DOKUZ EYLÜL UNIVERSITY
GRADUATE SCHOOL OF NATURAL AND APPLIED SCIENCES

VIBRATION ANALYSIS OF ROLLING ELEMENT BEARINGS USING PARAMETRIC MODELING

by
Sıdıka Nur DURMUŞ

October, 2019
İZMİR

VIBRATION ANALYSIS OF ROLLING ELEMENT BEARINGS USING PARAMETRIC MODELING

A Thesis Submitted to the
Graduate School of Natural and Applied Sciences of Dokuz Eylül University
In Partial Fulfillment of the Requirements forthe Degree of Master of Science in Mechanical Engineering,Machine Theory and Dynamics Program

by

Sıdıka Nur DURMUŞ

October, 2019
İZMİR

M.Sc THESIS EXAMINATON RESULT FORM

We have read the thesis entitled **"VIBRATION ANALYSIS OF ROLLING ELEMENT BEARINGS USING PARAMETRIC MODELING"** completed by **SIDIKA NUR DURMUŞ** under supervision of **PROF.DR. ZEKİ KIRAL** and we certify that in our opinion it is fully adequate, in scope and in quality, as a thesis for the degree of Master of Science.

Prof. Dr. Zeki KIRAL

Supervisor

Prof.Dr. Hasan ÖZTÜRK

(Jury Member)

Dr.Öğr.Üy. Aysun BALTACI

(Jury Member)

Prof. Dr. Kadriye ERTEKİN
Director
Graduate School of Natural and Applied Sciences

ACKNOWLEDGMENTS

I would like to present my deeply thanks to my esteemed professor, Prof. Dr. Zeki KIRAL, who has always supported me with his knowledge, experience, high patience and valuable ideas throughout the whole process of this study

I would like to thank the reference owners of the works and names I have mentioned in the reference section for their valuable work.

Finally, I would like to thank my dear friends, my dear family and most of all my mother, who have always supported me throughout my education life.

Sıdıka Nur DURMUŞ

VIBRATION ANALYSIS OF ROLLING ELEMENT BEARINGS USING PARAMETRIC MODELING

ABSTRACT

Bearings are standard machine elements used to increase the life and efficiency of the machine between the fixed and moving elements in the machines, reducing the friction and wear associated with it during operation. Bearings in which the load is transmitted by rotating elements between two surfaces are widely used in machine manufacturing and industrial applications due to their low friction characteristics and superior bearing properties. The fact that roller bearings perform their functions in a healthy way is important in terms of preventing machine performance, safety, human health,long-term and costly production downtime. For this reason, many methods have been developed for periodic maintenance of bearings and regular monitoring of their condition. Vibration analysis and condition monitoring are the most commonly used methods in industrial applications.

In this study, kinematic characteristics of a single row deep groove rolling element bearing weretaken into consideration and constant amplitude-constant direction loading model was obtained with a program developed in VisualBASIC programming language. In the finite element model of a bearing housing which is created parametrically with ANSYS APDL language, time varying forces were created forthe nodes at which the balls and outer ring are contacted and vibration analyseswere performed by the finite element method. Vibration analyzes were performed for the rolling element bearings with healthy and defect on the outer ring casesand standard statistical indicators are calculated by using the velocity and acceleration responses obtained from the numerical vibration analyzes. By examining the frequency contents of vibration responses, effects of the localized defects on the vibration response are analyzed.

Keywords: Rolling element bearing, bearing defect, parametric modeling, vibration analysis, Ansys, condition monitoring

RULMANLI YATAKLARIN PARAMETRİK MODELLEME İLE TİTREŞİM ANALİZİ

ÖZ

Rulmanlar, makinelerdeki duran ve hareket eden elemanlar arasında, çalışma esnasında meydana gelen sürtünmeyi ve buna bağlı aşınmayı azaltıp, makinenin ömrünü ve verimini artırmak için kullanılan standart makine elemanlarıdır. Yükün iki yüzey arasında dönel elemanlarla iletildiği rulmanlar, düşük sürtünme karakteristiği ve üstün yataklama özelliklerine sahip olmaları nedeniyle makine imalatı ve endüstriyel uygulamalarda yaygın şekilde kullanılmaktadırlar. Rulmanlı yatakların fonksiyonlarını sağlıklı bir şekilde yerine getiriyor olmaları, makine performansı, emniyeti, insan sağlığı, uzun süreli ve yüksek maliyetli üretim duruşlarının önüne geçilmesi açısından oldukça önemlidir. Bu sebeple rulmanlı yatakların periyodik bakımlarının yapılması ve durumlarının düzenli bir şekilde izlenilmesi adına bir çok yöntem geliştirilmiştir. Titreşim analizi ile durum izleme endüstriyel uygulamalarda en çok kullanılan yöntemdir.

Bu çalışmada, tek sıra bilyalı bir rulmanlı yatağın kinematik karakteristikleri dikkate alınarak, sabit genlik ve sabit doğrultulu yükleme modeli Visual BASIC programlama dilinde geliştirilen bir program ile elde edilmiştir. ANSYS APDL dili ile parametrik olarak oluşturulan yatak gövdesine ait sonlu elemanlar modeli üzerinde, bilyeler ve dış bileziğinin temas ettiği düğüm noktalarında zamana bağlı olarak değişen kuvvetler oluşturulmuş ve sonlu elemanlar yöntemi ile titreşim analizleri gerçekleştirilmiştir. Titreşim analizleri sağlıklı ve dış bileziği üzerinde bölgesel hata bulunan rulmanlı yataklar için yapılmış olup, sayısal titreşim analizlerinden elde edilen hız ve ivme cevapları kullanılarak standart istatistiksel göstergeler hesaplanmıştır. Titreşim cevaplarının frekans içerikleri incelenerek bölgesel hatanın titreşim cevabına etkileri analiz edilmiştir.

Anahtar Kelimeler: Rulmanlı yatak, rulman arızası, parametrik modelleme, titreşim analizi, Ansys, durum izleme

CONTENTS

Page

M.Sc THESIS EXAMINATON RESULT FORM ii
ACKNOWLEDGMENTS iii
ABSTRACT iv
ÖZ iv
LIST OF FIGURES x
LIST OF TABLES xv

CHAPTER ONE - INTRODUCTION 1

CHAPTER TWO - BEARINGS 12

CHAPTER THREE - THEORY OF VIBRATION 22

3.1 Introduction 22
3.2 Vibration Basics 23
3.2.1 Mass (m) 24
3.2.2 Stiffness (k) 24
3.2.3 Damping (c) 25
3.3 Vibration Terms and Definitions 25
3.3.1 Cycle 25
3.3.2 Amplitude 26
3.3.3 Period of Oscillation (T) 27
3.3.4 Frequency of Oscillation (f) 27
3.3.5 Phase(ø) 28
3.3.6 Angular Frequency (ω) 28
3.3.7 Natural Frequency 29
3.3.8 Resonance 29
3.4 Harmonic Motion, Displacement, Velocity and Acceleration 30
3.5 Classification of Vibration 32

3.5.1 Free Vibration 32
3.5.2 Forced Vibration 32
3.5.3 Undamped Vibration 33
3.5.4 Damped Vibration 33
3.5.5 Linear and Nonlinear Vibration 34
3.5.6 Deterministic and Random Vibration 34
3.6 Quantifying the Vibration Level 35
3.6.1 Peak to Peak 35
3.6.2 Zero to Peak 35
3.6.3 Root Mean Square (RMS) 35
3.6.4 Average 36
3.7Vibration Analysis Techniques 36
3.7.1 Time Domain Analysis 37
3.7.2 Frequency-Domain Analysis 39

CHAPTER FOUR - BEARING DEFECTS 40

4.1 Introduction 40
4.2 Types of the Bearing Defects and Reasons 41
4.2.1 Normal Fatigue Failure (flaking, pitting) 41
4.2.2 Cracks and Chips 41
4.2.3 Cage Damages 42
4.2.4 Brinelling 43
4.2.5 Creeping 43
4.2.6 Wear and Fretting 44
4.2.7 Scratch 45
4.2.8 Smearing 45
4.2.9 Score Marks 46
4.2.10 Peeling 46
4.2.11. Fracture 47

CHAPTER FIVE - SIMULATION OF VIBRATION SIGNALS IN ROLLING ELEMENT BEARING STRUCTURES 48

5.1 Structure and Bearing Forces 48
5.2 Creating Nodal Excitation Functions 52
5.3 Numerical Simulation..... 56

CHAPTER SIX - VIBRATION ANALYSIS OF BEARINGS AND FAULT DETECTION USING STATISTICAL FEATURES..... 59

6.1 Introduction 59
6.2 Time Waveform Analysis 59
6.3 Frequency Domain Analysis 78
6.4 Determining Ideal Sensor Positions According To Statistical Parameters 88

CHAPTER SEVEN - CONCLUSIONS 97

REFERENCES..... 100

APPENDICES 107

APPENDIX 1: Creation of Parametric Model and Obtaining the Natural Frequency 107
APPENDIX 2: 0 Degree Radial Loading Position for Vibration Analysis and Sample Code File on 152th Node..... 110
APPENDIX 3: Code Created to Process Data in Visual Program and Run It in Ansys Program 112
APPENDIX 4: An Example View of the ASCII File with Dynamic Extension Prg 116
APPENDIX 5: Installation Dates Applied with Interpolation with Code Created in Visual Basic Program to Carry Out Ansys Analysis..... 117

APPENDIX6: Frequency and Time Code Used for Creating Domain Analysis and Obtaining Statistical Indicators 118
APPENDIX 7: Code for Comparing Rms, Kurtosis, Peak to Peak and Crest Factor Values According to Sensor Positions 121
APPENDIX 8: Nomenclature 124

LIST OF FIGURES

Page

Figure 2.1 History of rolling element bearings 12
Figure 2.2 1500 years before the modern set of ball bearings, sketched by Leonardo da Vinci in Codex Madrid 13
Figure 2.3 Type of bearing a) rolling b) sliding 14
Figure 2.4 Type of contacts: point and line 14
Figure 2.5 Linear bearing 15
Figure 2.6 Journal bearing 15
Figure 2.7 Bearing components 16
Figure 2.8 Inner Ring 17
Figure 2.9 Outer Ring 17
Figure 2.10 Types of rolling elements 18
Figure 2.11 Cage 18
Figure 2.12 Force directions on the shaft 19
Figure 2.13 Radial bearings a) deep groove b) angular contact 20
Figure 2.14 Single Direction Thrust Ball Bearings 21
Figure 2.15 Double Direction Thrust Ball Bearings 21
Figure 2.16 Double direction angular contact thrust ball bearing 21
Figure 3.1 Spring-mass system 23
Figure 3.2 Rigid Mass 24
Figure 3.3 Linear Spring System 25
Figure 3.4 Viscous damper 25
Figure 3.5 Comparison of waves with different amplitudes 26
Figure 3.6 Different amplitude values 27
Figure 3.7 Frequency of Oscillation 28
Figure 3.8 Phase relationship between different waves 28
Figure 3.9 Resonance frequency 30
Figure 3.10 Resonant and non-resonant frequency values 30
Figure 3.11 Harmonic motion 31
Figure 3.12 A simple pendulum and spring-mass system 32
Figure 3.13 Forced vibration (mass, spring and damper system) 33

Figure 3.14 Undamped Vibration (mass-spring system) 33
Figure 3.15 Damped vibration (mass, spring and damper system)..... 34
Figure 3.16 Vibration amplitudes for sinusoidal wave 35
Figure 3.17 Guide to vibration severity as per ISO 10816 37
Figure 4.1 The reasons of the defects in rolling bearings 40
Figure 4.2 Inner ring, outer ring and balls are flaked..... 41
Figure 4.3 Cracks and chips defects..... 42
Figure 4.4 Examples of cage damages..... 42
Figure 4.5 Examples of brinelling..... 43
Figure 4.6 Creeping of inner rings 44
Figure 4.7 Wear and fretting failures 44
Figure 4.8 a) Inner ring of a spherical roller bearing b)Cage of a single-row ball bearing..... 45
Figure 4.9 Examples of smearing damage 46
Figure 4.10 Score marks 46
Figure 4.11 a) Inner ring of a spherical roller bearing b) Outer ring of a spherical roller bearing..... 47
Figure 4.12 a) Inner ring of a tapered roller bearing b) Outer ring of a solid needle roller bearing..... 47
Figure 5.1 Bearing housing dimensions and sensor locations in the finite element model..... 48
Figure 5.2 Dimensions of considered rolling element bearing 49
Figure 5.3 Load distribution in a rolling element bearing 51
Figure 5.4 Elements of the bearing and an instantaneous of dynamic loading..... 52
Figure 5.5 Dynamic loading of the bearing geometry $\theta = 0°$ and $\theta = 90°$ states 54
Figure 5.6 x component and y component of radial force acting on node f(x), f(y) function for 90° loading 55
Figure 5.7 Sample mode shapes a) at 1705.30 Hz b) at 3513.63 Hz c) at 4932.56 Hz d) at 5609.59 Hz e) at 7509.21 Hz 58
Figure 6.25 Experimental Acceleration signals for bearings of different conditions a) Normal bearing, b) Bearing with outer-ring defect 68

Figure 6.26 Acceleration scatter plot of the bearing, load direction 0°and node number 152 69
Figure 6.27 Acceleration scatter plot of the bearing, load direction 0° and node number 262 70
Figure 6.28 Acceleration scatter plot of the bearing, load direction 0° and node number 372 70
Figure 6.29 Acceleration scatter plot of the bearing, load direction 90° and node number 152 71
Figure 6.30 Acceleration scatter plot of the bearing, load direction 90° and node number 262 71
Figure 6.31 Acceleration scatter plot of the bearing, load direction 90° and node number 372 72
Figure 6.32 Acceleration scatter plot of the bearing, load direction 180° and node number 152 72
Figure 6.33 Acceleration scatter plot of the bearing, load direction 180° and node number 262 73
Figure 6.34 Acceleration scatter plot of the bearing, load direction 180° and node number 372 73
Figure 6.35 Acceleration scatter plot of the bearing, load direction 270° and node number 152 74
Figure 6.36 Acceleration scatter plot of the bearing, load direction 270°and node number 262 74
Figure 6.37 Acceleration scatter plot of the bearing, load direction 270° and node number 372 75
Figure 6.38 Frequency waveform of the bearing, 0° load direction on the x axis and node number 152 a) healthy bearing b) defect bearing 80
Figure 6.39 Frequency waveform of the bearing, 0° load direction on the y axis and node number 152 a) healthy bearing b) defect bearing 80
Figure 6.40 Frequency waveform of the bearing, 0° load direction on the x axis and node number 262 a) healthy bearing b) defect bearing 80
Figure 6.41 Frequency waveform of the bearing, 0° load direction on the y axis and node number 262 a) healthy bearing b) defect bearing 81

Figure 6.42 Frequency waveform of the bearing, 0° load direction on the x axis and node number 372 a) healthy bearing b) defect bearing 81
Figure 6.43 Frequency waveform of the bearing, 0° load direction on the y axis and node number 372 a) healthy bearing b) defect bearing 81
Figure 6.44 Frequency waveform of the bearing, 90° load direction on the x axis and node number 152 a) healthy bearing b) defect bearing 82
Figure 6.45 Frequency waveform of the bearing, 90° load direction on the y axis and node number 152 a) healthy bearing b) defect bearing 82
Figure 6.46 Frequency waveform of the bearing, 90° load direction on the x axis and node number 262 a) healthy bearing b) defect bearing 82
Figure 6.47 Frequency waveform of the bearing, 90° load direction on the y axis and node number 262 a) healthy bearing b) defect bearing 83
Figure 6.48 Frequency waveform of the bearing, 90° load direction on the x axis and node number 372 a) healthy bearing b) defect bearing 83
Figure 6.49 Frequency waveform of the bearing, 90° load direction on the y axis and node number 372 a) healthy bearing b) defect bearing 83
Figure 6.50 Frequency waveform of the bearing, 180° load direction on the x axis and node number 152 a) healthy bearing b) defect bearing..... 84
Figure 6.51 Frequency waveform of the bearing, 180° load direction on the y axis and node number 152 a) healthy bearing b) defect bearing..... 84
Figure 6.52 Frequency waveform of the bearing, 180° load direction on the x axis and node number 262 a) healthy bearing b) defect bearing..... 84
Figure 6.53 Frequency waveform of the bearing, 180° load direction on the y axis and node number 262 a) healthy bearing b) defect bearing..... 85
Figure 6.54 Frequency waveform of the bearing, 180° load direction on the x axis and node number 372 a) healthy bearing b) defect bearing..... 85
Figure 6.55 Frequency waveform of the bearing, 180° load direction on the y axis and node number 372 a) healthy bearing b) defect bearing..... 85
Figure 6.56 Frequency waveform of the bearing, 270° load direction on the x axis and node number 152 a) healthy bearing b) defect bearing..... 86
Figure 6.57 Frequency waveform of the bearing, 270° load direction on the y axis and node number 152 a) healthy bearing b) defect bearing..... 86

Figure 6.58 Frequency waveform of the bearing, 270° load direction on the x axis and node number 262 a) healthy bearing b) defect bearing..... 86
Figure 6.59 Frequency waveform of the bearing, 270° load direction on the y axis and node number 262 a) healthy bearing b) defect bearing..... 87
Figure 6.60 Frequency waveform of the bearing, 270° load direction on the x axis and node number 372 a) healthy bearing b) defect bearing..... 87
Figure 6.61 Frequency waveform of the bearing, 270° load direction on the y axis and node number 372 a) healthy bearing b) defect bearing..... 87
Figure 6.62 Kurtosis ratios of an faulty bearing for x component of a) acceleration responses b) velocity responses 89
Figure 6.63 Kurtosis ratios of an faulty bearing for y component of a) acceleration responses b) velocity responses 90
Figure 6.64 Crest Factorratios of an faulty bearing for x component of a) acceleration responses b) velocity responses..... 91
Figure 6.65 Crest Factor ratios of an faulty bearing for y component of a) acceleration responses b) velocity responses..... 92
Figure 6.66 RMS ratios of an faulty bearing for x component of a) acceleration responses b) velocity responses 93
Figure 6.67 RMS ratios of an faulty bearing for y component of a) acceleration responses b) velocity responses 94
Figure 6.68 Peak to Peak ratios of an faulty bearing for x component of a) acceleration responses b) velocity responses..... 95
Figure 6.69 RMS ratios of an faulty bearing for y component of a) acceleration responses b) velocity responses 96

LIST OF TABLES

Page

Table 5.1 Material properties of bearing structure 49
Table 5.2 Natural frequencies of the bearing structure 57
Table 6.1 Statistical parameters related to acceleration of defective and healty bearing, 152 node and x direction 76
Table 6.2 Statistical parameters related to acceleration of defective and healty bearing, 152 node and y direction 76
Table 6.3 Statistical parameters related to acceleration of defective and healty bearing, 262 node and x direction 77
Table 6.4 Statistical parameters related to acceleration of defective and healty bearing, 262 node and y direction 77
Table 6.5 Statistical parameters related to acceleration of defective and healty bearing, 372 node and x direction 77
Table 6.6 Statistical parameters related to acceleration of defective and healty bearing, 372 node and y direction 78

CHAPTER ONE
INTRODUCTION

All rotating objects that move under a certain amount of load stretch slightly due to the applied load and flatten on the contact surface, making both rotation and shifting (sliding) movement. This results in friction. Bearings are a kind of supporting elements between the standing and moving elements of the machines. Roller bearings are commonly used in many applications in the industry, from electronic appliances to helicopter gearboxes, as they reduce wear and friction during operation and increase machine life and efficiency. The fact that roller bearings perform their functions in a healthy way is of great importance both in terms of the performance and safety of the machine they are part of, as well as preventing long-term and costly production downtime and safety of human health. For this reason, periodic maintenance of roller bearings and their condition should be monitored regularly. Bearings in general; they consist an outer ring, an inner ring, cage and balls and are in contact with relatively high speeds and heavy dynamic loads. The Hertzian theme is one of the basic mechanisms that directly relate to the working conditions and stresses between rings and rolling elements (balls). The mechanism promotes a localized defect.

The load to the housing structure and machine frame through the rolling elements are carried by rolling materials bearings. It may be differently formed to transfer the load. The direction and magnitude of the transferred load relative to the shaft speed remains unchanged. The rolling material's radial load effective bearing is composed as a distributed load thanks to geometry (McFadden & Smith, 1984). Also there are empty places in the bearing structure in the course of the operation in similar states of the loading. Load transmission is carried out by the rolling elements. The kinematics of roller bearings can be derived using the kinematics of planetary gears. In general, the inner ring is the rotating component in most industrial applications and the outer ring is fixed. The movement of the planetary gears and rolling elements is the same and they rotate around the bearing axis. The moving elements transfer the load to the machine frame. Therefore, the loading of the bearing housing can be

referred to as a moving load problem in which various parameters are very important, such as the shape of the transferred load, the position of the roller elements (according to the load region and housing structure). Moving load pre requisites are an engineering subject that has been studied for many years. There are many studies of the moving load problem, and these studies usually focus on the moving load in beams that are elastically supported or not.

The successful monitoring of the condition monitoring technique of roller bearings depends on the selection of the appropriate signal processing technique. Many methods used to detect machine damage can be listed as follows: vibration analysis, acoustic emission measurements, motor current signature analysis (MCSA), noise monitoring, temperature monitoring, wear debris analysis, shock pulse method (SPM). Vibration analysis using experimental or simulated signals is one of the most successful methods used in condition monitoring studies. Secondly, it is to compare the vibrational data obtained by forming a defecton the bearing with the transmission data in the healthy bearing. Thirdly, to create and analyze bearing models with the help of computer-aided programs and to compare healthy and damaged bearings with the obtained vibration data.

McFadden & Smith (1984) created a point defect on the bearing inner ring under constant radial load and established a mathematical model to determine the vibration produced as a single point defect. The model reflects the effects of bearing load distribution, bearing geometry, shaft speed and exponential vibration disturbances and showed that the theoretical and empirical results are compatible with each other.

Mathew & Alfredson (1984) monitored and analyzed the vibration signals of several rolling element bearings in order to detect the failure of newly damaged bearings. They stated that frequency domain parameters provide better results than thetime domain parameters in fault detection, but it is still not correct to rely on a single method to detect bearing failures.

Lawry (1998) modeled a carrier structure using I-DEAS computer-aided engineering (CAE) software to obtain the finite element discretization and perform the finite element vibration analysis based on the mode superposition method.

Tandon & Choudhury (1999) discussed the acoustic measurement and vibration methods in bearing failure detection. At the end of the study, they showed that sound density technique, which is one of the acoustic measurement methods, is a more accurate method than sound pressure measurements. In addition, they suggested that among all the measurable values such as the peak to peak, probability density, RMS and kurtosis, the most accurate result would be obtained from the kurtosis value.

Kıral & Karagülle (2002) modeled the dynamic loading of a rolling bearing structure with a computer program and obtained the vibration responses of the structure using the IDEAS CAE package. They compared the values of displacement, velocity and acceleration responses obtained for faulty and healthy bearings at different sensor positions and rotational speeds. They showed that it is possible to make fault detection by using the envelope (HFRT) method.

Liewa & Limb (2004) used linear, semi-static and time-invariant theory to expand the time-varying rolling element formulation containing hardness formulation. The formulation takes into account the effect of the shaft rotation speed and the nature of the time unfunded stiffness coefficients is generally examined by converting the dependence on the shaft speed and time into a function of the normalized orbital position angle. They concluded that, with the help of the theory, the results of direct numerical integration for a gear pair sample can be compared and an improved time-averaged bearing hardness model can be established.

Mazanoglu (2004) studied the analysis of local defect in a bearing using vibrational analysis. In the study, the actual bearings under different loads were tested in both healthy and fault conditions and vibration signals were evaluated in frequency, time and combined time-frequency domains. As a result, it has been found that the existence of a fault occurs over time. The frequency peaks determined

by the envelope analysis were observed at the characteristic frequency of the fault component. By applying combined time-frequency analysis, the error indicators were detected only at the vibration energy levels at which the bearing components are in contact with the defect.

Tandon & Choudhury (2006) modeled the rotor bearing mechanism under radial load as a three degree of freedom system using the mass-spring-damper model. They obtained vibration reactions by forming defects in bearing elements under load and compared theoretical and experimental vibration values at different loads, faults and speeds. They showed that the amplitude values of bearing fault frequencies and harmonics are very close to theoretical and experimental conditions. They also concluded that the frequency amplitude obtained for the defect in the outer ring of the roller bearing was higher thanthatobtained for the inner ring and the rolling element under similar load and speed conditions.

Orhan et al. (2006) studied the real systems including cylindrical roller bearings and ball bearings in the condition monitoring and detection of defects by usingvibration and spectral analysis methods. The study showed that ball bearing slack causes outer ring fault. Time wave, frequency spectrum and vibration level values were obtained from various vibration samples. They performed vibration analyses at certain intervals and showed that possible errors can be prevented easily by vibration monitoring.

Kıral & Karagülle (2006) modeled a bearing structureconsidering theloading mechanism with different local defects under the action of an unbalanced load. In order to simulate bearing vibration signals, asone of the most reliable analysis methods,the finite elementmethod was proposed to be used. In this study, the effects of different parameters such as type of defect (inner ring failure and rolling element failure), rotational speed, defect'sangular position, sensor position and number of outer ring failure,on vibration monitoring methods were investigated by using time and frequency domain parameters. They found that the envelope method can be used

effectively to detect inner and outer ring faults, but rolling element faults have been difficult to detect by band energy ratio procedures and envelope technique.

Al-Ghamd & Mba (2006) studied the relationship between kurtosis and AE RMS amplitude for a number of fault conditions. The data obtained from the experimental test device were classified. Then, it was compared with vibration analysis and AE results under various speed and load conditions.It was found that AE maximum amplitude and kurtosis were very sensitive to the on set and development of faults according to vibration measurements.

Khalid et al. (2007) proposed a new method to detect localized errors in the outer and inner rings of a rolling element. In the model, a rolling element with internal and external race defects weregiven and a new method for the localized ball bearing faults was applied. In this study, wavelet shape parameters (ejaculation center and factor frequency) and wavelet transform coefficients were optimized for vibration signal thanks to maximizing kurtosis value.

Jayaswal et al. (2008) conducted a study examining condition monitoring methods applied to rotating equipment such as vibration analysis, noise analysis, temperature monitoring, visual inspection, acoustic emission analysis, wear debris analysis, motor current signature analysis and nondestructive testing. They concluded that vibration signature analysis was the most accurate method for fault detection.

Tomovic et al. (2010) described a vibration model of a rigid rotor supported by rolling element bearings. Parametric analysis of the effect of the the rolling elements and internal radial clearance on the rigid rotor vibrations in the unloaded rolling element bearings was performed using the proposed model. Vibration model and parametric analysis, which was defined by experimental methods were confirmed.

Randall & Antoni (2010) conducted a study directing the diagnostic analysis of strong masking signals from other machine components such as gears and acceleration signals comingfrom rolling element bearings. They found that, the

specific properties of the rolling element bearing signals were stochastic, not periodic, and were therefore distinguished from deterministic signals such as gears.

Kankar et al. (2011) considered seven different base wavelets for defect diagnosis of bearings with localized defects on bearing components and used the complex Morlet wavelet methodology based on the minimum Shannon entropy criterion to derive statistical characteristics from the wavelet coefficients of raw vibration signals. Accordingly, a feature extraction based on the wavelet theory showing error information from raw signals was made and then three different artificial information techniques were investigated to estimate the type of the fault in the bearings. Of these, it was found that the rolling vector of the support vector machine more accurately defined the error categories and was a much more accurate diagnostic method compared to the learning vector quantification and self-organizing maps.

Segla et al. (2012) developed a test apparatus with the aid of high frequency resonance technique (HFRT) to pinpoint the bearing failure. They created a local error on the inner ring and collected vibration signals from three different measuring points. They calculated the statistical parameters such as square factor, square root, and kurtosis. They found that characteristic defect frequencies of the carrier elements were also found on the obtained spectrum and showed that the source of the error could be determined with the HFRT method.

Xiang et al. (2015) proposed a hybrid approach to detect rolling element bearing failuresusing the spectral kurtosis (SK) and probabilistic principal component analysis (PPCA). Accordingly, the signal-to-noise ratio (SNR) of the PPCA denoising model was first developed by the selection of two basic parameters, main information and fault signals. In the next step, they designed a bandpass filter for denoising the signal. This filter determine the optimal bandwidth and center frequency using the fast spectral kurtosis procedure. Using filtered signal, the Hilbert envelope spectrum analysis was performed to remove the fault frequencies of the rolling element bearings. In this study, the PPCA and SK methods were found as

effective methods to be employed in fault detection and it was confirmed experimentally by considering different fault types.

Laha (2016) interested in increasing the fault mark in rolling element bearings and thus applying the balancing method of non-terrestrial vehicles for diagnostics. The parameters for the NL-mediator method were obtained by maximizing the kurtosis value of the bearing vibration signal. At the end of the study, the method was compared with the minimum entropy deconvolution (MED) technique and it was found to be more ideal method for diagnosing the fault. It was also shown that the envelope spectrum of the bearing vibration signal can beused to obtain characteristic bearing defect frequencies.

Nabhan et al. (2016) simulated the ball bearing and bearing housing by creating a three-dimensional finite element model. They formed defects in the outer ring at regular intervals, and they found compatibility by comparing the faults in the experimental and simulation results.

Sarabjeet et al. (2017) numerically modeled the vibration response of a rolling element bearing with a localized outer ring defect. In the study, the finite element model (FE) of a defective bearing was created by using the FE software package LS-DYNA. Time domain results including displacement, velocity and acceleration time traces showed that the modeled signals contain the fundamental characteristics corresponding to unloading and reloading of the rolling elements, respectively when entering and exiting the defective element. From frequency and time domain analyzes, they found that the numerical and analytical results were consistent.

Zhang et al. (2017) proposed a new diagnostic method based on variable mode separation in roller bearing failures in centrifugal pumps. In this method called VMD, the rolling bearing mechanism of outer ring fault, inner ring fault and bearing element fault was studied using the model of dynamic response. The unbalance and gravitational force were taken into account for the dynamic response modeling. Different types of faults were generated and simulation of these faults was obtaind as

vibration signals and the gaussian noise. As a result of the comparisons, they showed that the VMD was able to correctly givethe main mode of the bearing failure signal and performed better than the EMD by removing bearing defect characteristics.

Similarly et al. (2018) presented a new analytical bearing stiffness model that could overcome these problems by softening the non-linear bearing strength and stiffness-displacement properties in discontinuous regions and applied a deformation scale correction. In the study, a modular type model was used which allows each rolling element in contact to define a certain value of the flattening. It was observed that a small softening value can greatly increase the numerical calculation of the selected system in terms of speed and stability.

Chen & Kurfess (2018) developed a new technique to find the bearing fault size from input and output signals. When using an experimental model based signal processing method to find the entry point of the bearing vibration response, the output point was differentiated and determined by applying a threshold to the signal. The proposed method was verified in the bearing system of a 3-axis CNC machine tool shaft. Speed range was selected as 500-3000 rpm. As a result of the experiments, it was observed that the proposed techniques give less biased results in terms of spindle speed and more accurate estimates.

Yang et al. (2018) designed a rotor bearing frame system using a finite element method in aero motors where main shaft bearings play an important role in the efficient and safe operation of the entire motor. They studied the effect of roller bearing failures on performance and transmission characteristics. Mixed and single localized bearing faults are simulated in the model. At the end of the study, it was found that the simulation has a good prediction on the components of bearing failure characteristics and modulation frequencies. As long as the characteristic frequencies are different, it was proved that when the bearing failure with two different rolling elements occurs, the faults can be identified separately by this method.

Schmidt et al. (2018) proposed a rolling element with a novel detection methodology depend on novelty detection for machines operating under variable speed conditions. Accordingly, the rolling element with diagnostic methodology was verified on data fromtwo experimental data sets and a phenomenological transmission model. It has also been shown that it can easily detect, localize and direct an existing damage to the bearing. One of the most important aspects of the method discussed is to learn the characteristics of the healthy bearing signal such that it is used to generate an inconsistency signal then the condition of the bearing emerges under varying speed conditions.

Peng et al. (2019) have developed a new approach that uses the online wear debris characteristics to determine the wear condition of rolling element bearings. For this purpose, a dynamic particle imaging system was used to obtain multi-image particle images in the sequences. Target particles were detected and monitored based on moving particles, Gaussian mixing model and bubble detection algorithm. The amount of particles was obtained to show the trend and change in wear rates. Two-dimensional particle properties such as circumference, area, length, width, aspect ratio and roundness were also obtained. The results showed that oxidized, fatigue, slip and shear wear debris can be detected in real time, and thus the method studied can be applied for in-depth wear characterization of rolling element bearings in online condition monitoring.

Shah & Patel (2019) have developed a dynamic model to estimate vibration generated by a defective and healthy deep groove ball bearing, taking into account shaft masses, grooves, balls and seats. The hardness and damping effect with lubricating film and non-linear Hertz contact were also indicated in the established model. The derived equations of the motion were solved analytically using Matlab software employingthe fourth order Runge-Kutta method. In the simulation, it was found that the vibration amplitude of the balls passing over the defect increased and was affected by the presence of lubricant radial load, shaft rotation speed, defect size and position. The results of the current dynamic model are also confirmed by the

results obtained from the experimental methods and it can be safely used to estimate the frequency and amplitude produced by defective and healthy bearings.

Hizarci et al. (2019) carried out a vibration zone extraction study in order to detect the faults causing gear performance deterioration and to monitor the status of the gearboxes in detail. In the study, there is an experimental apparatus consisting of a two-stage helical gear box and a worm gear box. The apparatus using image processing algorithms were also used as an input to the artificial neural network for the classification of fault severity. At the end of the study, it was found that the method can fully monitor the status of the gearboxes and classify the severity of the faults.

Within the scope of this thesis, ANSYS APDL language was used for parametric modeling of the the bearing housing structure and numerical vibration analyses were performed by finite element method. In general, standard finite element packages are not usually installed to apply moving and time-varying loads to engineering structures. In this thesis, a dynamic loading model, which is the couse of the rolling element bearing vibrations, was obtained according to the requirements of the ANSYS transient analysis for healthy and faulty bearing conditions.

The computer code developed within this thesis reads the nodal informations (node labels and spatial positions) from an input file and generates time-dependent excitation functions for all excited nodes. In the program, dynamic loading model has been formed by considering bearing kinematics, loading status and bearing characteristics. The developed computer code can be used in vibration analysis of all structures containing rolling element bearings. Experimental studies are costly and it is very difficult to obtain mathematically simulated vibration signals to contain structural information. This work has been done to overcome these two difficulties and the method can be used to generate a vibration signal containing dynamic information of the housing structure or machine frame where the vibration sensor is placed without an experimental work. The resonances of the bearing structure are influenced by the operating speed of the shaft and the pulses at distinct frequencies

governed by the geometry of the bearings. The vibration signal of a defective bearing is bifurcated and modulated by the natural frequencies of the bearing system and/or the machine frame. Symptoms of erroneous statuscan be extracted from the vibration signals and its frequency domain parameters.

Organization of this thesis is as follows:

Chapter 1 consists of literature reviews on the problem of moving load, healty and defective modeling of vibration signals of rolling element bearings and condition monitoring techniques of rolling element bearings.

Chapter 2 summarizes the history of the bearing element, the basic elements of the rolling element bearings and the bearing types encountered in the industrial applications.

Chapter 3 gives brief information on the vibration theory and some monitoring techniques.

Chapter 4 includes general bearing failures with examples. The majority of the information wastaken from the bearing manufacturers.

Chapter 5 provides information about the selected bearing type, the formed bearing geometry and the finite element model. Dynamic modeling of bearing structure is explained. Dynamic responses from the nodes, data processing and vibration analysis are explained.

Chapter 6 describes the graphs and tables obtained fromthe acceleration values of the calculatedvibration signals. Healthy and damaged bearingsare compared according to statistical parameters under different loading directions.

Chapter 7 concludes the findings of the numerical vibration analysis of the considered rolling element bearing and gives some suggestions for future studies.

CHAPTER TWO
BEARINGS

2.1 Brief History of Bearings

In the ancient times, people had to push, pull, or rotate objects that they could not move with their own forces because of some of their needs. These needs also brought some inventions as shown in Figure 2.1.

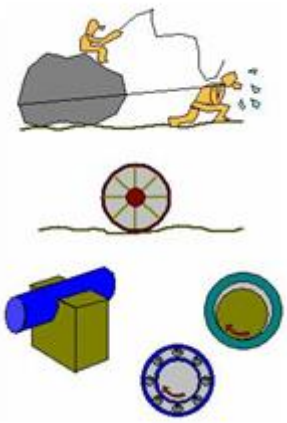

Figure 2.1 History of rolling element bearings (SKF, 1996)

This working to move objects was reduced significantly meanwhile he discovered simple forms of fattening like mud or water. The portrait of transportable bearings made of wooden cylinders prior to the Great Antiquity and earlier times. It is said that Egyptian used bearings and same tools to make use of trees around the slides. By the innovation of the wheel, it became manifest that rolling movement requires less effort and is lesser damaging to planes than sliding movement. It is not surprising for this reason, that bearings, using only rolling movement, were in the end improved for use in machines, where metal sliding on metal causes significantly abrasion.

The first machine designs used journal (plain) bearings which is consisted of hollow cylindirical steel without any rolling element supplied with lubricant. As the industry devoloped and manufacturing methods got better, the bearings also changed,

rolling elements are added and much better material is used which resulted in more life cycle and better efficiency.

An illustration of a ball bearing by Leonardo da Vinci from 1500s is shown in Figure 2.2. The first bearing patent was taken by Philip Vaughn in 1794 in Carmarthen, England. With the emergence of industrial evolution, steel became easier to process the material, and in 1883 a machine was designed by Frederick Fisher (FAG founder) to produce exactly circular and equal sized balls. With the help of balls produced with higher precision, the amount of friction between the metal surfaces and the resulting energy loss is minimized.

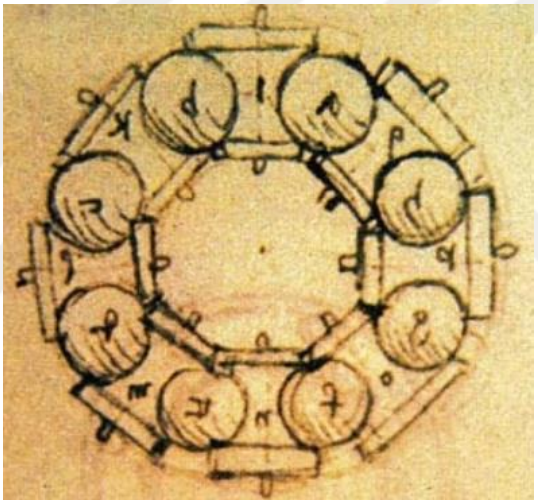

Figure 2.2 1500 years before the modern set of ball bearings, sketched by Leonardo da Vinci in Codex Madrid (UNESCO, n.d.)

2.2 Bearing Theory

As the bearings move between the outer and inner rings by means of rolling elements, the bearings providing the possibility of working with minimum friction are generally divided into two groups as rolling (Figure 2.3.a) and sliding (Figure 2.3.b). Sliding bearings, which are free to move horizontally or vertically, can tolerate axial displacement of the shaft within certain limits and are often preferred in precision engineering applications.

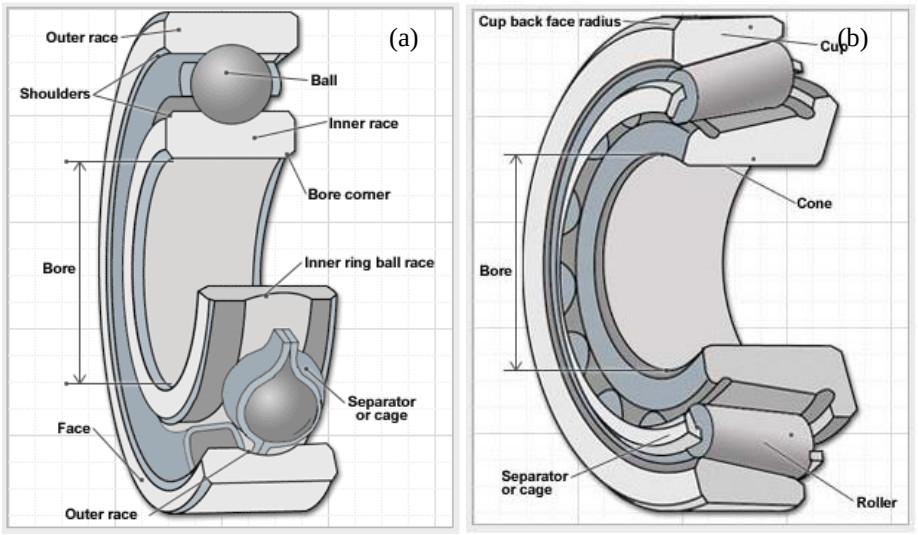

Figure 2.3 Type of bearing a) rolling b) sliding (SKF, 2019)

The bearings can be examined under two main categories, which are ball and roller bearings. The spherical parts which are called balls in the bearing reduces the friction by reducing the contact area **point contact** (Figure 2.4). In the bearing while the rollers transfer the force along a line **line contact** (Figure 2.4). Therefore generating much more load-bearing capacity.

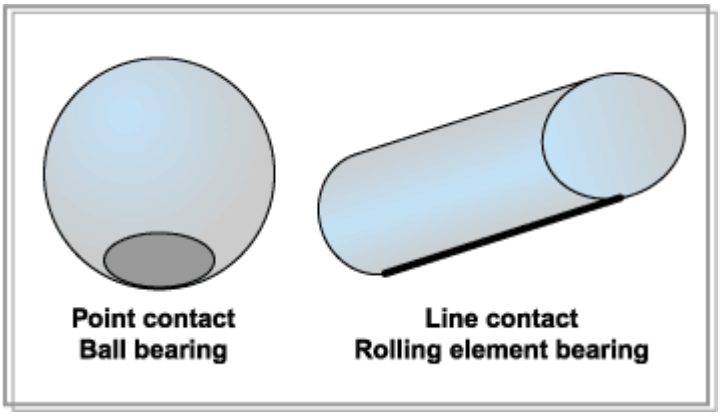

Figure 2.4 Type of contacts: point and line (FAG, 2001)

2.2.1 Sliding Bearing

Plain bearings are bearings that make sliding movement between their surfaces. To prevent friction, these surfaces include an oil film. There are two kinds of plain bearings, linear bearings and journal bearings. They are generally made in two parts, the movable element (shaft) and fixed element (bearing).

Linear bearings produced for linear direction movements cannot make rotational movements due to their design. Figure 2.5 shows a linear bearing.

Figure 2.5 Linear bearing (Meta Rulman, 2019)

Journal bearings are thebearings capable of sliding between two surfaces as well as rotational movement. As with linear bearings, there is an oil film between the surfaces to prevent friction. They have vibration and sound damping properties as well as very carryingheavy loads. Figure 2.6 shows an exemplary bearing housing.

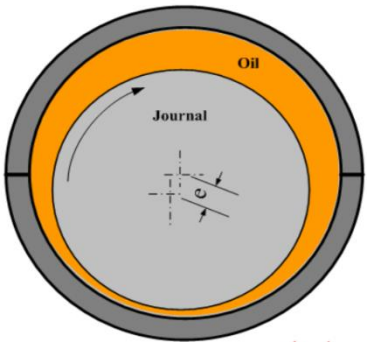

Figure 2.6 Journal bearing (Substech, 2019)

2.2.2 Rolling Bearings

They are carrier elements that allow relative movement between two machine elements with minimum friction, preventing movement in the force direction. Bearings with rolling elements are used for the bearing of machine elements such as bicycles, compressors and wheels. While the inner ring of the roller bearing is in contact with the shaft, the outerring is in contact with the machine body and rolling elements are provided between the two rings.

2.2.2.1 Bearing Components

Although some bearing types have extra components, the bearings are generallyconsist ofthe inner ring, the outer ring, the cage and the rolling elements as shown in Figure 2.7. The rolling element may vary depending on the bearing type.

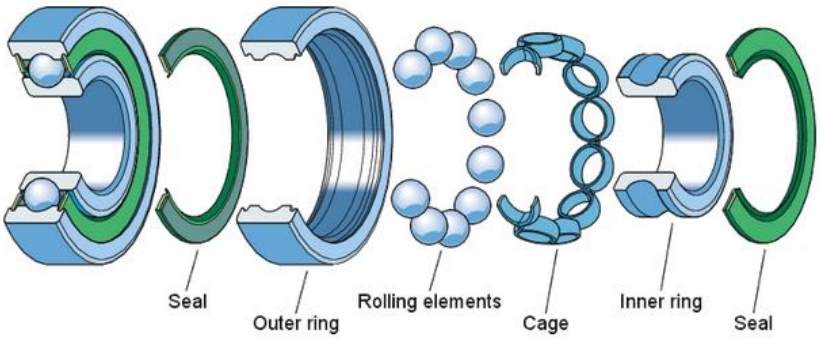

Figure 2.7 Bearing components (SKF, 2013)

2.2.2.2 Inner Ring

Itis installed on the shaft and rotating part of the machine as shown in Figure 2.8. The hole may be cylindirical or conical. The inner rings usually made of special, high purity, chrome alloy steel. They have different forms such as cylindrical, spherical and conical depending on the type of rolling elements.

Figure 2.8 Inner Ring (NPTEL, 2019)

2.2.2.3 Outer Ring

It is installed in the housing of the machine and in most situations, it does not rotate. Similar to the inner rings, they are usually made of special, high purtiy, chrome alloy steel, as shown in Figure 2.9. The forms of the raceways may be spherical, sylindirical or conical.

Figure 2.9 Outer Ring (NPTEL, 2019)

2.2.2.4 Rolling Elements

They are balls, rollers, cones, spheres or needles. They are made of special, high purity, chrome alloy steel. Special materials such as ceramic and plastic are also used. The rolling elements are separated and guided by the cage, where the rings or discs are specially closed and rotated. They transfer the loads they carry by this way. Rolling element types are shown in Figure 2.10.

Figure 2.10 Types of rolling elements (SDP/SI, 2018)

2.2.2.5 Cage

It is responsible for keeping and guiding the rotating elements apart. The materials used include steel, brass and plastic. While robust metal cages can be produced by processing techniques, pressed cages are made of sheet metal. Similarly, plastic cages can be processed from solid plastic or produced by injection molding. Cage is shown in Figure 2.11.

Figure 2.11 Cage (NPTEL, 2019)

2.2.2.6 Seals

They are necessary for a long and safe life of the bearing. They protect the bearing from defilement and keep the lubricant inside the bearings.

2.2.2.7 Guide Rings

They are used in some spherical roller bearings that claim deeply better quality. The main function of theguide rings is to guide the bearings so that they can rotate parallel to the shaft and deploy the load equally to the raceways.

2.2.2.8 Bearings According to Load Direction

When the bearings are running, they are divided into two groups as thrust and radial bearings according to the direction of the force they carry. Radial loads acting bearing's axis of rotation. Axial (thrust) acts parallel to the axis of rotation. The directions of the forces loaded on the shaft are shown in Figure 2.12.

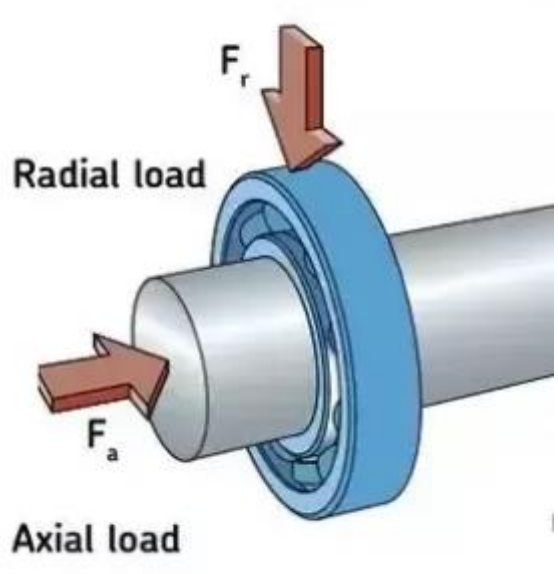

Figure 2.12 Force directions on the shaft (Kaydon Bearing Solutions, 2018)

2.2.2.8.1 Radial Bearings. Deep groove ball bearings are the maximum speed limit of all bearing types. Due to the spherical nature of the balls in these bearings, only the top point of the balls contacts the rings of the bearing. Therefore, they provide lower surface contact than roller bearings, so higher speeds with less friction can be achieved. While radial bearings are able to carry both radial and axial forces depending on the angle of contact, they can also carry radial forces only when the angle of contact is zero. The radial bearings are shown in Figure 2.13.

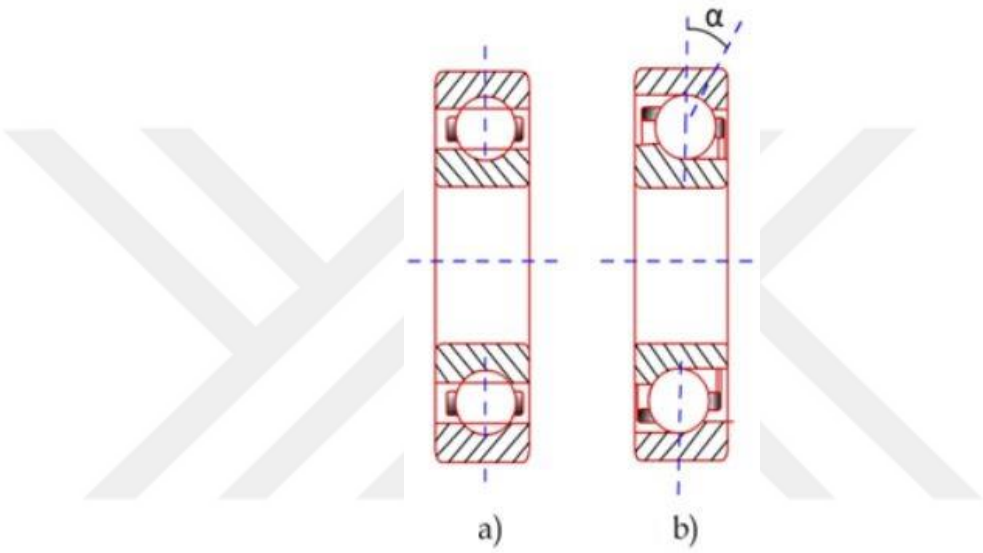

Figure 2.13 Radial bearings a) deep groove b) angular contact (NPTEL, 2019)

2.2.2.8.2 Thrust or Axial Bearings. Axial ball bearings can be dismantled. These bearings are manufactured in both single and double direction types. One-way axial bearings consist of spindle ring, ball assembly and body ring. Parts of bidirectional thrust bearings are two body rings, two ball sets and spacer rings. Both bearing types can bear large axial loads. The forces acting on the bearing must be smaller than a certain value so that the balls under the influence of centrifugal force do not come out of the channels during operation. Single direction thrust ball bearing is shown in Figure 2.14 and double direction thrust ball bearing is shown in Figure 2.15. Some types of them can also carry some radial forces. In Figure 2.16, an axial bearing that carries a radial force is shown.

Figure 2.14 Single Direction Thrust Ball Bearings (SKF, 2017)

Figure 2.15 Double Direction Thrust Ball Bearings (SKF, 2017)

Figure 2.16 Double direction angular contact thrust ball bearing (SKF, 2012)

CHAPTER THREE
THEORY OF VIBRATION

3.1 Introduction

A system has done around the equilibrium position oscillation is called vibration. Eardrum and associated mechanism vibrate with the aim to perform hearing, the tongue and vocal cords vibrate to speak. Most of the musical instruments, especially in stringed instruments, vibration is a desirable event. Other vibration on the side is undesirable for many mechanical systems, in some cases also it is destructive. For example, vibrations in the fuselage cause fatigue and consequently damage. Earthquake-induced vibrations can cause cracks and damage to buildings. Vibration is a common effect in everyday life and vibration reduction is the main area of interest.

Vibration is available everywhere and is a phenomenon affecting the structure of engineering designs. Vibration characteristics can be the determining factor for engineering designs. Vibration can sometimes be harmful and avoided, sometimes very useful and desirable. How to vibrate in both cases it is important information for engineering to analyze, measure and control.

The vehicles are more robust and provide more insulation than road inputs than before. Today's more robust vehicles are less susceptible to many of the vibrations that may occur in vehicles of previous designs, but vibrations can still be detected in a more modern vehicle if a transmission path is formed between a rotating component and the vehicle's body.

3.2 Vibration Basics

In vibration systems, springs are used for stroing potential energy, mass and inertia for kinetic energy and damping for gradually lost energy. The vibration system constantly changes its energy between potential energyand kineticenergy. For this reason, vibrating systems have elements that store potential and kinetic energies. Elements that store potential energy are spring or elastic elements; elements that store kinetic energy are mass or inertia elements. The elastic elements store potential energy and return this energy to the inertia element as kinetic energy.

In damped systems few percantange of the total energy is lost at each vibration cycle and additional energy source should be added to the system if steady vibration wants to be maintained. Only lumped parameter systems composed of ideal mass, spring, and damper elements are studied in this chapter. There are twotypesof motion; translational and rotational motion. Displacement is represented as linear distances in the translational motion, and displacement is represented as angular distance in the rotational motion.

Below is the explanation of how a spring-mass system reacts against an external force F. Figure 3.1 shows a spring-mass system.

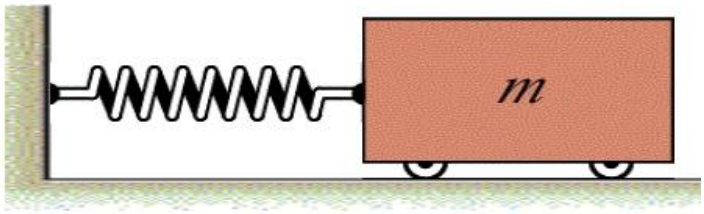

Figure 3.1 Spring-mass system (Universty Of Southern Queesland Lecture Notes, 2019)

The applied force F moves the mass by getting over the inertia of the mass and the reactions of the spring.

Machines have three main features in order to determine how they react to forces that lead to vibration. These are mass (m), stiffness (k) and damping (c).

These features can be used to explain how machines respond to vibration.

3.2.1 Mass (m)

The acceleration of a mass is proportional to the resultant F of all forces acting on the mass according to Newton's second law. It is measured in kg. The rigid mass is shown in Figure 3.2 and its element equation is given in Equation 3.1.

$$F = m\ddot{x} \tag{3.1}$$

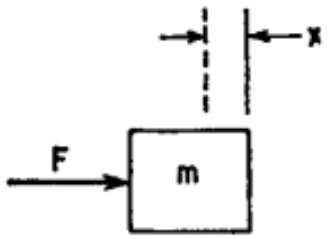

Figure 3.2 Rigid Mass (Rao, 2004)

3.2.2 Stiffness (k)

Figure 3.3 shows a linear spring. In linear springs, the amount of extension of spring is proportional to the force. It is described by Equation 3.2.

$$F = k(x - u) \tag{3.2}$$

It is considered that the ideal springs have no mass; therefore, the force acting on one end is equal and opposite to the force acting on the other end. The constant k defines stiffness or spring constant. It is measured in N/m.

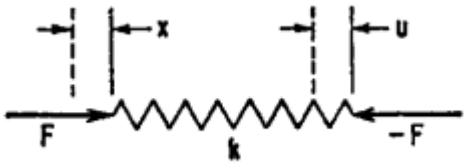

Figure 3.3 Linear Spring System (Rao, 2004)

3.2.3 Damping (c)

Aviscous damper is shown in Figure 3.4. The applied force to the viscous damper is proportional to the relative velocity of its connection points and it is described by Equation 3.3.

$$F = c(\dot{x} - \dot{u}) \tag{3.3}$$

The constant c defines the damping coefficient and the characteristic parameter of the damper. It is considered that the ideal dampers have no mass; therefore the force at one end is equal and opposite to the force at the other end. It is measured in N/(m/s).

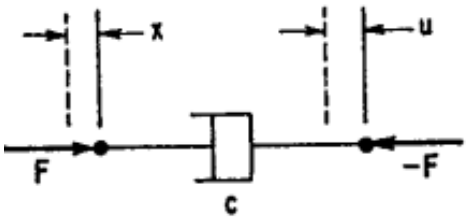

Figure 3.4 Viscous damper (Rao, 2004)

3.3 Vibration Terms and Definitions

3.3.1 Cycle

A cycle is defined as a full vibration. In Figure 3.5, waves with different amplitudes are shown. The cycle is defined as a vibrating body moves from stable

position (point A) to a high level (point B), then to stable position again (point C), then to reverse high position (point D) and then back to stable position (point E) again.

3.3.2 Amplitude

It is defined as the maximum magnitude of the movement of the object from equilibrium in one direction. In other words, it is half of the vertical distance it takes from the top of a wave to its trough in the vibration graph. These are B and D points in Figure 3.5. Also, Figure 3.6 shows the different amplitude values in the graph.

Vibration amplitude is expressed in three different ways. These are: peak to peak (P-P), zero to peak (0-P) and RMS (root mean square).

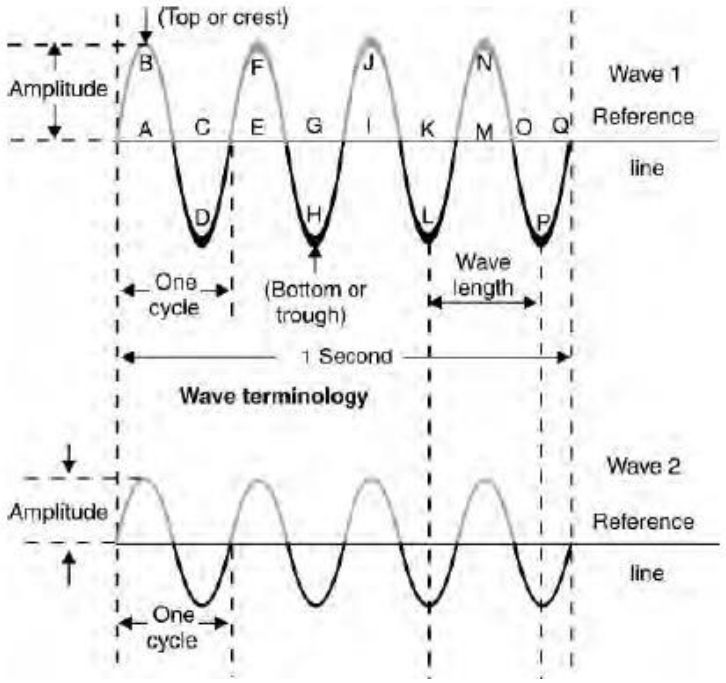

Figure 3.5 Comparison of waves with different amplitudes(Scheffer, 2004)

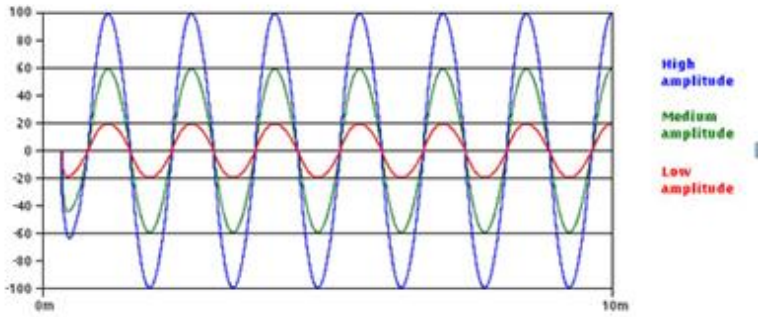

Figure 3.6 Different amplitude values (Scheffer, 2004)

3.3.3 Period of Oscillation (T)

It is the time it takes for a vibrating body to complete its movement. It is measured withthe second. Period of oscillation is calculated as given in Equation 3.4, where ω is the angular frequency of the ascillation.

$$\tau = \frac{2\pi}{\omega}[s] \tag{3.4}$$

3.3.4 Frequency of Oscillation (f)

Frequency can be expressed as the number of repetations within 1 second and it is measured in Hertz. Frequency of oscillation is shown in Figure 3.7 and it is described by Equation 3.5.

$$f = \frac{1}{\tau} = \frac{\omega}{2\pi}[Hz] \tag{3.5}$$

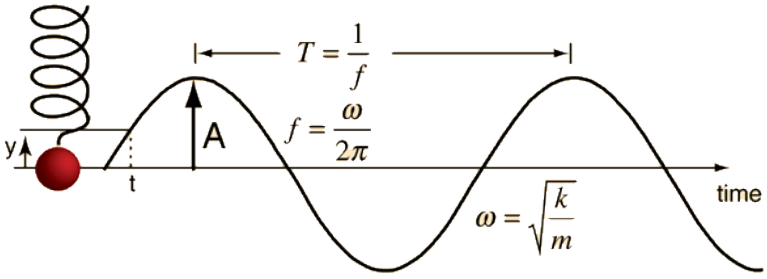

Figure 3.7 Frequency of Oscillation (Rao, 2000)

3.3.5 Phase(ø)

The term phase angle in vectors and phasors represents the angular component of the polar coordinate system. For the quantity of the vector, amplitude and the phase angle in the representation are called the polar representation. In periodic events such as wave, the phase angle is synchronized with the phase.

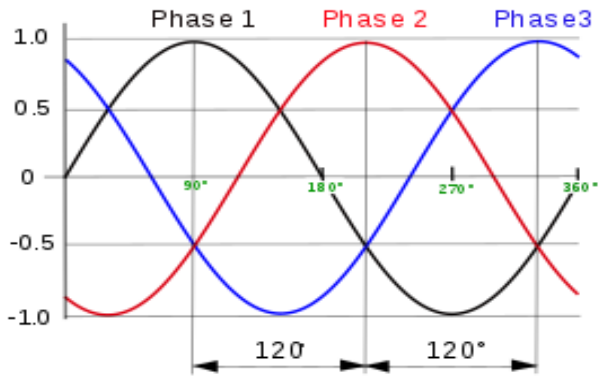

Figure 3.8 Phase relationship between different waves (SKF,2019)

3.3.6 Angular Frequency (ω)

Angular frequency is a measure of the number of radians per unit of time in periodic motion. Its unit isdegrees (or radians) per second. Angular frequency is calculated as given in Equation 3.6.

$$\omega = 2\pi f = \frac{2\pi}{T} \tag{3.6}$$

3.3.7 Natural Frequency

Natural frequency (eigenfrequency) is the frequency at which a system tends to oscillate in the absence of any driving and damping force. Natural frequency is calculated as given in Equation 3.7.

$$\text{Natural frequency: } \omega_n = \sqrt{\frac{k_{eff}}{m_{eff}}} \text{ [rad/s]} \tag{3.7}$$

where k_{eff} and m_{eff} are the effective mass and effective stiffness values of the considered system, respectively.

3.3.8 Resonance

Every object oscillates at its natural frequency under any initial condition. The natural frequency valuedepends on the shape and the materialof the object.For the undamped case, if an harmonic force is applied to the object at a frequency equal to its natural frequency, the resonance condition occurs. In the case of resonance, the object vibrates with maximum amplitudes. An example of the resonance phenomenonin the frequency-amplitude graph is shown in Figure 3.9. Figure 3.10 shows the resonant and non-resonant frequency values. Resonance frequency is calculated as given in Equation 3.8.

$$\text{Resonance frequency: } \omega_r = \omega_n \sqrt{1 - 2\zeta^2} \tag{3.8}$$

where ζ is the damping ratio of the system.

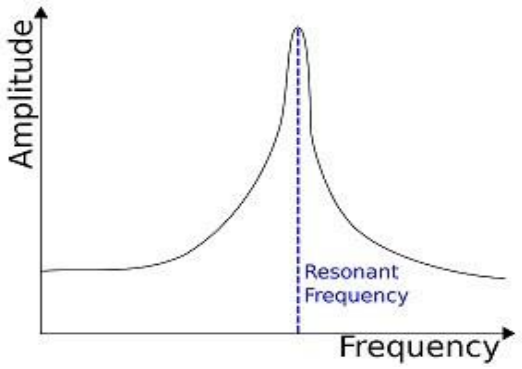

Figure 3.9 Resonance frequency (Vibration Institute, 2018)

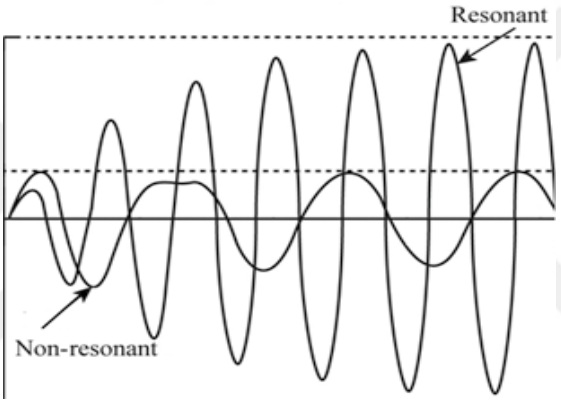

Figure 3.10 Resonant and non-resonant frequency values (Rao,2000)

3.4 Harmonic Motion, Displacement, Velocity and Acceleration

When the objects connected to the ends of the springs in Figure 3.11 are pulled out of the equilibrium position in the frictionless system, they move periodically between two equal points. With the effect of recalling forces to the equilibrium position, the movement of objects periodically commuting between two fixed points is called simple harmonic motion. This motion is called harmonic and periodic. Equation of a harmonic motion is given in Equation 3.9.

$$x = X_0 \sin \omega t \tag{3.9}$$

where;

x= displacement at any given instant t [m];

X_0= maximum displacement [m];

$\omega = 2\pi f$

t=time (seconds)

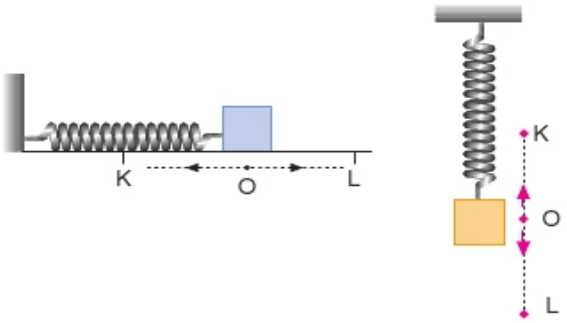

Figure 3.11 Harmonic motion (Vibration Institute, 2018)

There is a derivative-dependent relationship between acceleration, velocity and displacement. Velocity is equal to the derivative of displacement equation over time. Similarly, acceleration is obtained by taking the derivative of the velocity equation over time. Velocity is calculated as given in Equation 3.10 and acceleration is calculated as given in Equation 3.11.

$$Velocity = \frac{dX}{dt} = X_0 \omega \cos \omega t \tag{3.10}$$

$$Acceleration = \frac{dV}{dt} = -X_0 \omega^2 \sin \omega t \tag{3.11}$$

3.5 Classification of Vibration

3.5.1 Free Vibration

In vibrating systems, the initial effect applied as the position or speed of the system is called initial conditions. If a system oscillates with this input, this movement is called asfree vibration. During free vibration, the potential and kinetic energy of the system is in change, but in conservative systems the sum of the potential and kinetic energy of the system is constant and does not change over time. Figure 3.12 shows the movement of a simple pendulum and spring-mass system.

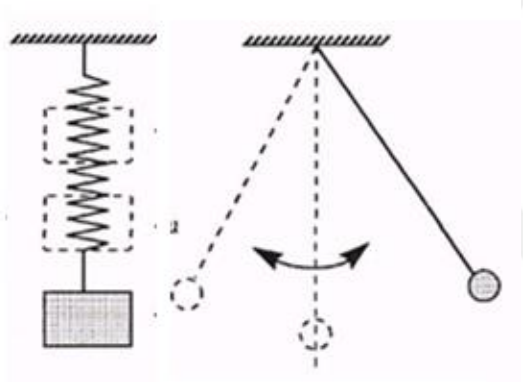

Figure 3.12 A simple pendulum and spring-mass system (Rao, 2000)

3.5.2 Forced Vibration

If a system oscillates with the effect of an external harmonic force, this is called forced vibration. When the forcing frequency and the natural frequency of the system are close enough to be the same, the system enters the resonance. If resonance occurs in a mechanical system, it may be harmful enough to cause a final deterioration of the system. One of the most important reasons for vibration analysis is to predict when resonance will occur and to decide what to do to prevent it from happening. Forcing effect on a mass-spring-damper system is shown in Figure 3.13.

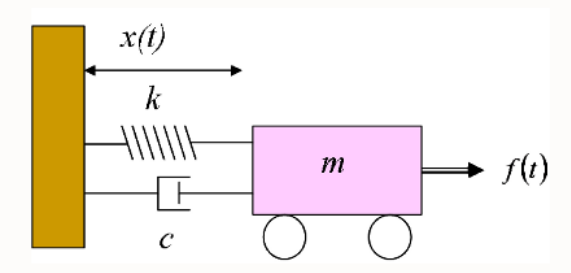

Figure 3.13 Forced vibration (mass, spring and damper system) (Vibration Institute, 2018)

3.5.3 Undamped Vibration

If there is no loss in the system due to friction or other resistances, the system moves undamped. If there is no damping in a free-vibrating system that moves with the initial conditions, the system continues its motion with the first input forever. The mass-spring system is shown in Figure 3.14.

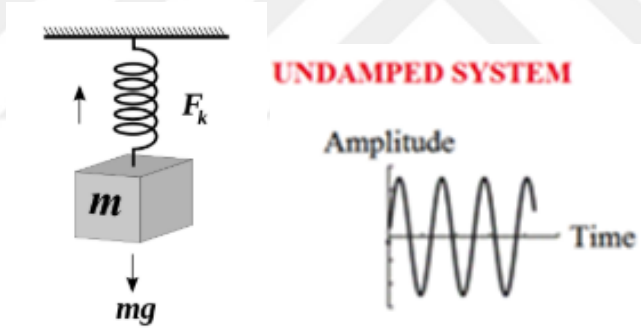

Figure 3.14 Undamped Vibration (mass-spring system) (Rao,2004)

3.5.4 Damped Vibration

The elements that cause loss of energy or movement in the system and move in the direction of slowing or stopping the system are called damping element, and the movement made by such systems is called damped vibration. In fact, there is a slight loss in all systems for different reasons. Figure 3.15 shows a spring-mass-damper system.

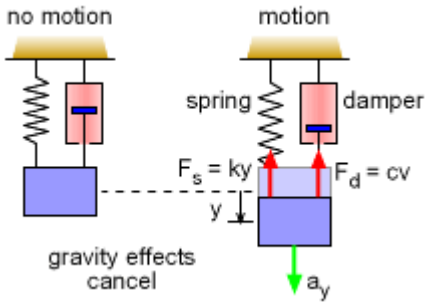

Figure 3.15 Damped vibration (mass, spring and damper system) (Vibration Institute, 2018)

3.5.5 Linear and Nonlinear Vibration

In a system that makes vibration movement, if all the components of the system make a linear movement, the resulting vibration is called linear vibration. If any element exhibits a non-linear behavior, it is called a non-linear vibration. Many vibration systems are found in nonlinear form, especially due to large amplitudes (Rao, 2010).

3.5.6 Deterministic and Random Vibration

In a vibrating system, it is called deterministic vibrations, if possible, to know the magnitude of the forcing effect at any given time. Vibrations caused by rotation unbalance in shafts can be given as examples.

If the magnitude of the coercive effect in the system cannot be estimated over time, it is called random vibration. In such vibrations, the motion of the system and the effect of coercive force are analyzed statistically. Vibrations caused by wind effects, road profiles and earthquakes can be given as examples.

3.6 Quantifying the Vibration Level

It is possible to find four different values from the time domain vibration resonse of a system. These are: peak to peak, zero to peak, root mean square (RMS) and average. They are shown in Figure 3.16.

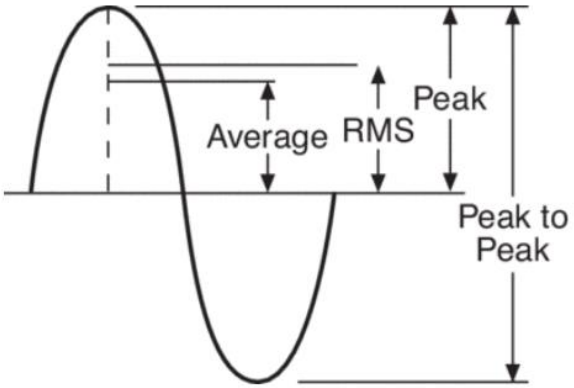

Figure 3.16 Vibration amplitudes for sinusoidal wave (MKS,2019)

3.6.1 Peak to Peak

This value is defined as the difference between positive and negative points where the absolute amplitude is highest. In some applications in the industry, a limit peak to peak value is determined to define the vibration level and condition monitoring is carried outaccordingly.

3.6.2 Zero to Peak

The distance between the equilibrium point and the maximum point of the signal. It can also be expressed as half of the peak to peak value.

3.6.3 Root Mean Square (RMS)

The RMS (Mean Average Square) value of a signal is called the normalized second statistical moment of the signal, or the valued average vibration square

measured at a given time period. Vibration amplitude is the most commonly used measure in condition monitoring. RMS is often preferred to define the "constant state" or "continuous" amplitude of a time-varying signal. In a simple harmonic motion, it is 0.7071 times the peak value of zero. The RMS value is used in ISO 10816 standard. For a harmonic signal RMS value is calculated thanks to Equation 3.12 and Equation 3.13.

$$\tau = \frac{2\pi}{\omega} \tag{3.12}$$

$$RMS = \sqrt{\frac{1}{\tau}\int_0^{\tau} x^2 dt} = \frac{Peak}{\sqrt{2}} \tag{3.13}$$

3.6.4 Average

It is a method in which vibration amplitudes are measured at certain time intervals and arithmetically averaged. It is not as widely used as other methods.

3.7 Vibration Analysis Techniques

Nowadays, vibration analysis is the most reliable and practical method for monitoring the status of machines. With vibration analysis, vibration signals from certain points in the machine body are analyzed in time and frequency environment. By comparing with the reference value which is healthy, the error status is determined according to the degree of deviation. The desired result is to be detected at the initial stage of the error and to prevent faults. The permissible vibration levels for the machines are determined in the ISO 10816 standard given in Figure 3.17.

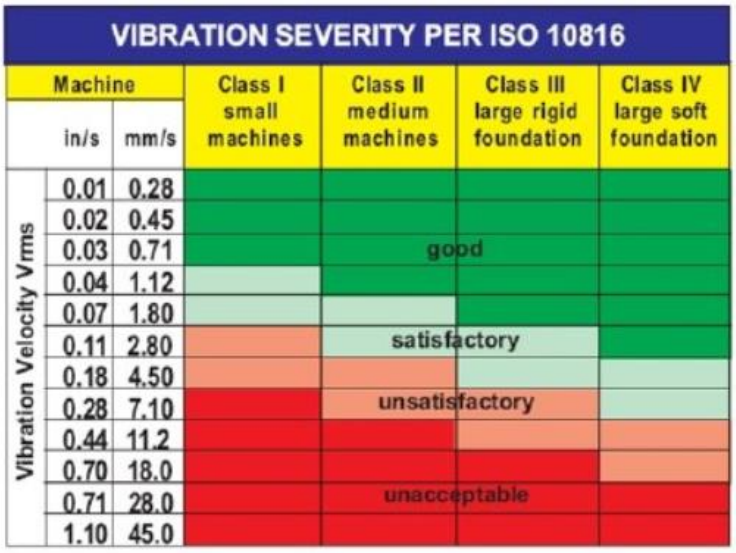

Figure 3.17 Guide to vibration severity as per ISO 10816

3.7.1 Time Domain Analysis

Time domain analysis covers to examine the experimental or numerical vibration signals using different statistical features. By comparing the vibration signals obtained from a defective bearing and the vibration signals obtained from a healthy bearing, the distortions in waveforms and changes in amplitudes over time are monitored. The statistical indicators obtained from the amplitude-time graph to be obtained for the condition monitoring of the machines can be explained with the following headings.

3.7.1.1 Mean

The mean value is called the arithmetic mean of the vibration signal and generally does not provide reliable information about a widely distributed signal. The average value x of a discrete time signal with N samples is calculated using Equation 3.14 (Neter, Wasserman and Whitmore, 1988).

$$\text{Mean} = \overline{x} = \frac{1}{N}\sum_{i=1}^{N} x_i^2 \tag{3.14}$$

3.7.1.2 Standart Deviation (σ)

It is equal to the square root of the variance and if the vibration signals are close to the average, the standard deviation value is low, otherwise, it is high. (Heperkan, Kesgin, 2002). Standart deviation is calculated using Equation (3.15).

$$\text{Standard Deviation} = \sigma = \sqrt{\frac{1}{N}\sum_{i=1}^{N}\left(x_i - \bar{x}\right)^2} \tag{3.15}$$

3.7.1.3 Skewness

It is expressed as the third standardized moment of the vibration signal and shows the asymmetry of a distribution around the mean. A distribution with an asymmetric tail extending to positive values indicates positive skew. Given the negative skew, an asymmetric tailed distribution extending towards more negative values is observed. If the skew value is zero, a symmetric distribution is observed (Miettinen and Leinonen, 1999). Skewness is calculated using Equation 3.16.

$$\text{Skewness} = \frac{\sum_{i=1}^{N}\left(x_i - \bar{x}\right)^3}{N\sigma^3} \tag{3.16}$$

3.7.1.4 Kurtosis

Kurtosis shows the irregularity or flatness of the distribution compared to the normal distribution. Positive kurtosis shows the relatively highest distribution. Negative kurtosis is relatively flat (Neter et al., 1988). It is a frequently used method for detecting non-periodic shocks (Metravib Technologies, n.d.). Kurtosis is a valid measure of the deterioration of a machine but does not provide any indication for diagnosing the problem (Azima DLI, 2009). Kurtosis is calculated using Equation 3.17.

$$\text{Kurtosis} = \frac{\sum_{i=1}^{N}\left(x_i - \bar{x}\right)^4}{N\sigma^4} \tag{3.17}$$

3.7.1.5 Crest factor (cf)

The crest factor is defined as the ratio of the peak value to the RMS of the signal (Friedman, n.d.). Crest factor value is expected to be between 2 and 6 in healty situtation. Crest factor is calculated using Equation 3.18.

$$\text{cf} = \frac{x_{\max} - x_{\min}}{rms(x)} \tag{3.18}$$

3.7.2 Frequency-Domain Analysis

Frequency spectrum refers to a frequency-vibration amplitude graph and is the characteristic of the machines. As soon as damage to the machine under investigation begins to occur, the vibration level and frequency spectrum of the machine will change.

Methods in the frequency domain include Hilbert Transform Method (HTM), Fast Fourier Transform (FFT) and Power Cepstrum Analysis (PCA). Theoretically, the time domain signals can be transformed into a frequency domain using Fourier Transforms, and vice versa.

Since the changes caused by the fault can be detected more easily compared to the changes in the general vibration levels, this method can be used for bearings, gears, ... etc. and is often preferred in case of condition monitoring. (Rao, 2010).

CHAPTER FOUR
BEARING DEFECTS

4.1 Introduction

Rolling element bearings are the most popular used bearings in rotating machines. The smooth running of bearings is one of the most important factors affecting the performance and life of the machine. Since all forces are transmitted through the bearings in the machines. Rolling element bearings are very important research area for increasing accuracy and reliability of the machine. Inadequate lubrication, heavy loading, ineffective sealing, careless handling, dirt, dust are reasons for bearing damages. These factors cause different defects on the bearing. Types of the bearing defects and reasons are explained in detail below.

The reasons of the defects in rolling element bearings are shown in Figure 4.1. The most important problems are unsuitable lubricant, aged lubricant and solid contamination. About 0.35% of rolling bearings do not reach expected life (Antriebstechnik, 1979).

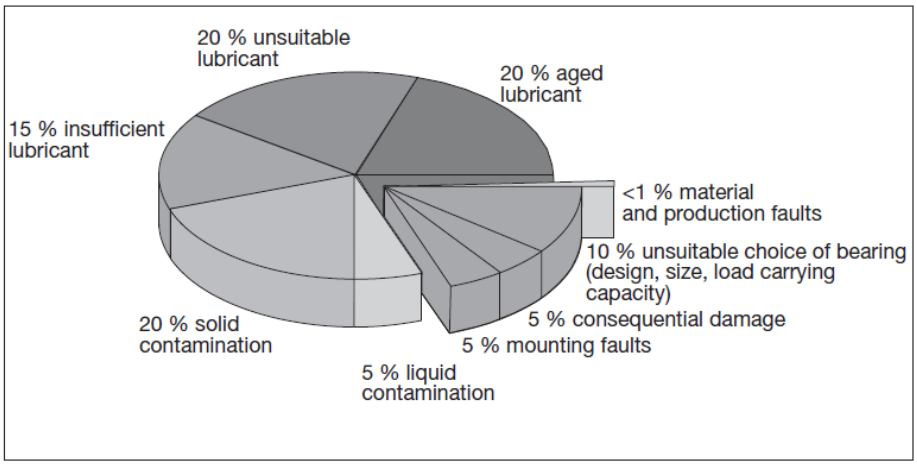

Figure 4.1 The reasons of the defects in rolling bearings (Antriebstechnik, 1979)

4.2 Types of the Bearing Defects and Reasons

4.2.1 Normal Fatigue Failure (flaking, pitting)

Flaking in the surface of the bearing elements is shown in Figure 4.2. Excessive load due to improper handling, overloading, housing or poor shaft accuracy, installation error, rusting, ingress of dirt or dust may cause piting and flaking (NTN, 2017). To prevent this damages, a bearing with a heavier nominal load, and a more viscose grease lubricant may be used.

Figure 4.2 Inner ring, outer ring and balls are flaked (NTN, 2017)

4.2.2 Cracks and Chips

Chips are thetype of failure occurring at a certain part of a bearing ring rib or corner of a roller (Koyo, 2015). Cracks and chips defects are shown in Figure 4.3. Some situations such as extreme tightness, overload, impact load, flaking progress, heat generation, and friction caused by contact between mounting parts and collar, creep-induced heat generation, weak taper angle of taper shaft, poor cylindricality of shaft may be cause cracks. Correct insertion tolerance, checking load conditions, improving assembly method are importants methods to prevent this problem.

Figure 4.3 Cracks and chips defects (Action Bearing, n.d)

4.2.3 Cage Damages

Cage damage consists of one or more case such as cage deformation, fracture and abrasion, breaking the cage column, deformation on the side surface, abrasion of the pocket surface, abrasion of the guide surface. Examples of cage damage are shown in Figure 4.4. Poor installation (misalignment), abuse, large torque load, impact and big vibration, extreme rotation speed, sudden acceleration and deceleration, insufficient lubrication, temperature rise are reasons for cage damages (NTN, 2017). Precautions can be taken by checking installation method, checking temperature, rotation and load conditions, choosing a different cage type, selecting a different lubrication method and/or a different lubricant.

Figure 4.4 Examples of cage damages (Koyo, 2015)

4.2.4 Brinelling

The definition of brinelling is the permanent indentation of a hard surface. Example of brinelling are shown in Figure 4.5. Brinelling may be caused by vibration and shaking of a stationary bearing during transport, small amplitude oscillating motion, insufficient lubrication. Securing shaft and bearing during transport, packing the inner and outer rings separately and transporting, reducing boot vibration, using the right oil are precaution methods for brinelling.

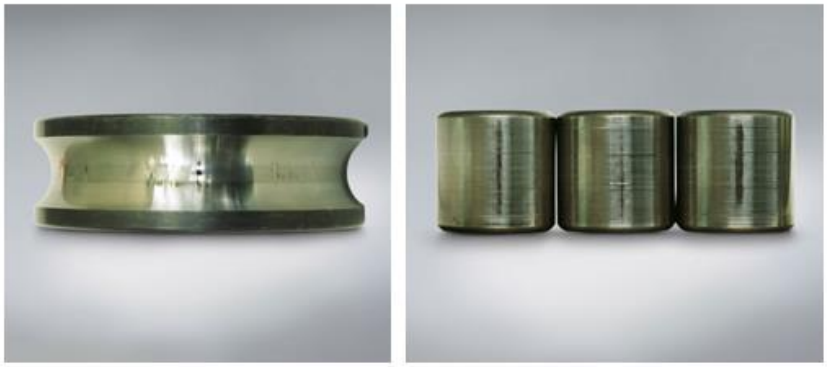

Figure 4.5 Examples of brinelling (Action Bearing, n.d)

4.2.5 Creeping

Creep is the displacement during operation of a bearing ring, relative to the shaft or housing. Examples of creep damage are shown in Figure 4.6. Insufficient tightness or loose fit, insufficient sleeve tightening may cause creeping. Precautions can be taken by checking tightness and prevent rotation, correcting sleeve tightening, inspecting shaft and bearing precision, appling adhesive to the mounting surface, appling an oil film to the mounting surface.

Figure 4.6 Creeping of inner rings (Barden, n.d.)

4.2.6 Wear and Fretting

Main reasons for the wear are sliding abrasion on parts including the roller end face and rib, cage, cage pocket surface, and the guide surface of the bearing ring. Wear and corrosion occur to the rolling and sliding surfaces because of contamination by foreign matter. If wear is low level, the bearings may be used after the bearing and housing thoroughly cleaned. Precautions can be taken byimprovement of lubricant and lubrication type, filtering of oil, improvement of sealing. Slight sliding is repeatedly caused on the contact surface causes fretting. Therefore, a rust like powder occurs on the fitting surface (Koyo, 2015). Wear and fretting damages are shown in Figure 4.7.

Figure 4.7 Wear and fretting failures (Koyo, 2015)

4.2.7 Scratch

Scratch is the surface damage caused by the accumulation of small scratches caused by scraping, incorrect lubrication or slipping under heavy operating conditions. Possible causesof scratch are overload, overboot, insufficient lubrication, particles captured on the surface, slope of inner and outer rings, shaft bending reduced precision in shaft and bearing housing.

Figure 4.8a shows an inner ring of a spherical roller bearing. Scratching occurs on large shoulder face of inner ring. Reason of the damage is reel slip due to sudden acceleration and deceleration. Figure 4.8b shows cage of a single-row ball bearing. Scrape occurs in press-steel cage pockets of the bearing. Reason of the damage is rash leaking.

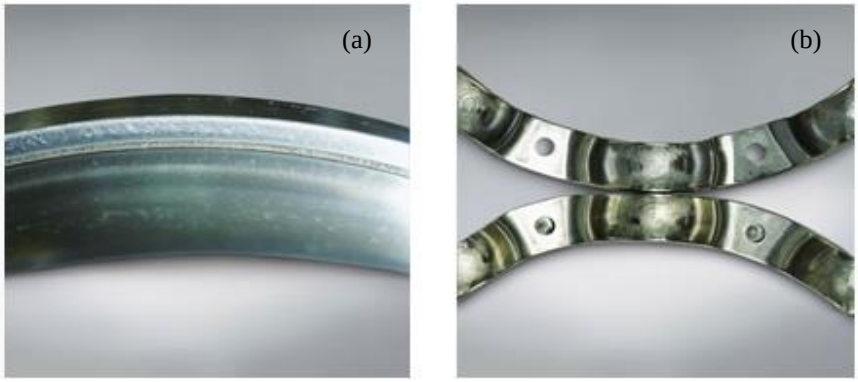

Figure 4.8 a) Inner ring of a spherical roller bearing b) Cage of a single-row ball bearing (NTN, 2017)

4.2.8 Smearing

Smearing is surface damage caused by heating between the bearing elements as a result of fracture and/or slipping of the oil film. In addition to melting, surface roughness is also observed. High speed and light load, sudden acceleration/deceleration, wrong oil, water inlet may cause smearing. Damage example are shown in Figure 4.9.

Figure 4.9 Examples of smearing damage (NTN, 2017)

4.2.9 Score Marks

Out-of-square insertion into rolling element set causes score marks on the raceway of the inner ring.

Figure 4.10 Score marks (FAG, 1985)

4.2.10 Peeling

Peeling may be caused by unsuitable lubricant, oil spil mix, rough surface due to insufficient lubrication, surface roughness of matching rotating parts. Figure 4.11a shows rounded peeling defect at the center of the raceway surface of a inner ring of a spherical roller bearing. Reason of the damage is insufficient lubrication. Figure 4.11b shows peeling defect around the shoulder of the raceway outer ring of a spherical roller bearing. Similar to other example, reason of the damage is insufficient lubrication. Choosing an appropriate oil, improving sealing system,

improving sealing, avoiding rust when inoperative, removing surface roughness of matching rotating parts are considered to prevent defect.

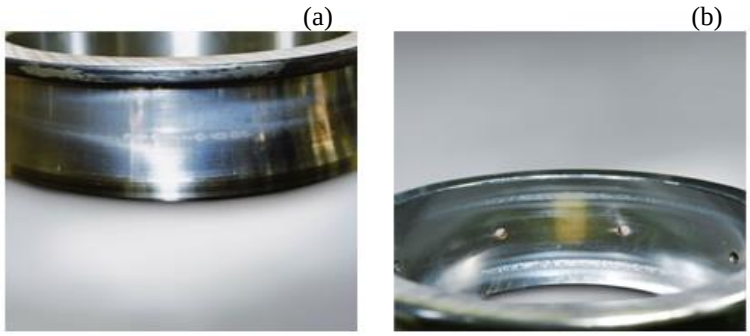

Figure 4.11 a) Inner ring of a spherical roller bearing b) Outer ring of a spherical roller bearing (Koyo, 2015)

4.2.11. Fracture

Fracture refers to small particles that have been broken by an overload or impact load that locally act on a pulley corner or sleeve. Impact during assembly, overload, poor handling may cause fracture damage. Figure 4.12a shows cone fracture on back shoulder of inner ring of a tapered roller bearing. Figure 4.12b shows outer ring fracture on shoulder of outer ring of a solid needle roller bearing. Reason of the damage is reel bending due to overload. Precautions can be taken by improving installation method (tight fit, use of correct tools etc.), reviewing installation conditions, providing sufficient support for the bearing shoulder.

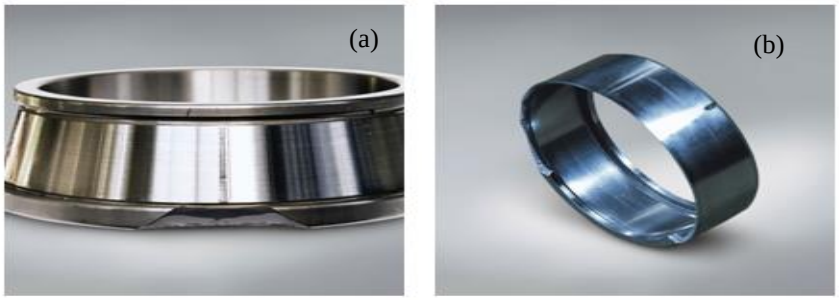

Figure 4.12 a) Inner ring of a tapered roller bearing b) Outer ring of a solid needle roller bearing (Barden, n.d.)

CHAPTER FIVE
SIMULATION OF VIBRATION SIGNALS IN ROLLING ELEMENT BEARING STRUCTURES

5.1 Structure and Bearing Forces

In this study, the radial load distribution in the bearing housing was considered to create a proper dynamic loading model considering the bearing kinematics and the angular positions of the nodes in the finite element model. For this purpose, a finite element model with the given dimensions shown in Figure 5.1 was created parametrically using the developed ANSYS APDL code. By using the developed code, parametric modeling of the bearing housing can be made for desired housing dimensions easily.

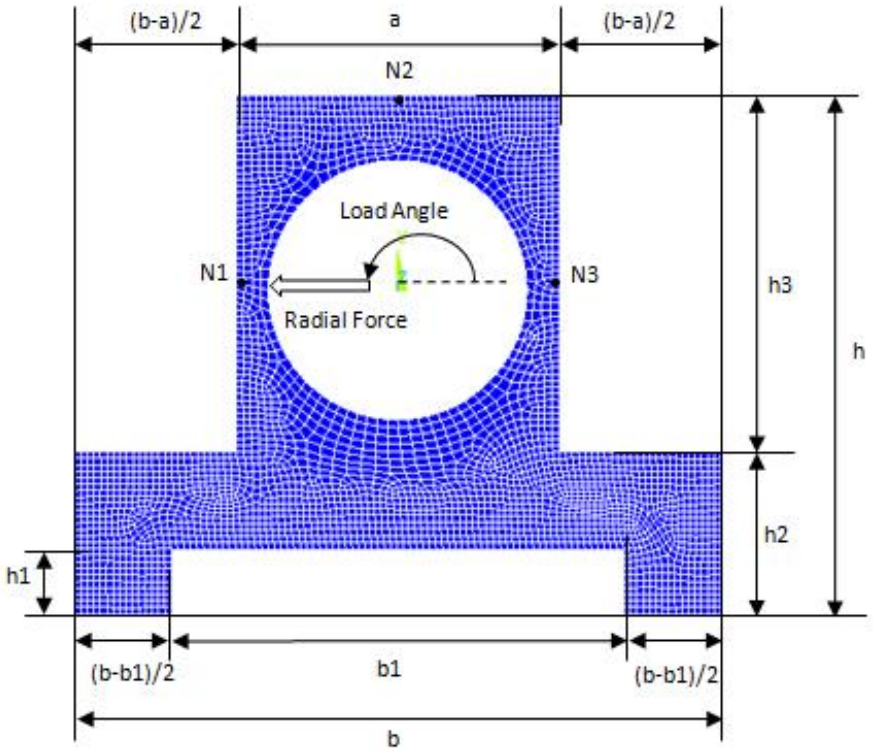

Figure 5.1 Bearing housing dimensions and sensor locations in the finite element model

The finite element model is modeled by using 10 node triangular elements with three degrees of freedom in each node. The present finite element model consists of 52786 nodes and 32586 elements. Here, only the bearing body was modeled and the dynamic loading was made from the inner circular geometry presenting the outer ring. The basic dimensions of 6208 type rolling element bearing used to create the dynamic loading model are shown in Figure 5.2.

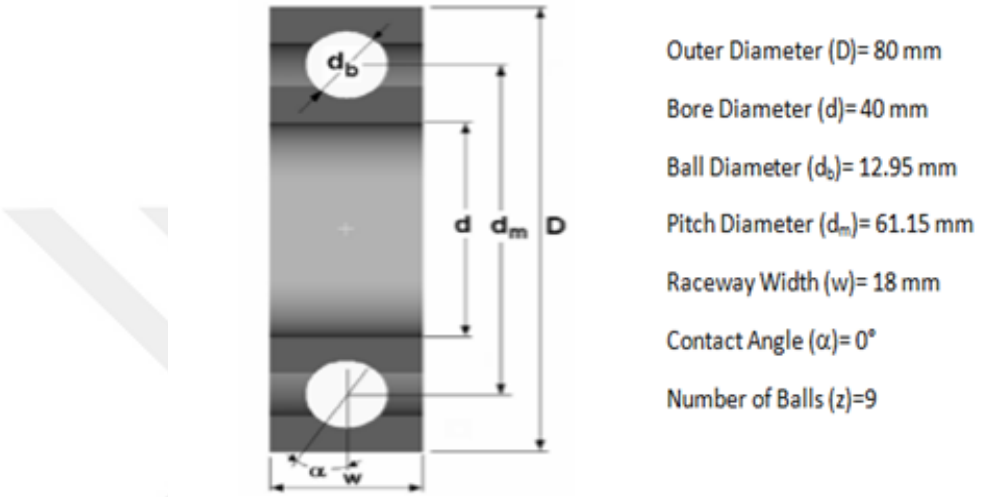

Figure 5.2 Dimensions of considered rolling element bearing

The material properties of the bearing housing are given in Table 5.1.

Table 5.1 Material properties of bearing structure

	Young Modulus	**Poisson Ratio**	**Mass Density**
Housing	206 GPa	0.29	7860 kg/m^3

The outer ring, inner ring, rolling elements and cage form the rolling element bearing and they have different rotational frequencies depending on bearing kinematics, bearing geometry and shaft rotation frequency. The outer ring and inner ring frequencies are equal to the shaft rotation frequency (f_s), depending on whether the inner ring or the outer ring is fixed. The cage (f_c) that holds the balls together at an equal distance and the balls have their own rotational frequencies (f_r). The cage

and ball frequencies can be calculated as follows for a rolling bearing with the outer ring fixed and inner ring rotating with shaft (Tandon & Choudhury, 1999).

$$f_c = \frac{f_s}{2}\left(1 - \frac{d_1}{d_m}\cos\alpha\right) \tag{5.1}$$

$$f_r = \frac{d_m f_s}{2d_b}\left(1 - \frac{d_b^2}{d_m^2}\cos^2\alpha\right) \tag{5.2}$$

In Equation 5.1 and 5.2, f_s is the shaft rotation frequency in Hertz and α is the contact angle. In this study, the contactangle is assumed to be "0" considering that the bearing carries pure radial load.

In single row ball bearings, the outer ring contact with the balls takes place from the inner surface of the ring and along a line. Bearing faults usually occur in this area which is loaded dynamically during operation. In the work performed, the bearing load is taken as aradialforce acting from the shaft. The radial load has a constant direction and the bearing outer ring is partially loaded. The radial force on the shaft is transmitted to the inner ring-balls-outer ring and finally to the bearing housing. Due to the geometry of the bearing, the radial load is transferred to the bearing structure by means of a group of balls passing through the loading zoneshown in Figure 5.3. The radial load distribution in the bearing is defined by the Stribeck Equation 5.3 (McFadden and Smith, 1984).

$$q(\Phi) = q_0\left(1 - \frac{1}{2\varepsilon}(1-\cos\Phi)\right)^n \tag{5.3}$$

Where q_0 represents the largest load amplitude, ε represents the load distribution factor and φ represents the angular coordinate relative to the load distribution axis. The load distribution in the bearing is shown in Figure 5.3.

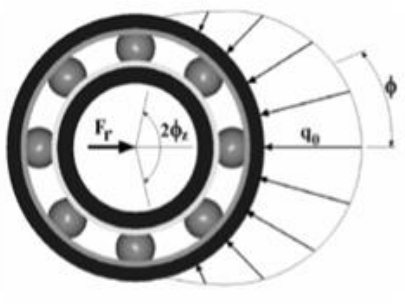

Figure 5.3 Load distribution in a rolling element bearing (Kıral and Karagülle, 2005)

The exponent "n" depends on the type of bearings. For ball bearings, the "n" exponent is taken as 10/9. As shown in Figure 5.4, only a certain part of the bearing is loaded at a certain time, the other part does not bear the load. The load amount of each ball in the load zone can be calculated from Equation 5.4. The composition of the loads carried by the balls with respect to the bearing axis is equal to the radial load (F_r) and their torque is equal to zero. The load distribution on the outer ring can generally be expressed as (Holm-Hansen and Gao, 1999).

$$q(\Phi)=\begin{Bmatrix} q_0\left[1-\frac{1}{2\varepsilon}(1-\cos\Phi)\right]^n \\ 0 \end{Bmatrix} \begin{matrix} for \\ elsewhere \end{matrix} -\Phi_z<\Phi<\Phi_z \tag{5.4}$$

Where $q_0$on the load distribution symmetry axis indicates the maximum load. The maximum load, number of balls (Z), radial load value and contact angle can be calculated using Equation 5.5.

$$q_0=\frac{5f_r}{Z\cos\alpha} \tag{5.5}$$

The angle of the load zone depends on the load distribution factor. For bearings with positive backlash (ball diameter smaller than the gap between the outer ring and inner ring), the load distribution factor ε is between 0 and 0.5 and φ_z is between 0° and 90°. In this study, $\varepsilon = 0.45$ is taken and the load region angle φ_z is calculated with Equation 5.6 (Holm-Hansen and Gao, 2000).

$$\Phi_z = \cos^{-1}(1-2\varepsilon) \tag{5.6}$$

In this study, the finite element model has been created for the housing structure and the outer ring has been represented with a circular line. Total of 80 nodes have been used to create the dynamic loading model.

5.2 Creating Nodal Excitation Functions

Standard finite element softwares are not generally designed to describe complex dynamic loads. Therefore, an additional study is necessary to identify the external loads affecting the structure. In this thesis, a computer program written in Visual BASIC programming language was developed to create the load distribution by considering both bearing kinematics and load distribution (Norton, 1998). Thus, the forces transmitted to the bearing outer ring during the operation, and therefore to the bearing body, are defined as time-dependent loading functions for each node. The distributed radial load travels respectively from the shaft to the inner ring, the balls, the outer ring and finally to the bearing body. The balls transfer the load to the nodes on the rolling path on the inner surface of the bearing outer ring. These time dependent forces cause the bearing body vibrations. The definitions based on the dynamic loading model are shown in Figure 5.4.

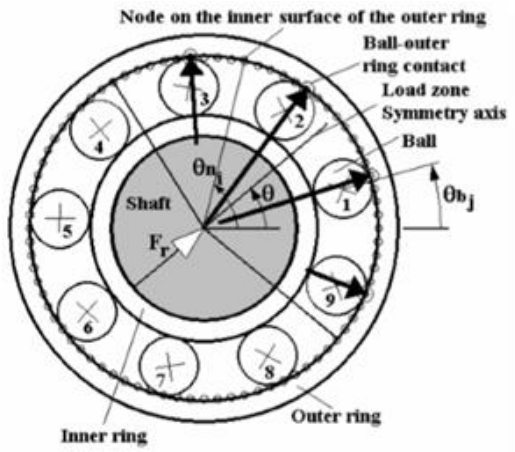

Figure 5.4 Elements of the bearing and an instantaneous of dynamic loading (Kıral, 2002)

There are 80 nodes at the angle intervals of $\Delta\theta$ = 4.5 ° on the outer ring rolling track for the rolling bearing geometry, which is assumed to be in point contact with the inner surface of the outer ring. For the definition of radial load, forcing functions are defined in *x* and *y* directions ateach node and the total number of forcing functions used is 160. In Figure 5.5, where the definitions based on the dynamic loading model are shown, the rotation of the shaft and the radial load θ is the angular positions θ_{ni} (i = 1 ... 80) of the nodes on the outer ring rolling surface, and the angular positions of the balls θ_{bj} (j = 1 ... Z). The balls rotate around the shaft rotation axis with cage frequency (f_c). Due to the geometry of the bearing, the cage frequency is lower than the shaft rotation frequency. The number of balls remaining in the load zone is determined by the load zone angle, load angle and angles of the balls. The total number of nodes remaining in the load zone is constant and is determined by the angle of the load zone. Furthermore, the remaining nodes in the load zone are constantly changing. When the load distribution angle is considered, the total number of nodes remaining in the load zone for the bearing geometry is found using Equation 5.7.

$$N_z = 2N - 1 \tag{5.7}$$

Here *N* is the number of nodes that satisfy the condition $|\theta_{ni}-\theta|<\varphi_z$. The nodes near the ball are exposed to radial load. If a node satisfies the requirement of Equation 5.8, the correction function is included in the group of nodes to be defined. Here $\Delta\theta$ is the angular distance between two adjacent nodes.

$$\left|\theta_{ni} - \theta_{bj}\right| \le 0.5\Delta\theta \text{ i=1to } N_z, \text{ j=1 to Z} \tag{5.8}$$

The load acting on a node whose node number is determined is calculated with the help of Equation 5.4 according to the position of the node in the load region. The $\theta=0°$ and $\theta=90°$ states of the constant direction loading of the bearing geometry are shown in Figure 5.5. As shown here, the nodes satisfying the condition given in Equation 5.5 carry a certain portion of the radial load. This condition is provided for all nodes at different instant of times, so that all nodes on the contact circle bear

theload at certain moments. However, the load amplitudes are constantly different due to the kinematics of the bearing and the radial load rotating.

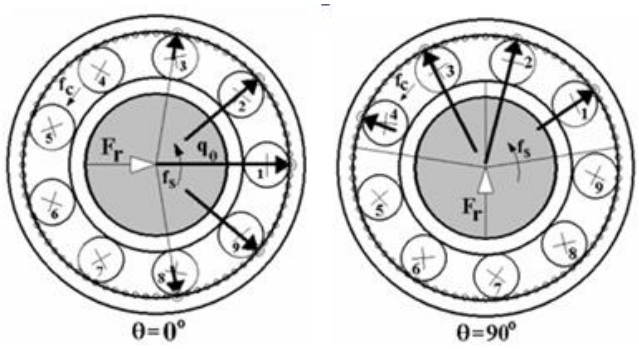

Figure 5.5 Dynamic loading of the bearing geometry θ= 0° and θ=90° states (Kıral, 2002)

Nodal forcing functions are obtained by a program developed in Visual BASIC programming language. The position of the balls, the labels of the nodes in the load zone, the time of effect and the amplitudes of the forces effecting on the nodes are determined by the program.

With the help of the developed computer program, forcing functions of all ball bearings with contact angle $\alpha=0°$ are created in ASCII file format which can be run in ANSYS APDL program for the desired number of shaft rotations. In order for this code to work, the radial positions, the labels of the nodes in the circular path, the bearing geometry (pitch diameter, ball diameter and number of balls and number), the magnitude of the radial load and the shaft frequency must be known. An example graph of an excitation function in node x direction and y direction at 90° radial loadingfor values of F_r = 50000 N and shaft frequency f_s= 16.66 Hz (1000 rpm) are shown in Figure 5.6. An example view of the ASCII file is given in Appendix 4.

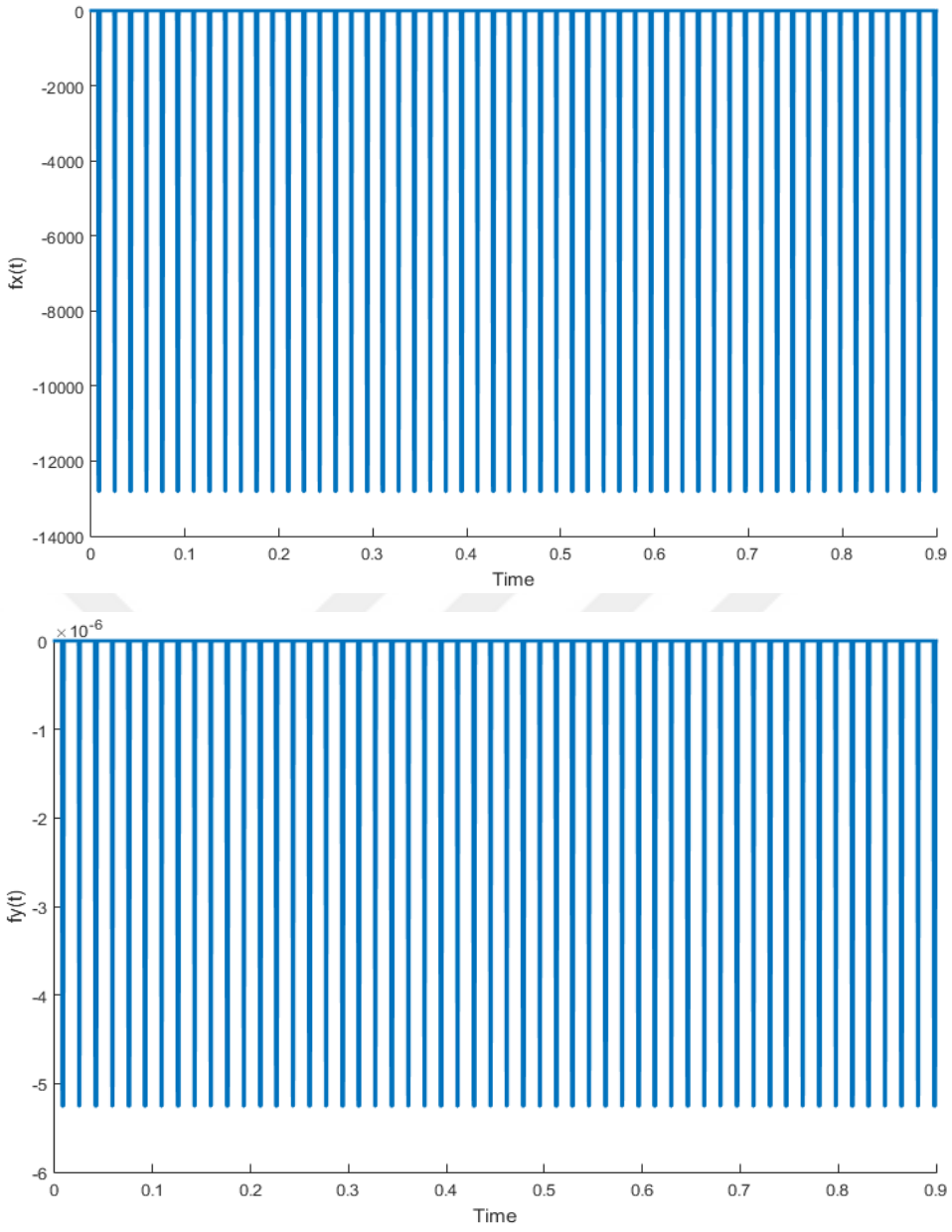

Figure 5.6 x component and y component of radial force acting on node f(x), f(y) function for 90° loading

To perform the vibration analysis in the ANSYS APDL program, it is necessary to edit the *.txt files to obtain the equally spaced time intervals. In these files, each force is applied to the corresponding node at different times with no equally-spaced time interval. The intermediate force values for different t values are obtained by interpolation, without disturbing the form of the forces. The aim here is; to introduce the same function with more points. Thus, when performing vibration analysis in

ANSYS APDL program, the value of time given for each node is determined. For this purpose, the code given in the Appendix 3 is created in the Visual BASIC program.

First, the rows and columns of the .prg extension files are read in the program. The smallest dt is found for each data, and the time parameter is rebuilt according to this value and all files in .txt format are obtained by using the code given in the Appendix 5.

5.3 Numerical Simulation

In the finite element method, which will be used for the modeling and vibration analysis of the system, the equations of motion can be formed as multi-degree of freedom systems in matrix form. The mode superposition technique is used for this equation system, which calculates the dynamic response of the structure. In this technique, it is necessary to pre-calculate the natural frequencies and the mode shapes of the structure to form the uncoupled equations. Then, an appropriate numerical method is selected and the dynamic response is calculated in modal coordinates.

The modal matrix of the system is used to convert modal results into real coordinates. ANSYS softwareuses the mode superposition technique in vibration analysis.

In this study, the dynamic response of the structure was calculated by consideringthe 10 natural frequencies and the corresponding mode shapes. The first 10 natural frequencies of the system are given in Table 5.2 and the five mode shapes in the *x-y* plane for bearing housing are shown in Figure 5.7. The time step is chosen as $T_{10}/20$ during the analysis in order to ensure that all the 10 modes contribute to the dynamic response. T_{10} is the period of the 10^{th} natural vibration mode.

Table 5.2 Natural frequencies of the bearing structure

Mode Number	Natural frequency (Hz)
1	685.356
2	1705.30
3	2172.28
4	2760.57
5	3513.63
6	4932.56
7	5609.59
8	5751.77
9	6004.58
10	7509.21

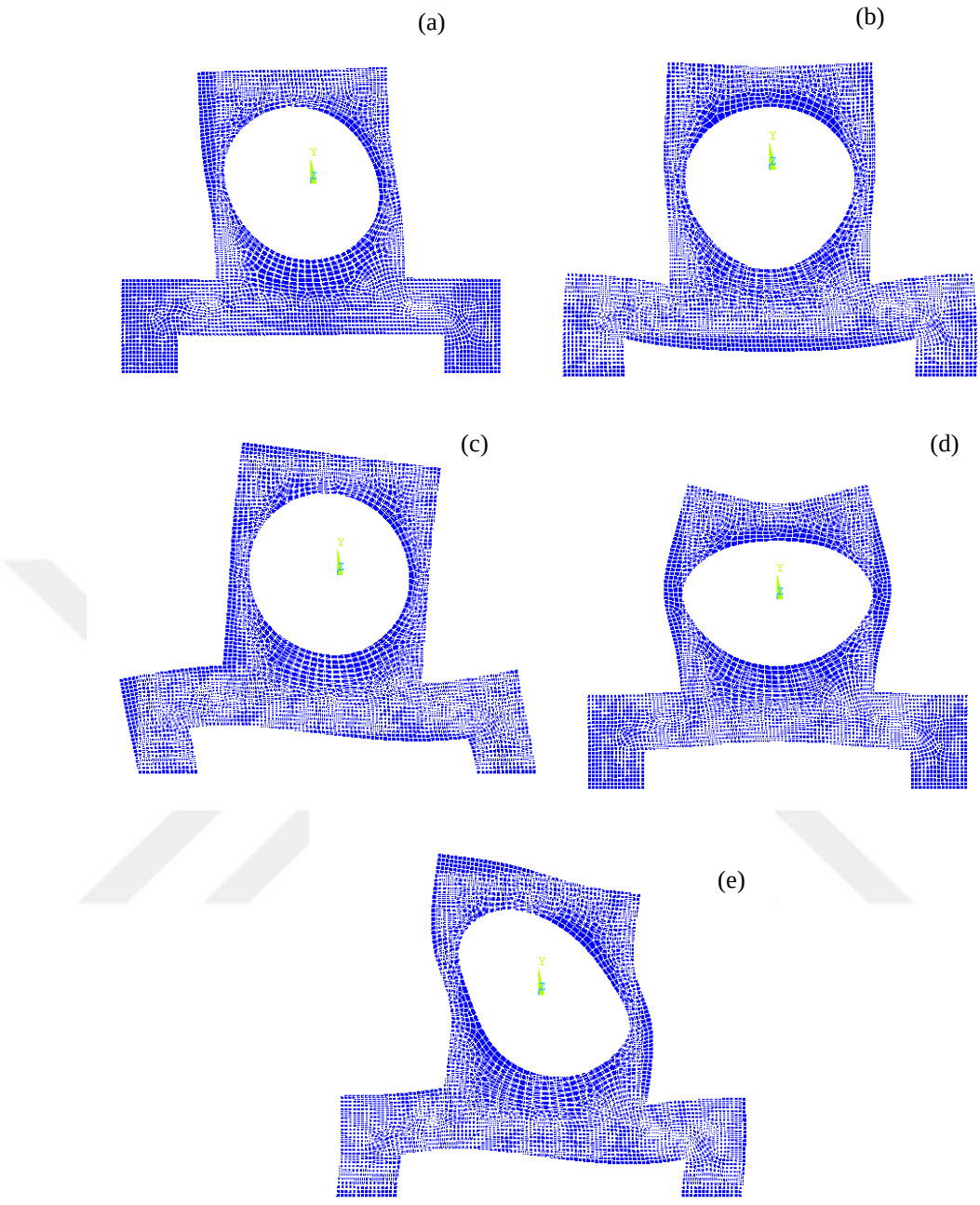

Figure 5.7 Sample mode shapes a) at 1705.30 Hz b) at 3513.63 Hz c) at 4932.56 Hz d) at 5609.59 Hz e) at 7509.21 Hz

CHAPTER SIX
VIBRATION ANALYSIS OF BEARINGS AND FAULT DETECTION USING STATISTICAL FEATURES

6.1 Introduction

In this section, loading models of rolling elements with healthy and faulty cases were created for different loading directions. Time and frequency domain analyzes were performed for condition monitoring and fault diagnosis of rolling element bearing structure. By applying radial loads at different loading directions, velocity and acceleration values were obtained as the vibration response. The statistical properties of vibration signals for healthy and faulty bearings were compared for different loading angles. For the fault modeling, the radial load is increased by 6 times at the ball-fault coincidence (Kıral, 2002). The local defect is located on the symmetry axis of the loading zone. Statistical parameters such as RMS, kurtosis, peak to peak and crest factor were calculated. By comparing these values, ideal sensor positions were alsodetermined. Local faultson the outer ring of the bearing and the effect of the load direction were examined.

6.2 Time Waveform Analysis

The time waveform consists of raw vibration amplitudes versus time. It contains all the vibration signals in the system because it is not subject to any filtration. There are some characteristic forms that are accepted according to the type of damage, but can be seen in cases where the damage is severe as there are raw vibration signals. The resulting graphics only allow the detection of defects in the bearing. It does not provide information about the location and magnitude of the error (Patidar and Soni, 2013).

In the graphs given in Figure 6.1-6.24, the waveform graphs obtained for the raw vibration signals are examined for healty andfaulty (outer ring) bearings at different loading directions (0, 90, 180 and 270 degrees). The graphs are discussed separately

in the *x-y* plane for each of the positions (node numbers in FE model) N_1=152, N_2=262 and N_3=372 defined in the bearing housing. In the graphs givenin Figure 6.1-6.24, it is observed that the bearingswith the outer ring fault show a more spikynature under the same load conditions. For all radial loading conditions, similar vibration characteristics were observed in faulty bearings. Based on this, it was understood that it would be correct to say that the time-dependent amplitude graphs show the existence of the fault.

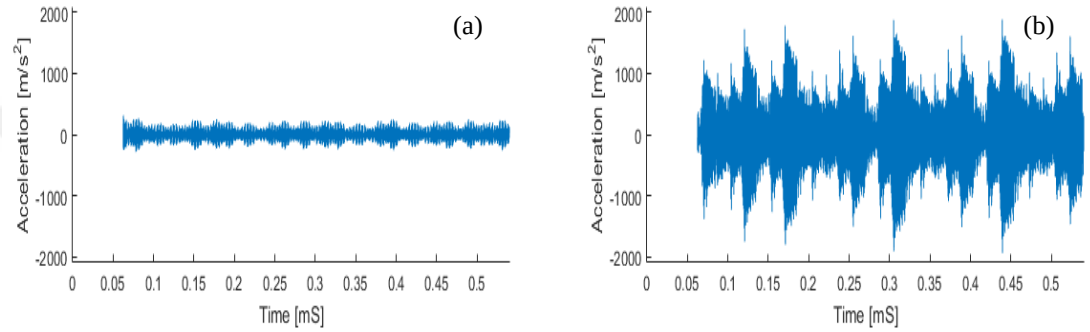

Figure 6.1 Time waveform of the bearing, 0° load direction on the x axis and node number 152 a) healthy bearing b) faulty bearing

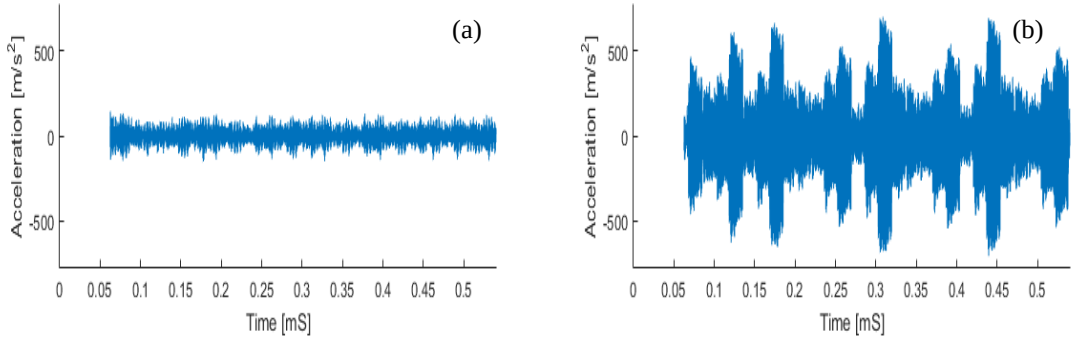

Figure 6.2 Time waveform of the bearing, 0° load direction on the y axis and node number 152 a) healthy bearing b) faulty bearing

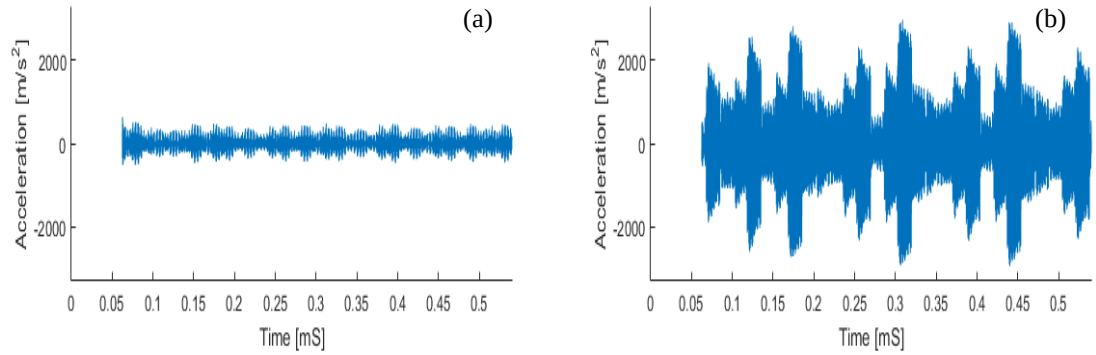

Figure 6.3 Time waveform of the bearing, 0° load direction on the x axis and node number 262 a) healthy bearing b) faulty bearing

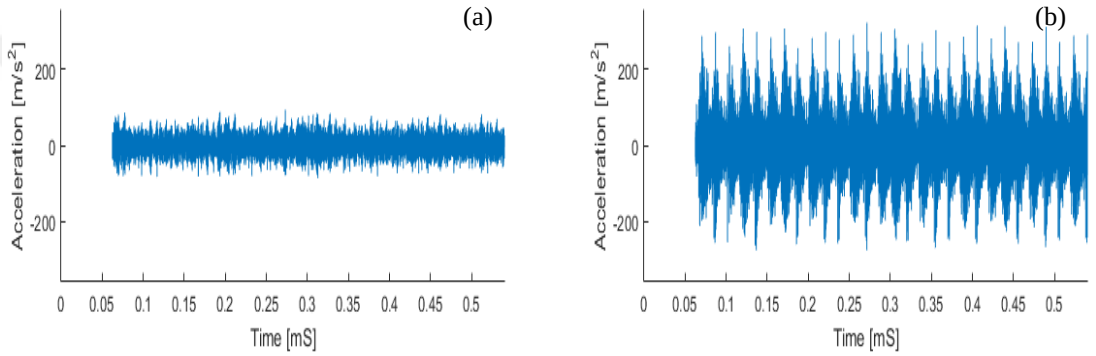

Figure 6.4 Time waveform of the bearing, 0° load direction on the y axis and node number 262 a) healthy bearing b) faulty bearing

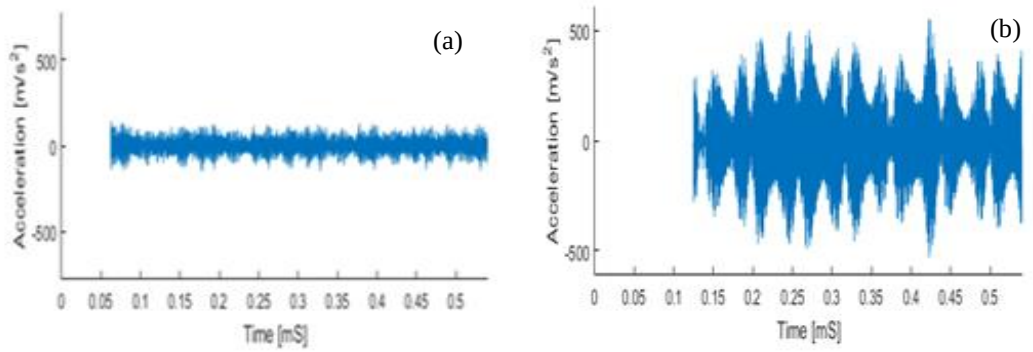

Figure 6.5 Time waveform of the bearing, 0° load direction on the x axis and node number 372 a) healthy bearing b) faulty bearing

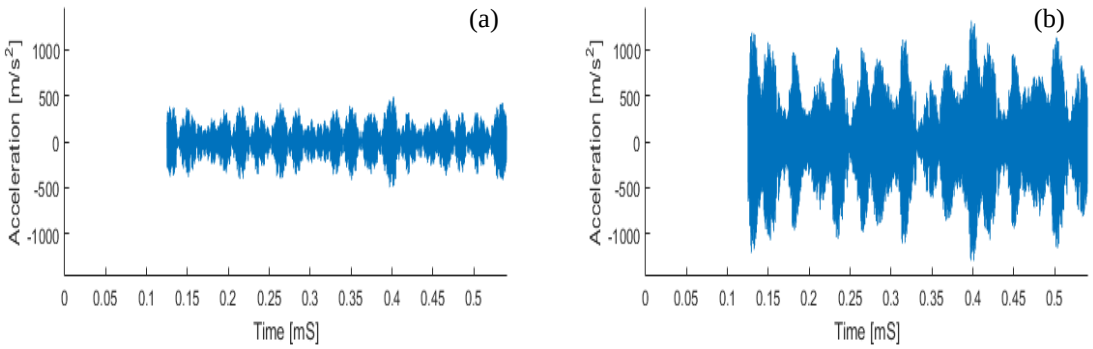

Figure 6.6 Time waveform of the bearing, 0° load direction on the y axis and node number 372 a) healthy bearing b) faulty bearing

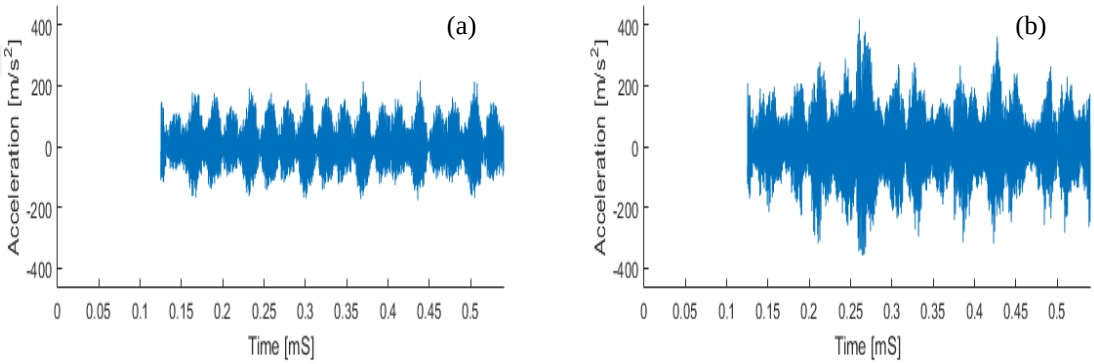

Figure 6.7 Time waveform of the bearing, 90° load direction on the x axis and node number 152 a) healthy bearing b) faulty bearing

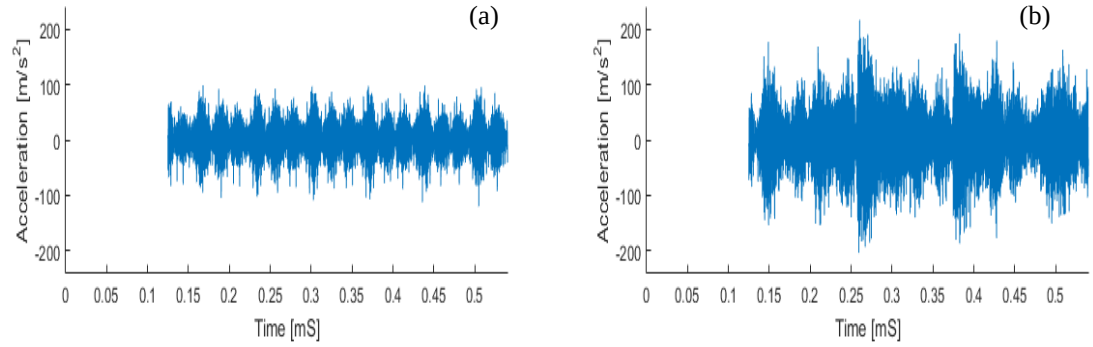

Figure 6.8 Time waveform of the bearing, 90° load direction on the y axis and node number 152 a) healthy bearing b) faulty bearing

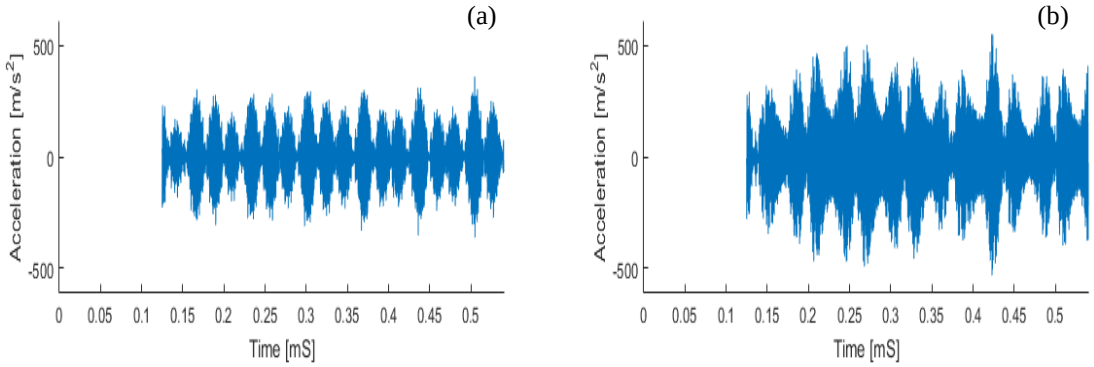

Figure 6.9 Time waveform of the bearing, 90° load direction on the x axis and node number 262 a) healthy bearing b) faulty bearing

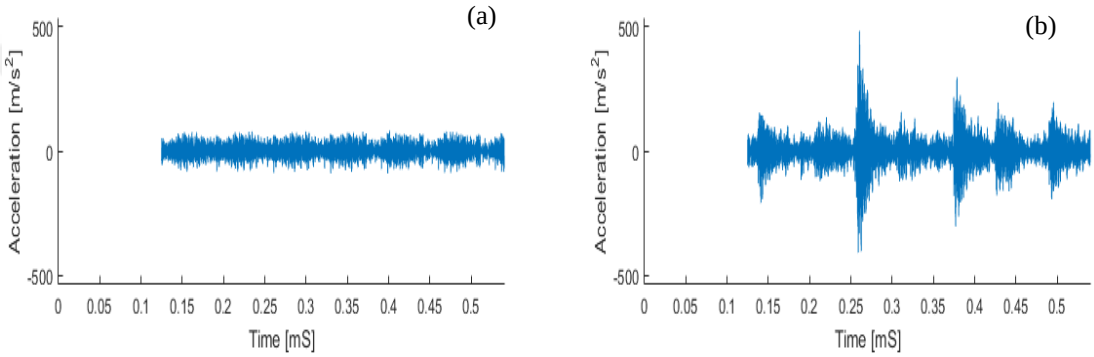

Figure 6.10 Time waveform of the bearing, 90° load direction on the y axis and node number 262 a) healthy bearing b) faulty bearing

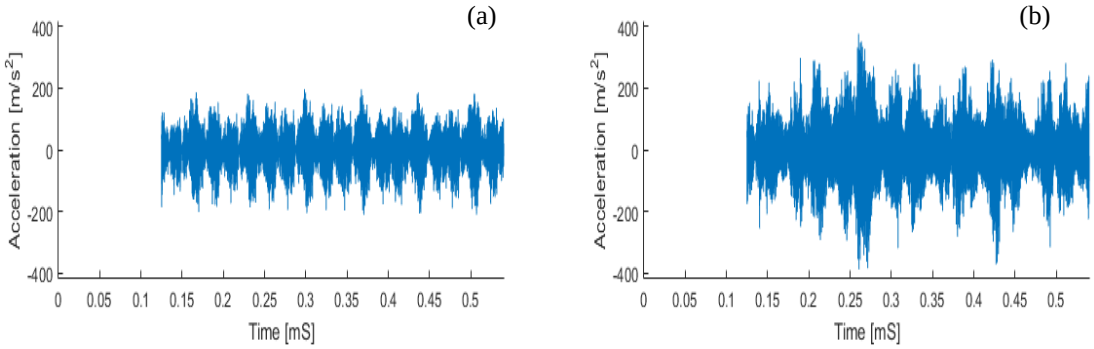

Figure 6.11 Time waveform of the bearing, 90° load direction on the x axis and node number 372 a) healthy bearing b) faulty bearing

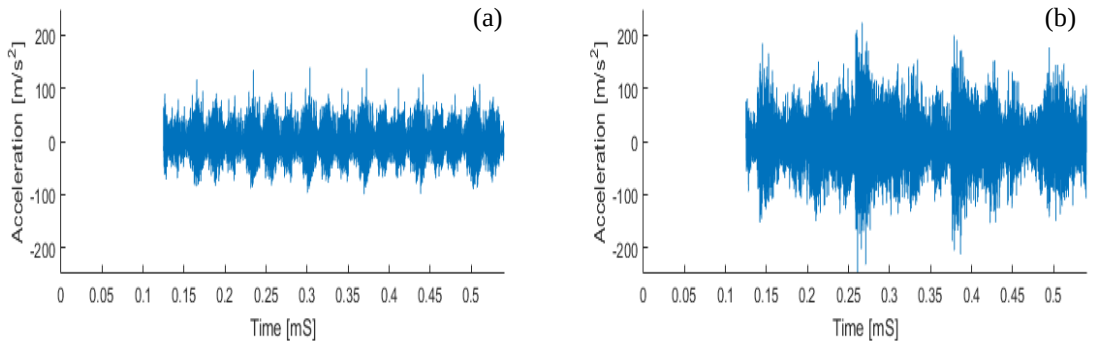

Figure 6.12 Time waveform of the bearing, 90° load direction on the y axis and node number 372 a) healthy bearing b) faulty bearing

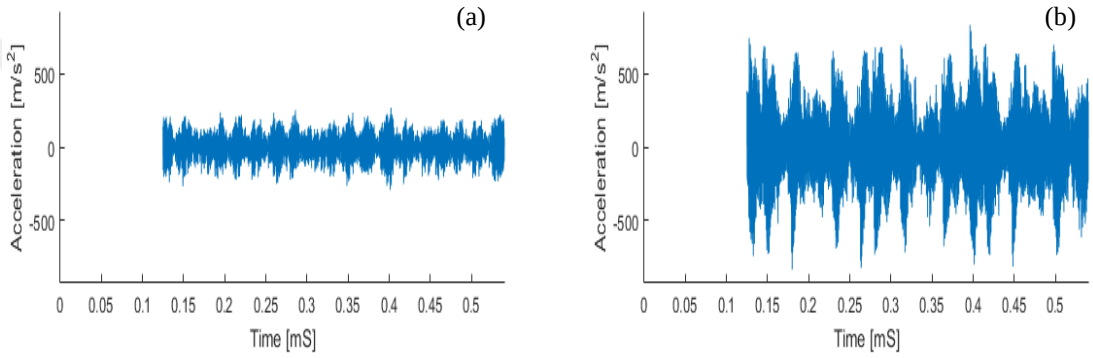

Figure 6.13 Time waveform of the bearing, 180° load direction on the x axis and node number 152 a) healthy bearing b) faulty bearing

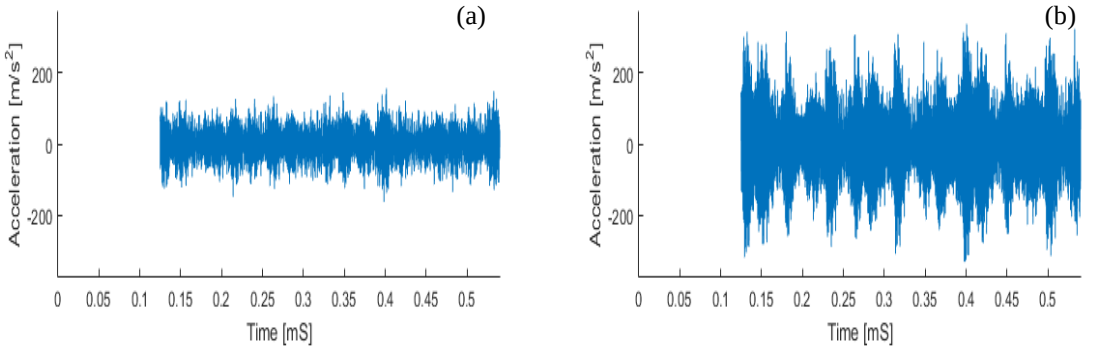

Figure 6.14 Time waveform of the bearing, 180° load direction on the y axis and node number 152 a) healthy bearing b) faulty bearing

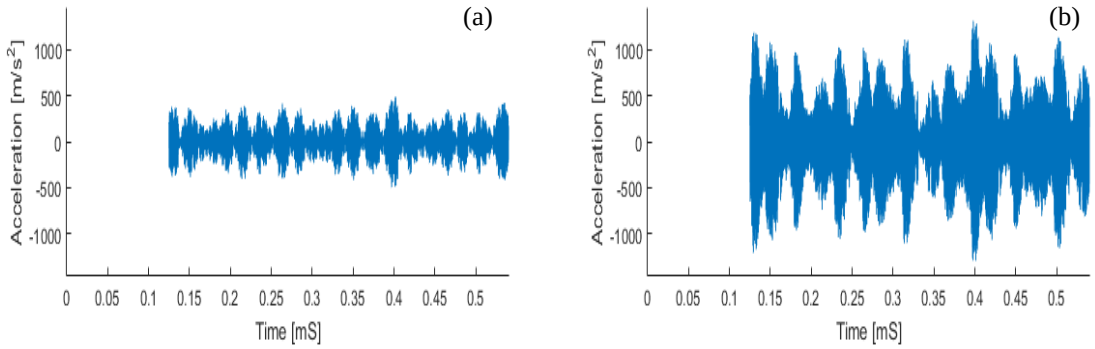

Figure 6.15 Time waveform of the bearing, 180° load direction on the x axis and node number 262 a) healthy bearing b) faulty bearing

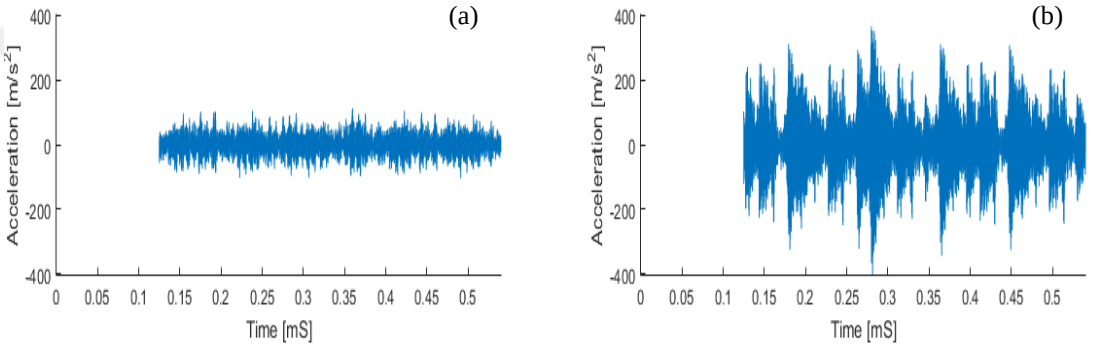

Figure 6.16 Time waveform of the bearing, 180° load direction on the y axis and node number 262 a) healthy bearing b) faulty bearing

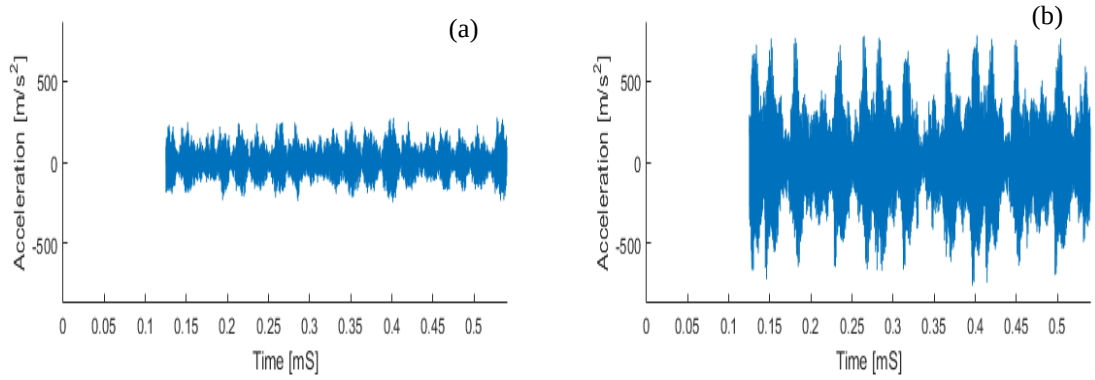

Figure 6.17 Time waveform of the bearing, 180° load direction on the x axis and node number 372 a) healthy bearing b) faulty bearing

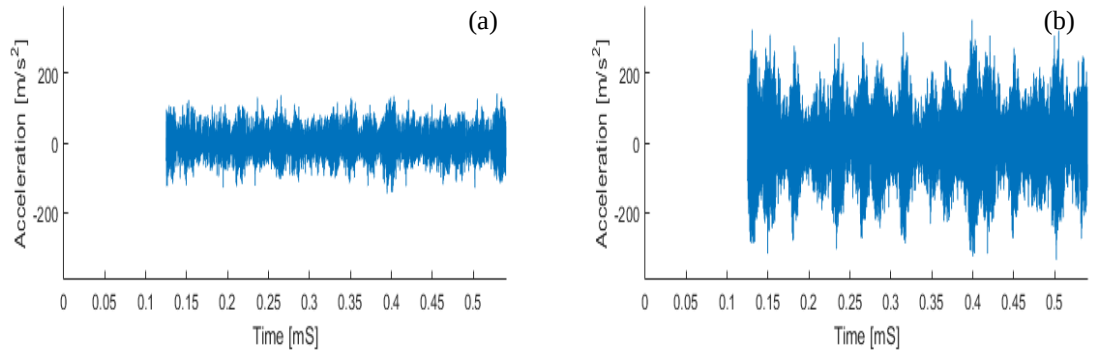

Figure 6.18 Time waveform of the bearing, 180° load direction on the y axis and node number 372 a) healthy bearing b) defect bearing

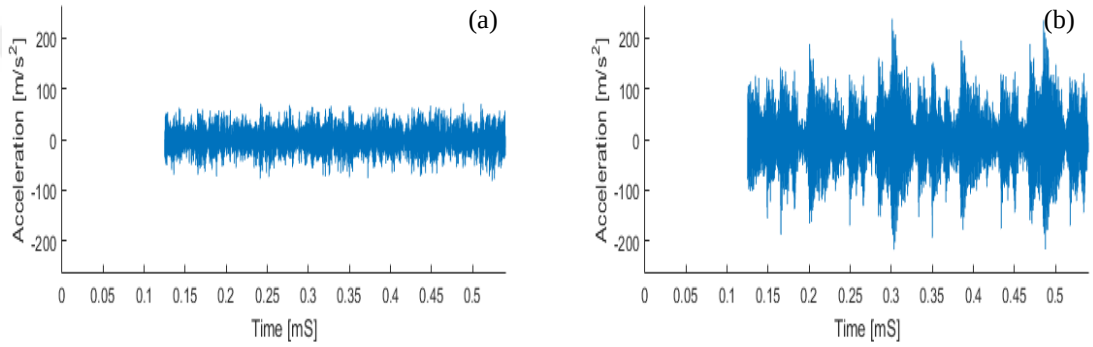

Figure 6.19 Time waveform of the bearing, 270° load direction on the x axis and node number 152 a) healthy bearing b) faulty bearing

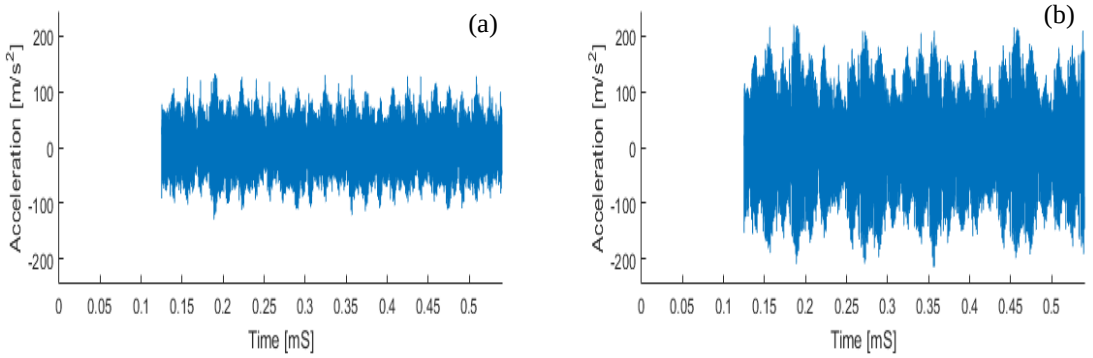

Figure 6.20 Time waveform of the bearing, 270° load direction on the y axis and node number 152 a) healthy bearing b) faulty bearing

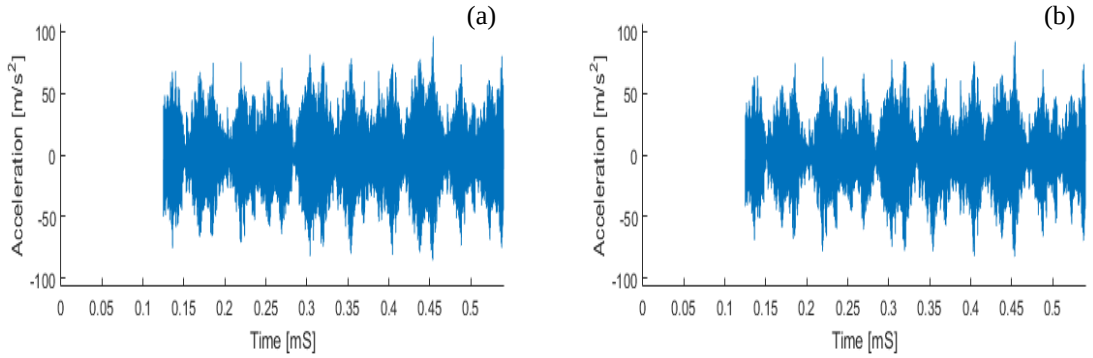

Figure 6.21 Time waveform of the bearing, 270° load direction on the x axis and node number 262 a) healthy bearing b) faulty bearing

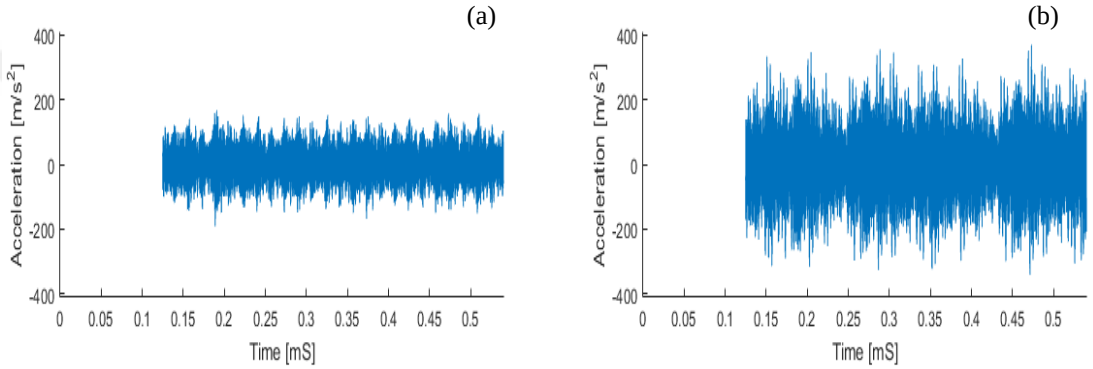

Figure 6.22 Time waveform of the bearing, 270° load direction on the y axis and node number 262 a) healthy bearing b) faulty bearing

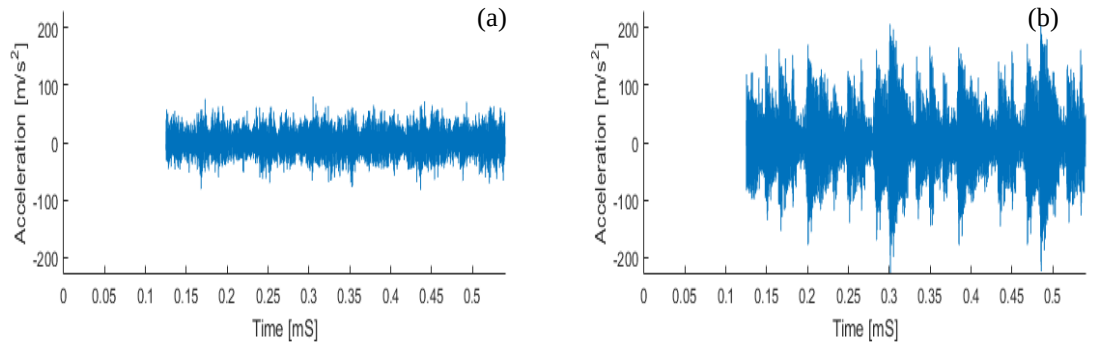

Figure 6.23 Time waveform of the bearing, 270° load direction on the x axis and node number 372 a) healthy bearing b) faulty bearing

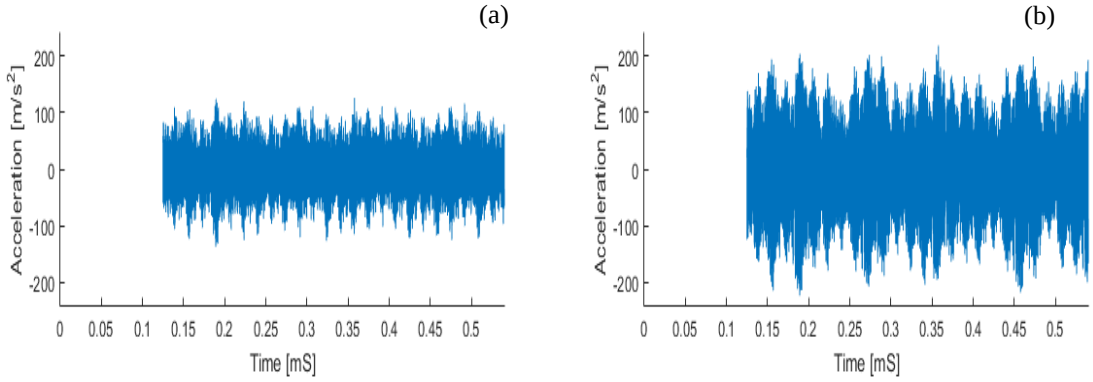

Figure 6.24 Time waveform of the bearing, 270° load direction on the y axis and node number 372 a) healthy bearing b) faulty bearing

For comparison, Figure 6.25 shows the experimental time-dependent acceleration signal presented by Li & Ma (1997). This graph of the experimental study is similar to the graphs given in Figure 6.1-6.24. It shows that faulty vibration signals have sharper characteristics than healthy signals and that the proposed method can be used to generate signals for vibration analysis and condition monitoring.

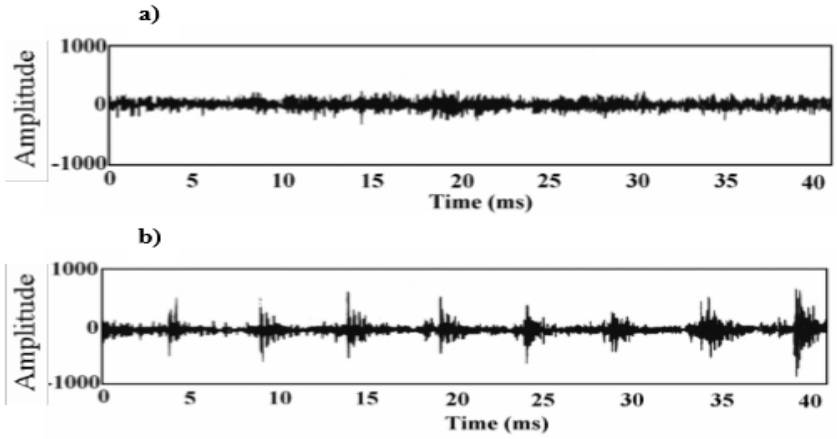

Figure 6.25 Experimental Acceleration signals for bearings of different conditions (Li & Ma, 1997) a) Normal bearing, b) Bearing with outer-ring defect

The time dependent acceleration values of the sensor points N_1, N_2 and N_3 for radial loading at 0, 90, 180 and 270 degrees at 1000 rpm are given in Figure 6.26-6.37respectively. The *x* and *y* components of the acceleration values for healty and faulty bearings are shown in a single graph.

In these graphs, the amplitude values of healthy bearings are centered, while the amplitude of faulty bearings have reached higher values and have a more irregular structure. The effect of positioning the sensor relative to the radial loading position was observed. In the 0, 90 and 180 degree radial loading zones, graphs plotted according to the readings of the N_3 sensor generally show positive correlation, while the N_1 sensor tends to show negative correlation. The N_2 sensor shows a distribution parallel to the x axis. In the 270 degree radial loading zones below the sensor positions, the signals generated for N_1, N_2 and N_3 all show a distribution parallel to the y axis. It has been found that the sensor positions relative to the angle of the acting radial load can be correlated with the signal reading capability of the sensor.

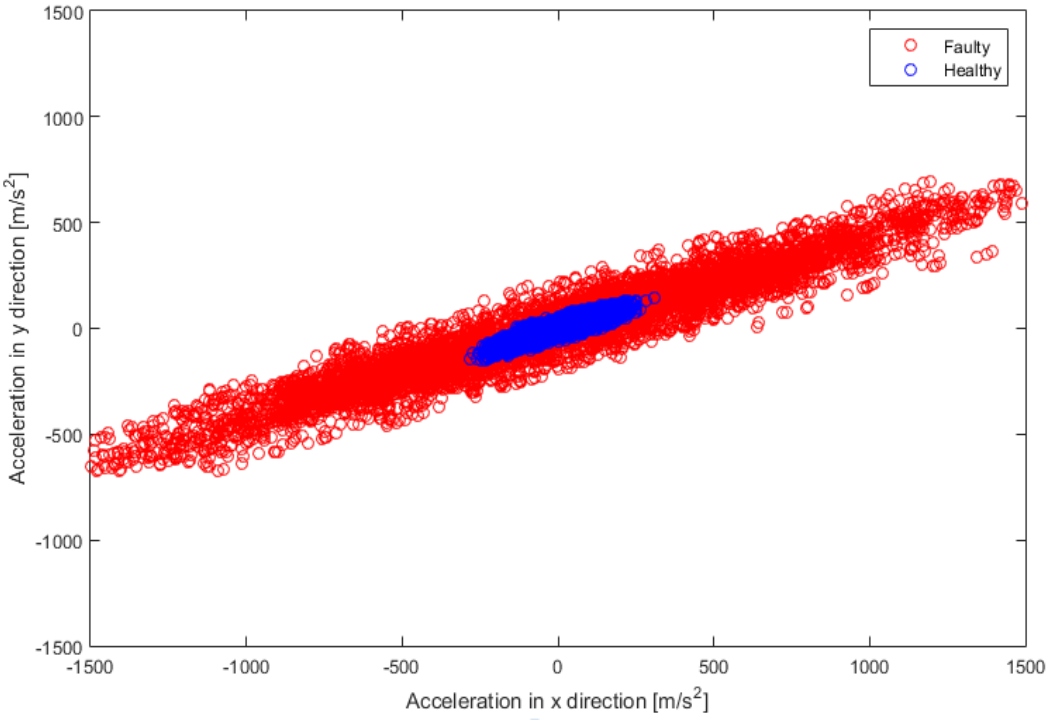

Figure 6.26 Acceleration scatter plot of the bearing, load direction 0°and node number 152

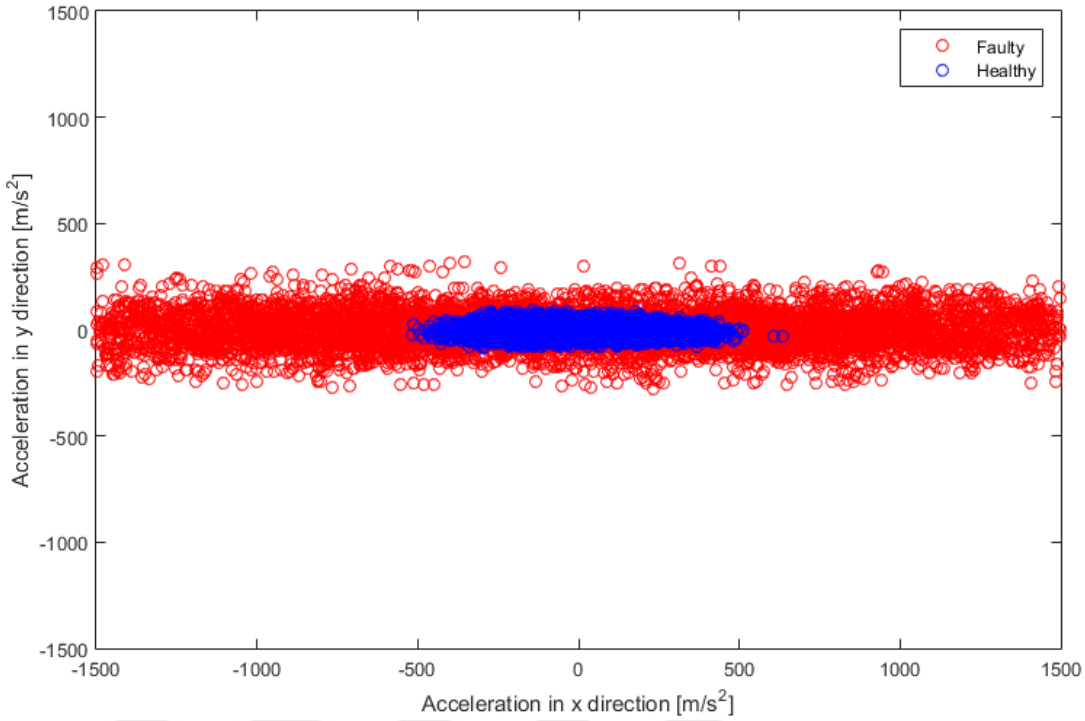

Figure 6.27 Acceleration scatter plot of the bearing, load direction 0° and node number 262

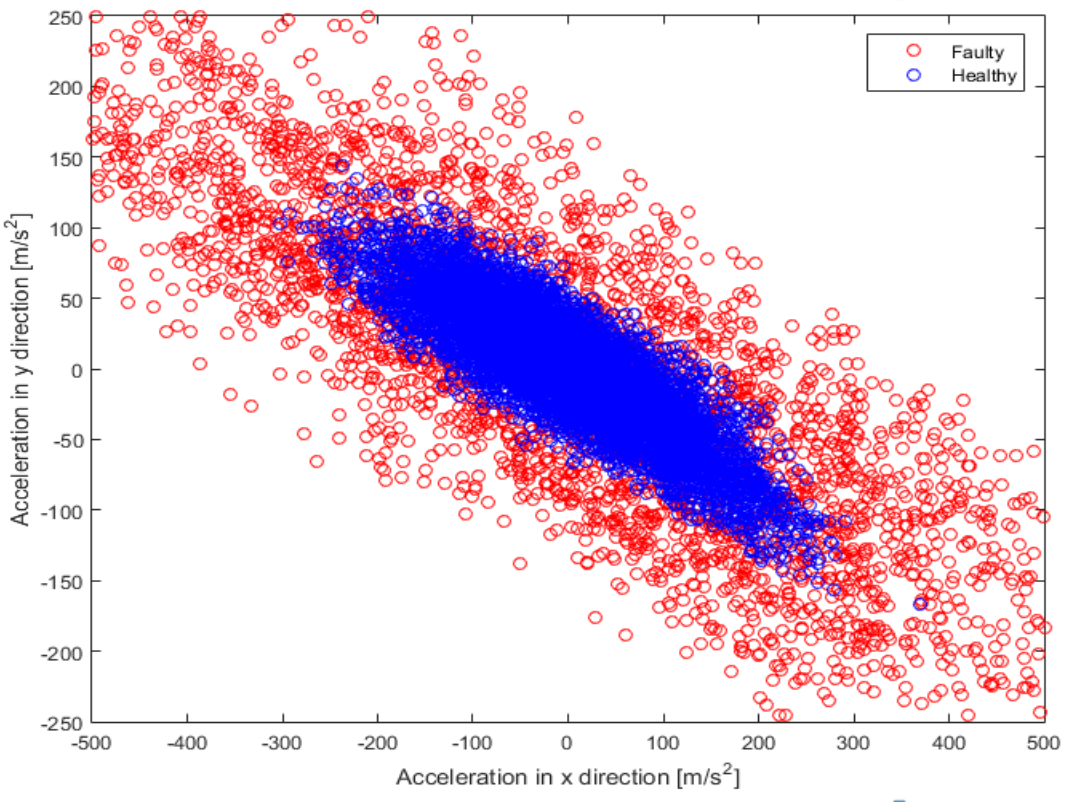

Figure 6.28 Acceleration scatter plot of the bearing, load direction 0° and node number 372

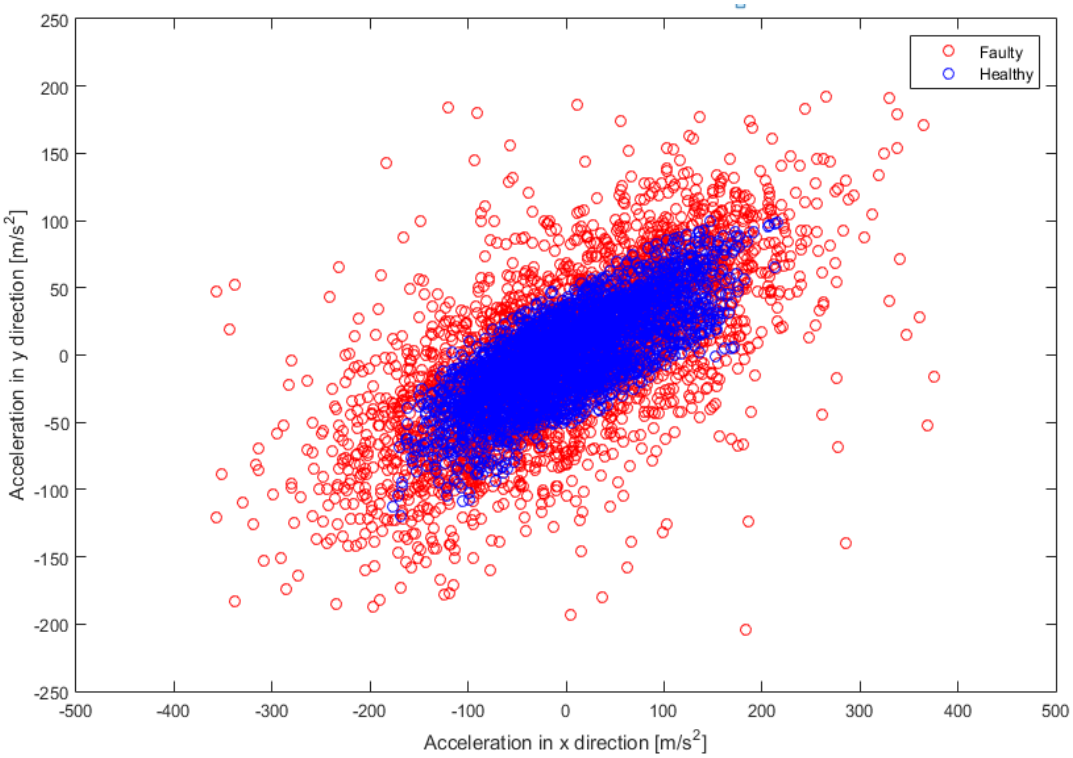

Figure 6.29 Acceleration scatter plot of the bearing, load direction 90° and node number 152

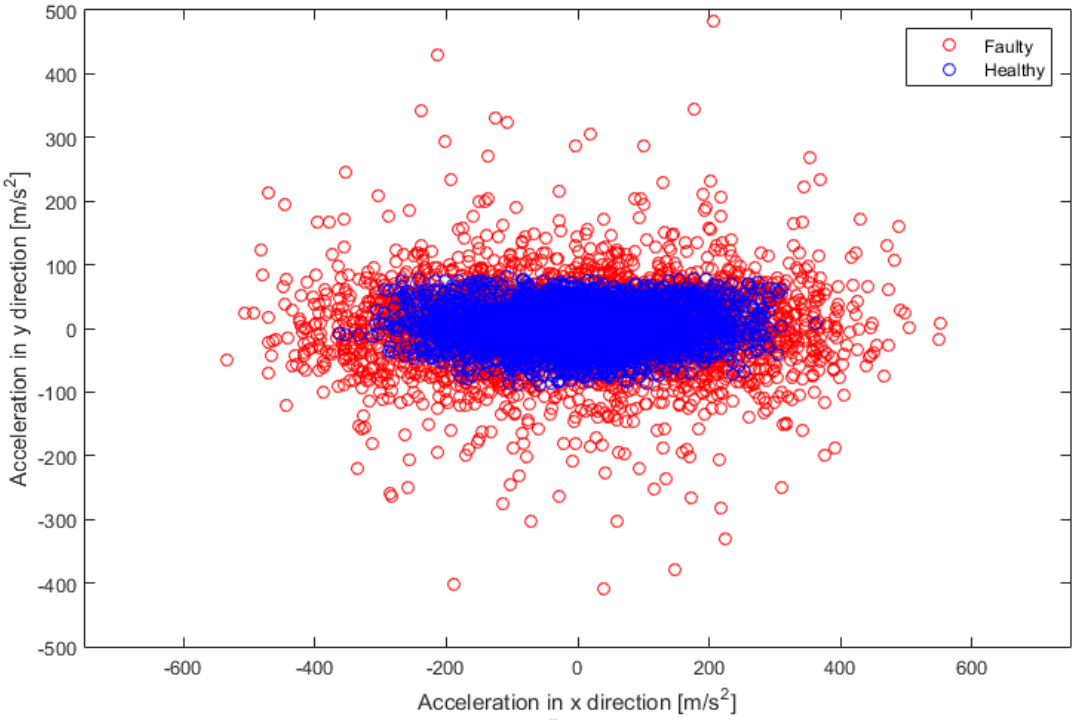

Figure 6.30 Acceleration scatter plot of the bearing, load direction 90° and node number 262

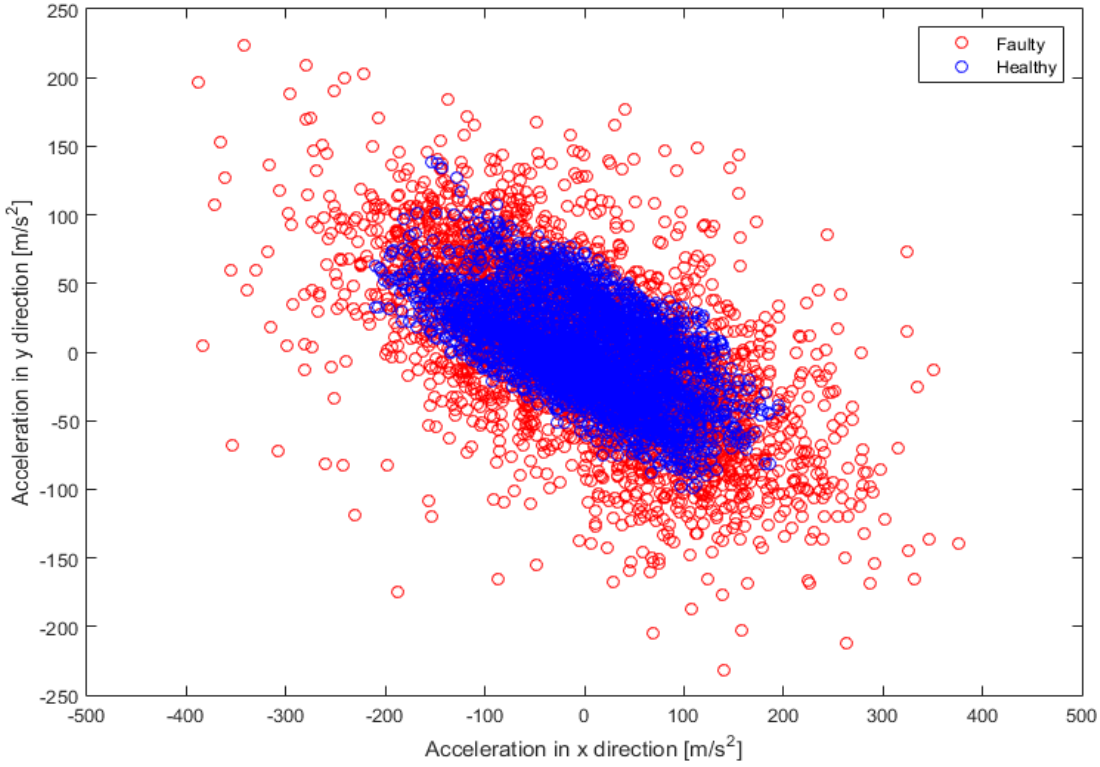

Figure 6.31 Acceleration scatter plot of the bearing, load direction 90° and node number 372

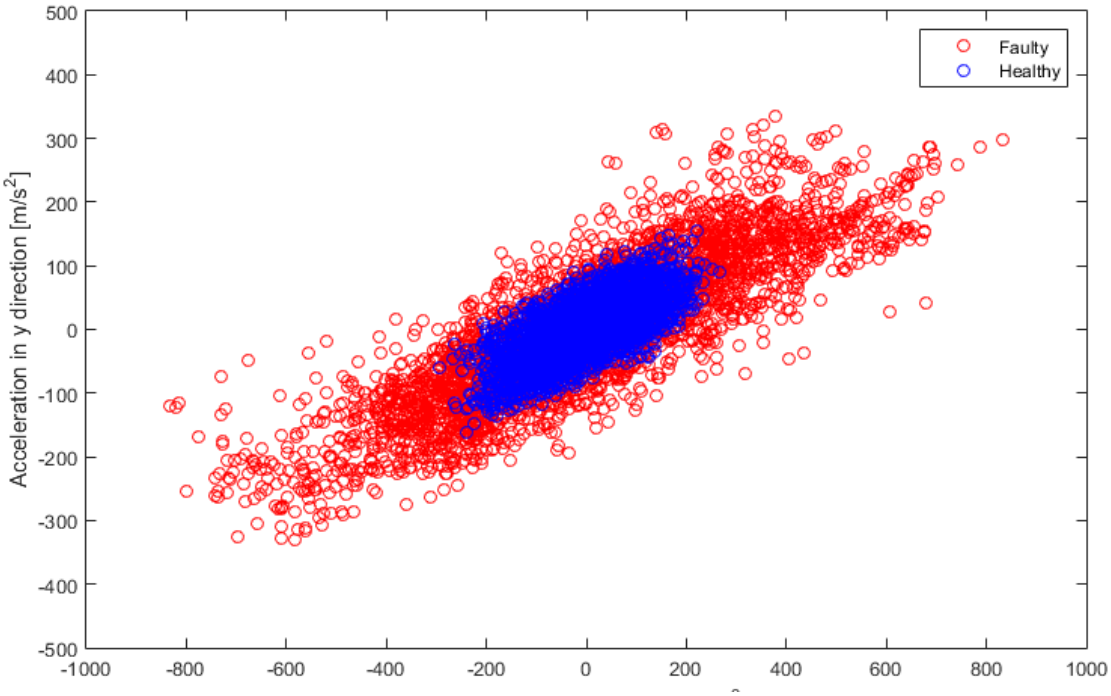

Figure 6.32 Acceleration scatter plot of the bearing, load direction 180° and node number 152

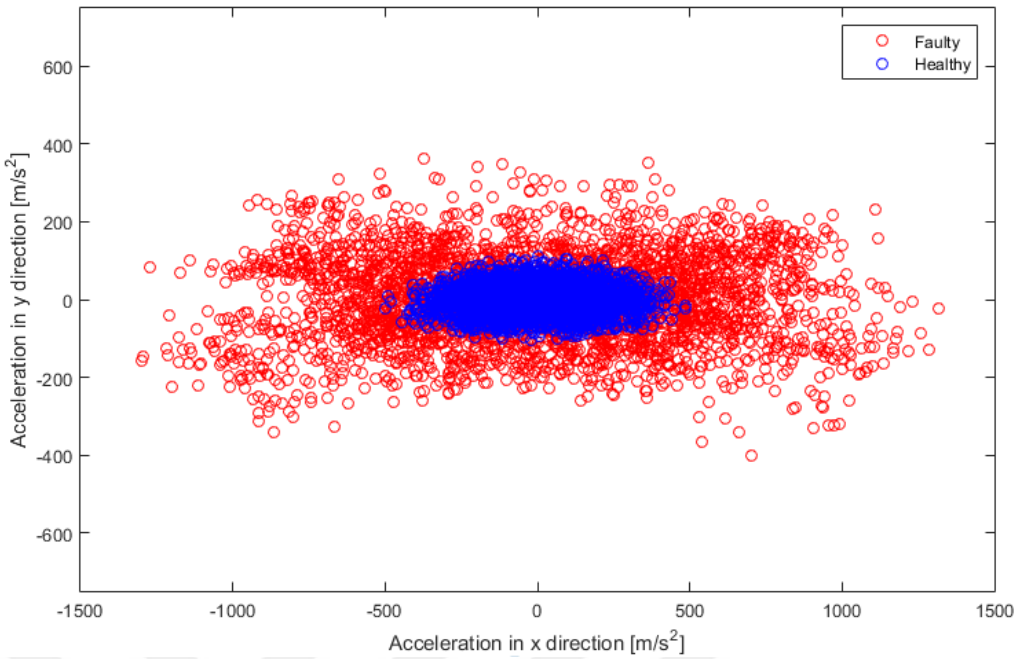

Figure 6.33 Acceleration scatter plot of the bearing, load direction 180° and node number 262

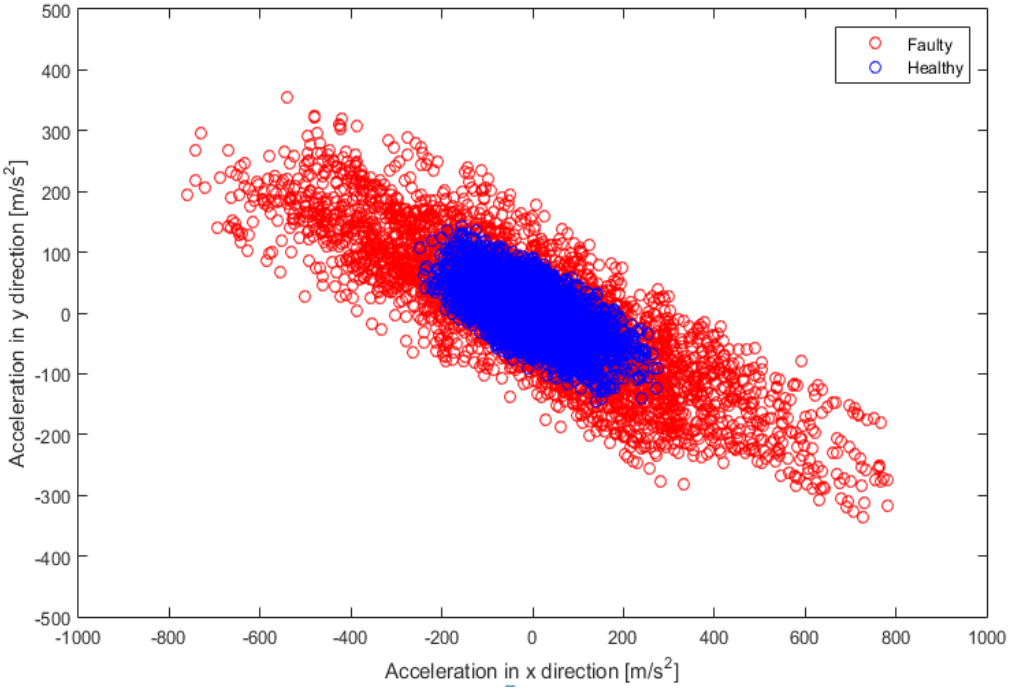

Figure 6.34 Acceleration scatter plot of the bearing, load direction 180° and node number 372

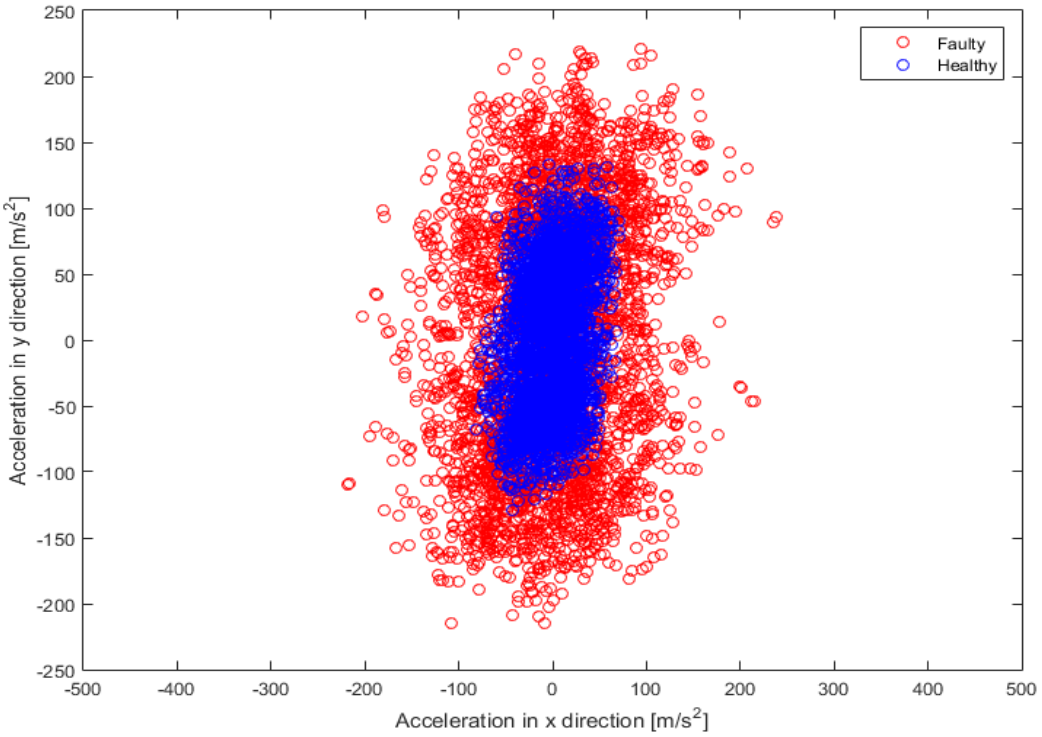

Figure 6.35 Acceleration scatter plot of the bearing, load direction 270° and node number 152

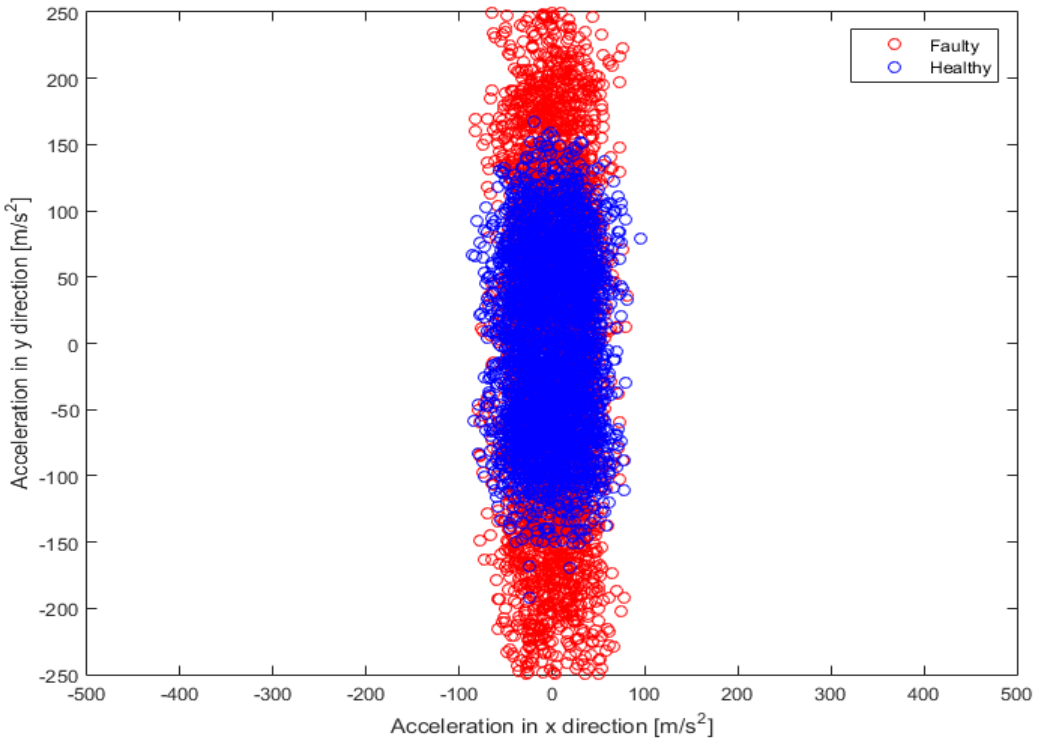

Figure 6.36 Acceleration scatter plot of the bearing, load direction 270° and node number 262

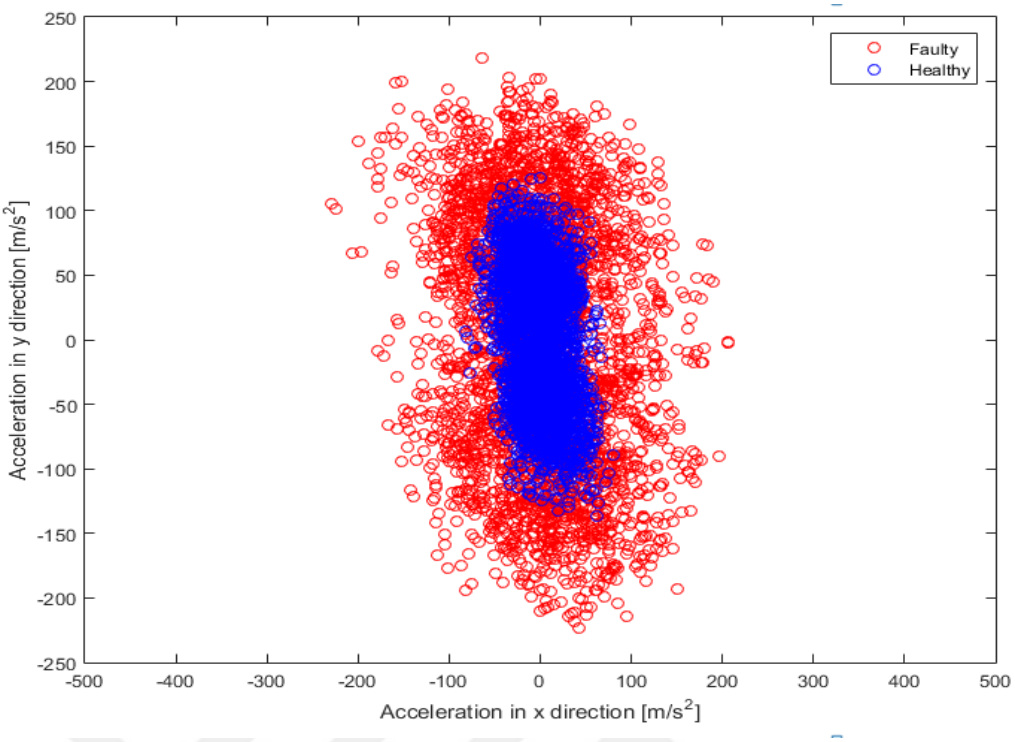

Figure 6.37 Acceleration scatter plot of the bearing, load direction 270° and node number 372

In Table 6.1-6.6, different parameters such as root mean square (RMS), Peak to Peak (P2P), Crest factor (Fc) and Curtosis were listed according to the data obtained from vibration analyses. The effects of the applied load direction and the location of the faultwere examined by using statistical features. For radial loading conditions at 0, 90, 180 and 270 degrees, measurements were taken from sensor points N_1, N_2 and N_3 on faulty and healty bearings and the x and y components of the measured amplitude values were obtained separately. The aim is to show that the amplitude values increase at the location of the fault on the outerring and to examine the reliability of statistical data.

The statistical parameters RMS, Peak to Peak, Crest Factor and Kurtosis were calculated and examined separately to select the most ideal sensor position sensitive to errors at four different angular positions.

The values in Table 6.1-6.6 were calculated for the x and y values of the acceleration responses at sensor positions, namely N_1, N_2 and N_3. Table 6.1-6.6 show

that the most ideal parameter to determine the presence of a local fault closest to the sensor is peak-to-peak and rms values. A defect at 90° can be easily detected by a sensor located in the x-axis of the bearing, such as N_1 and N_3. The N_2 point can be considered an ideal sensor position for detecting any angular position error using acceleration-dependent RMS and peak-to-peak ratios. Kurtosis and crest factor values are not as effective as peak to peak and RMS valuesat the speed of 1000 rpm to determine the sensor position due to acceleration.

Table 6.1 Statistical parameters related to acceleration of defective and healty bearing, 152node and x direction

STATİSTİCAL PARAMETER	0°- Faulty Bearing	0°- Healty Bearing	90°- Faulty Bearing	90°- Healty Bearing	180°- Faulty Bearing	180°- Healty Bearing	270°- Faulty Bearing	270°- Healty Bearing
Peak to Peak Value	3821.4	594.33	773.87	391.73	1665.6	559.10	455.91	153.2050
Root Mean Square Value (RMS)	561.2482	89.4087	111.0822	68.9773	279.23	93.5966	65.1423	26.2501
Crest Factor Value	6.8088	6.6473	6.9666	5.6791	5.9649	5.9735	6.9987	5.8364
Kurtosis Value	2.8077	2.7640	2.9411	2.6321	2.7145	2.5830	2.9250	2.7412

Table 6.2 Statistical parameters related to acceleration of defective and healty bearing, 152 node and y direction

STATİSTİCAL PARAMETER	0°- Faulty Bearing	0°- Healty Bearing	90°- Faulty Bearing	90°- Healty Bearing	180°- Faulty Bearing	180°- Healty Bearing	270°- Faulty Bearing	270°- Healty Bearing
Peak to Peak Value	1401.2	295.37	420.98	219.1580	665.94	317.51	435.69	262.42
Root Mean Square Value (RMS)	246.8834	44.9989	60.3170	33.8630	119.2442	47.5295	97.7451	53.6115
Crest Factor Value	5.6754	6.5639	6.9795	6.4719	5.5847	6.6803	4.4574	4.8948
Kurtosis Value	2.7498	2.8261	3.0260	2.9587	2.4889	2.8093	1.8906	1.9726

Table 6.3 Statistical parameters related to acceleration of defective and healty bearing, 262 node and x direction

STATİSTİCAL PARAMETER	0°- Faulty Bearing	0°- Healty Bearing	90°- Faulty Bearing	90°- Healty Bearing	180°- Faulty Bearing	180°- Healty Bearing	270°- Faulty Bearing	270°- Healty Bearing
Peak to Peak Value	5901.6	1152.3	1084.7	724.95	2617.1	985.91	173.8480	180.83
Root Mean Square Value (RMS)	1061.4	172.1481	192.0039	121.7249	489.3659	165.9162	28.8191	31.6055
Crest Factor Value	5.5601	6.6934	5.6493	5.9556	5.3479	5.9422	6.0324	5.7215
Kurtosis Value	2.6908	2.7616	2.3860	2.5983	2.3737	2.5896	2.5411	2.3160

Table 6.4 Statistical parameters related to acceleration of defective and healty bearing, 262 node and y direction

STATİSTİCAL PARAMETER	0°- Faulty Bearing	0°- Healty Bearing	90°- Faulty Bearing	90°- Healty Bearing	180°- Faulty Bearing	180°- Healty Bearing	270°- Faulty Bearing	270°- Healty Bearing
Peak to Peak Value	597.66	178.8840	891.0100	171.0120	766.07	215.25	712.35	358.90
Root Mean Square Value (RMS)	90.3380	27.8002	66.9113	33.2990	111.1448	36.5816	137.0339	68.3580
Crest Factor Value	6.6158	6.4346	13.3163	5.1357	6.8925	5.8841	5.1983	5.2503
Kurtosis Value	2.9993	2.7373	7.7980	2.3919	2.9169	2.6233	2.1774	1.9939

Table 6.5 Statistical parameters related to acceleration of defective and healty bearing, 372 node and x direction

STATİSTİCAL PARAMETER	0°- Faulty Bearing	0°- Healty Bearing	90°- Faulty Bearing	90°- Healty Bearing	180°- Faulty Bearing	180°- Healty Bearing	270°- Faulty Bearing	270°- Healty Bearing
Peak to Peak Value	4648.2	671.99	763.17	406.16	1543.2	523.52	434.90	162.1840
Root Mean Square Value (RMS)	527.68	95.1206	112.0191	71.4498	276.0973	93.1608	64.6074	24.8513
Crest Factor Value	6.8246	7.0646	6.8129	5.6846	5.5893	5.6195	6.7314	6.5262
Kurtosis Value	2.9003	2.7727	2.9689	2.7202	2.7134	2.5832	2.9506	2.7513

Table 6.6 Statistical parameters related to acceleration of defective and healty bearing, 372 node and y direction

STATİSTİCAL PARAMETER	0°- Faulty Bearing	0°- Healty Bearing	90°- Faulty Bearing	90°- Healty Bearing	180°- Faulty Bearing	180°- Healty Bearing	270°- Faulty Bearing	270°- Healty Bearing
Peak to Peak Value	3.7826	310.70	478.17	238.2820	690.27	287.46	442.19	262.78
Root Mean Square Value (RMS)	220.7453	44.0637	61.0847	35.5480	119.3893	48.2402	97.9477	54.0126
Crest Factor Value	7.1982	7.0512	7.8280	6.7031	5.7817	5.9589	4.5146	4.8652
Kurtosis Value	2.9843	2.9285	3.1255	2.8560	2.4633	2.6275	1.8950	1.9665

6.3 Frequency Domain Analysis

Another method of vibration analysis is the processing of vibration signals in the frequency domain. The presence of one of the error frequencies in the direct or processed frequency spectrum is a clear indication of the error (Kıral and Karagülle, 2003). Characteristic defect frequencies are related to the position of the defect in a bearing and the rotational speed (Tandon & Choudhury, 1999).

All components that make up the bearing have a very small surface roughness, so that all healthy and unhealthy bearings have a defect frequency. The characteristic defect frequencies for a rolling bearing are expressed by Equation 6.1-6.4.

$$\text{Fundamental Train (case) Frequency= FTF}=\frac{S}{2}\left(1-\frac{B_d}{P_d}\cos\phi\right) \tag{6.1}$$

$$\text{Ball Pass Frequency of the Inner Race= BPFI}=\frac{N_b}{2}S\left(1+\frac{B_d}{P_d}\cos\phi\right) \tag{6.2}$$

$$\text{Ball Pass Frequency of the Outer Race= BPFO}=\frac{N_b}{2}S\left(1-\frac{B_d}{P_d}\cos\phi\right) \tag{6.3}$$

$$\text{Ball Spin Frequency= BSF}=\frac{P_d}{2B_d}S\left[1-\left(\frac{B_d}{P_d}\right)^2\cos^2\phi\right] \tag{6.4}$$

The symbols used in the equations refer to the following terms respectively:

θ: Contact angle**, S:** Shaft speed, **N_b:** Number of balls or rollers**, B_d:** Ball or roller diameter**, P_d:** Pitch diameter

In this study, frequency spectra were obtained by Fast Fourier Transform (FFT) using Equation 6.5 in Matlab. The fast Fourier transform of a distrete time signal wasobtained by using the following formula

$$\sum_{n=0}^{N-1}x(n)e^{-jn\omega_k}\quad(k=0,1,2,...,N-1) \tag{6.5}$$

In this section, frequency spectra for healthy and faulty bearings were obtained and bearing failure frequencies wereinvestigated. Frequency analysis graphs were obtained to analyze the effect of loading angle and sensor positions. Failure frequencies and harmonics of healthy and faulty bearings were obtained for *x* and *y* components of acceleration-dependent values at each sensor point.

Frequency spectrum graphs at 0, 90, 180 and 270 degrees load conditions at the N_1, N_2 and N_3 measuring points of healthy and faulty bearingsare as shown in Figure 6.38-6.61 for 16.66 Hz rotational speed. In all graphs, it is seen that the amplitude and harmonics of the outer ring failure frequency of the faulty bearing are much higher than the healthy bearings. Thus, bearing failure is clearly identified in all graphics.

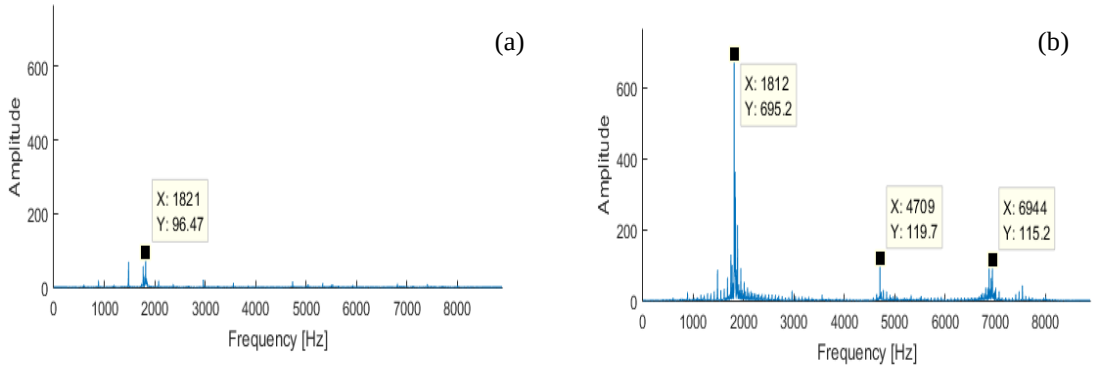

Figure 6.38 Frequency waveform of the bearing, 0° load direction on the x axis and node number 152 a) healthy bearing b) defect bearing

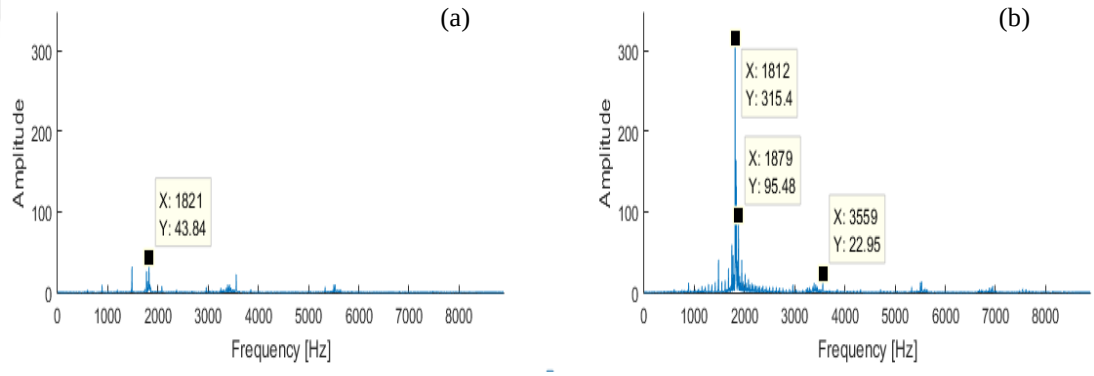

Figure 6.39 Frequency waveform of the bearing, 0° load direction on the y axis and node number 152 a) healthy bearing b) defect bearing

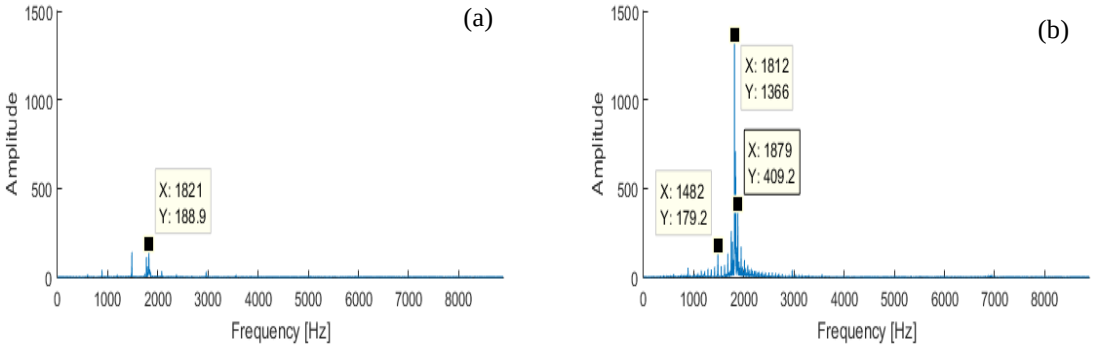

Figure 6.40 Frequency waveform of the bearing, 0° load direction on the x axis and node number 262 a) healthy bearing b) defect bearing

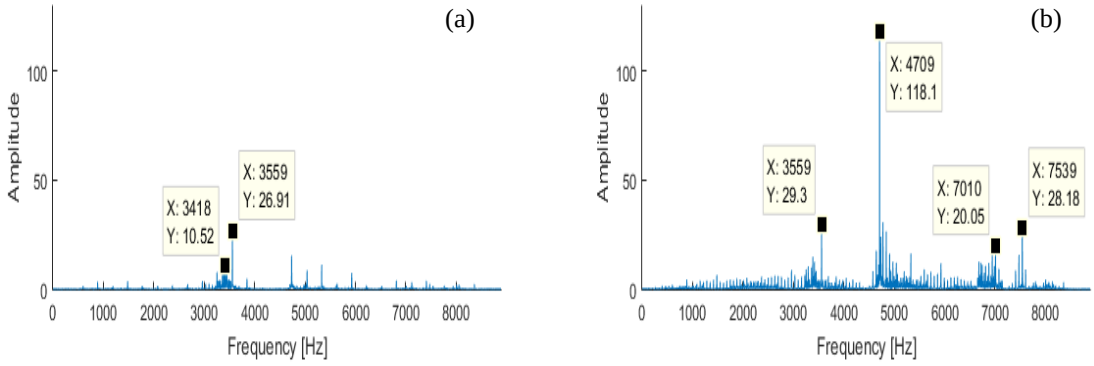

Figure 6.41 Frequency waveform of the bearing, 0° load direction on the y axis and node number 262 a) healthy bearing b) defect bearing

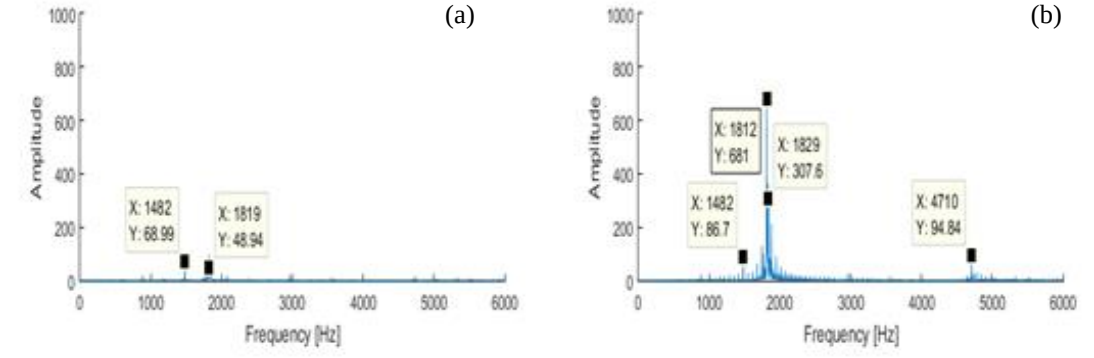

Figure 6.42 Frequency waveform of the bearing, 0° load direction on the x axis and node number 372 a) healthy bearing b) defect bearing

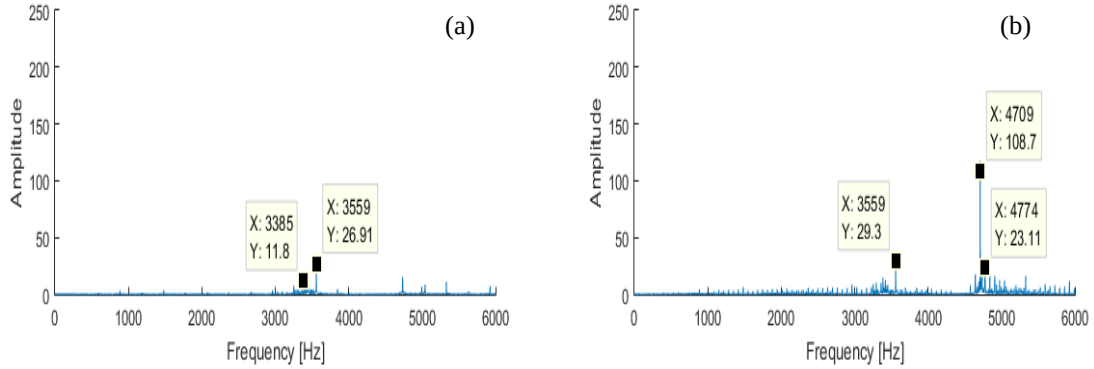

Figure 6.43 Frequency waveform of the bearing, 0° load direction on the y axis and node number 372 a) healthy bearing b) defect bearing

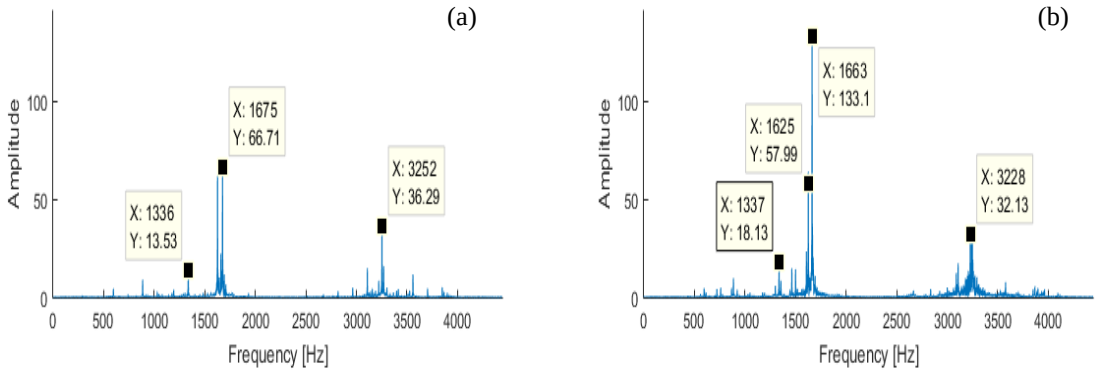

Figure 6.44 Frequency waveform of the bearing, 90° load direction on the x axis and node number 152 a) healthy bearing b) defect bearing

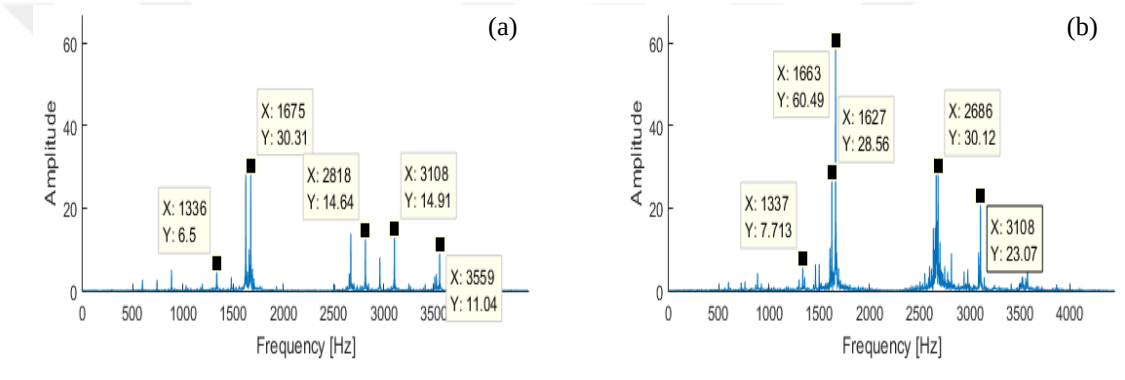

Figure 6.45 Frequency waveform of the bearing, 90° load direction on the y axis and node number 152 a) healthy bearing b) defect bearing

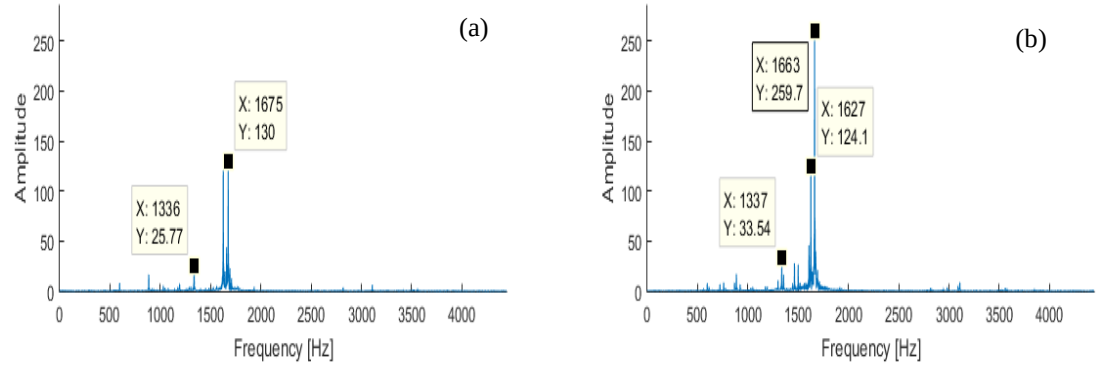

Figure 6.46 Frequency waveform of the bearing, 90° load direction on the x axis and node number 262 a) healthy bearing b) defect bearing

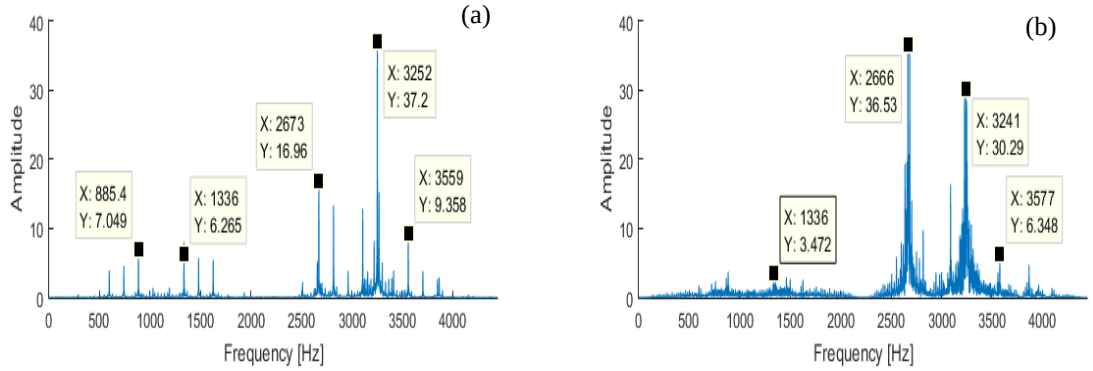

Figure 6.47 Frequency waveform of the bearing, 90° load direction on the y axis and node number 262 a) healthy bearing b) defect bearing

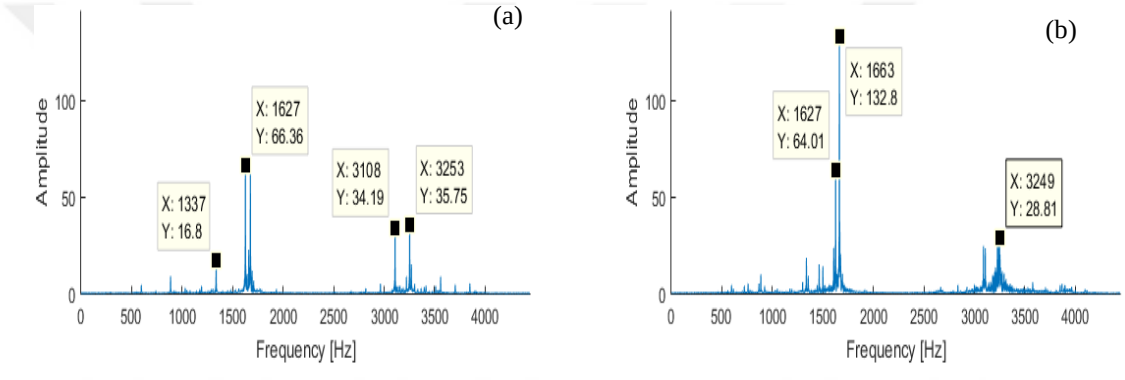

Figure 6.48 Frequency waveform of the bearing, 90° load direction on the x axis and node number 372 a) healthy bearing b) defect bearing

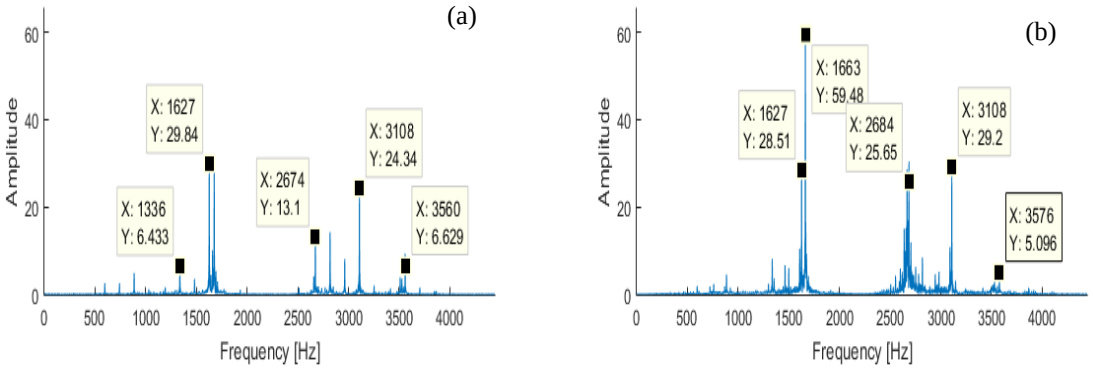

Figure 6.49 Frequency waveform of the bearing, 90° load direction on the y axis and node number 372 a) healthy bearing b) defect bearing

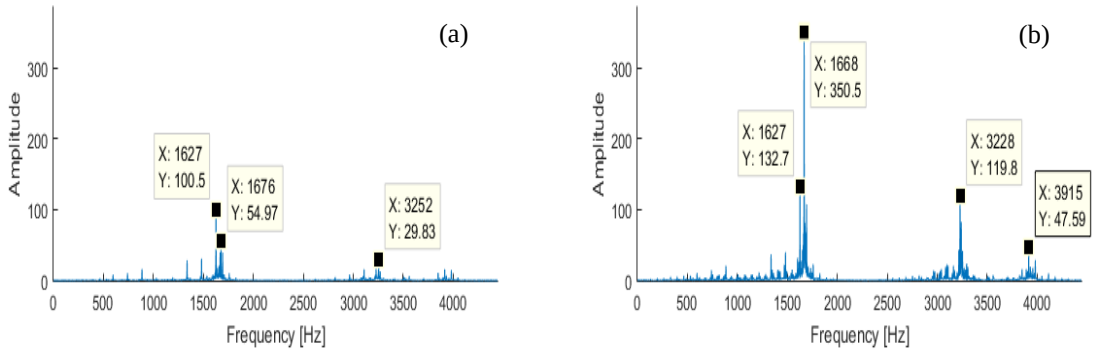

Figure 6.50 Frequency waveform of the bearing, 180° load direction on the x axis and node number 152 a) healthy bearing b) defect bearing

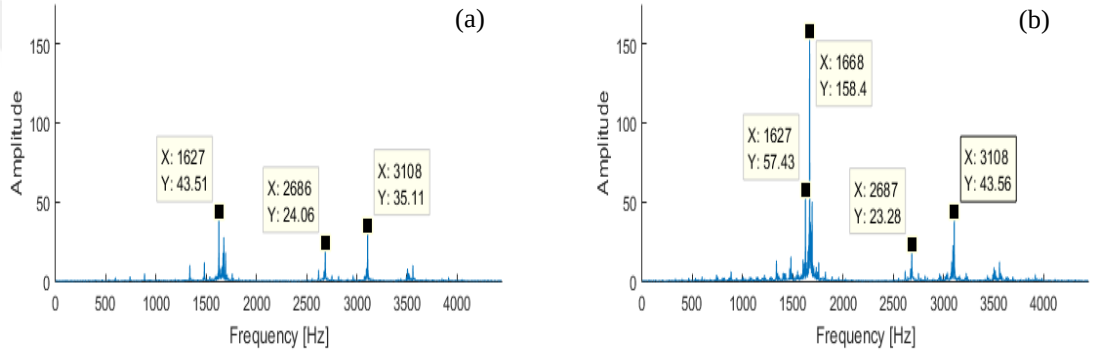

Figure 6.51 Frequency waveform of the bearing, 180° load direction on the y axis and node number 152 a) healthy bearing b) defect bearing

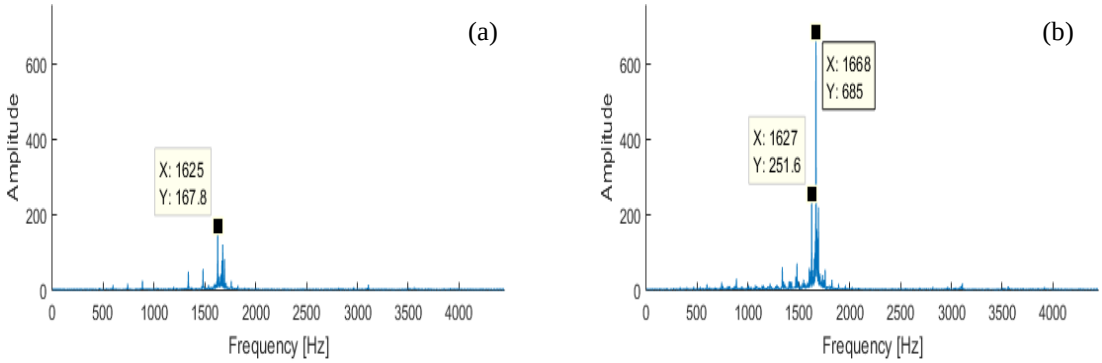

Figure 6.52 Frequency waveform of the bearing, 180° load direction on the x axis and node number 262 a) healthy bearing b) defect bearing

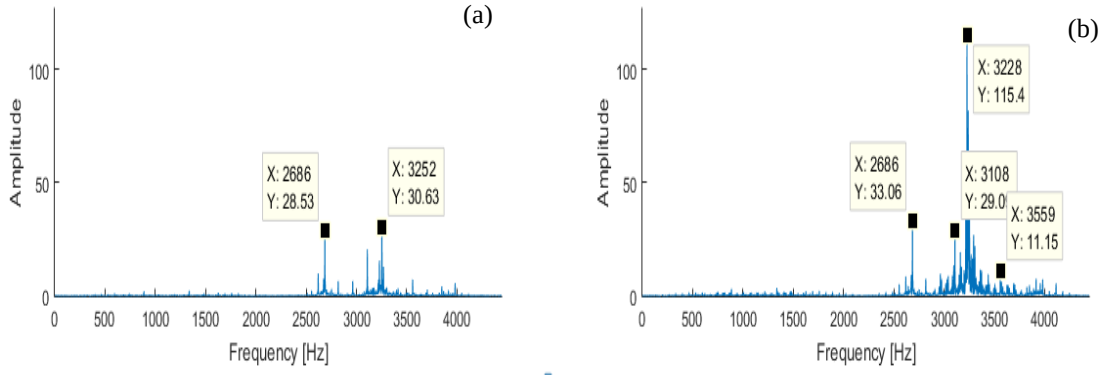

Figure 6.53 Frequency waveform of the bearing, 180° load direction on the y axis and node number 262 a) healthy bearing b) defect bearing

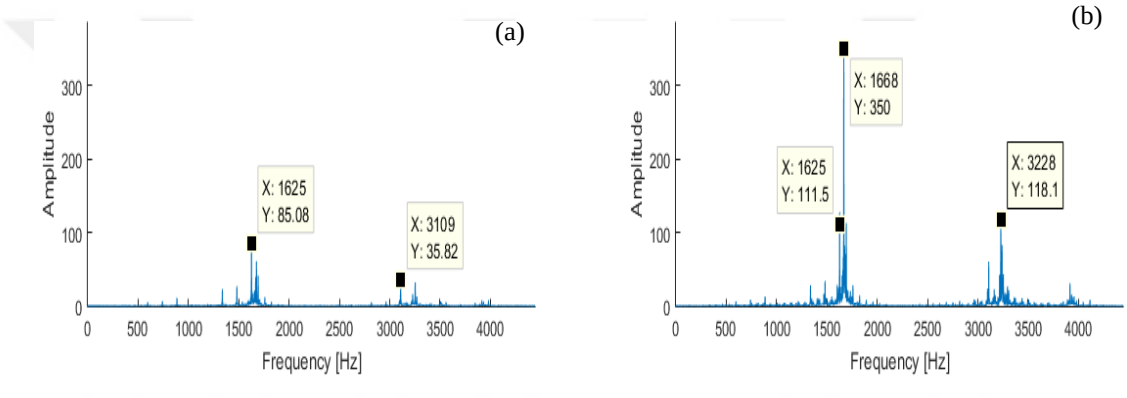

Figure 6.54 Frequency waveform of the bearing, 180° load direction on the x axis and node number 372 a) healthy bearing b) defect bearing

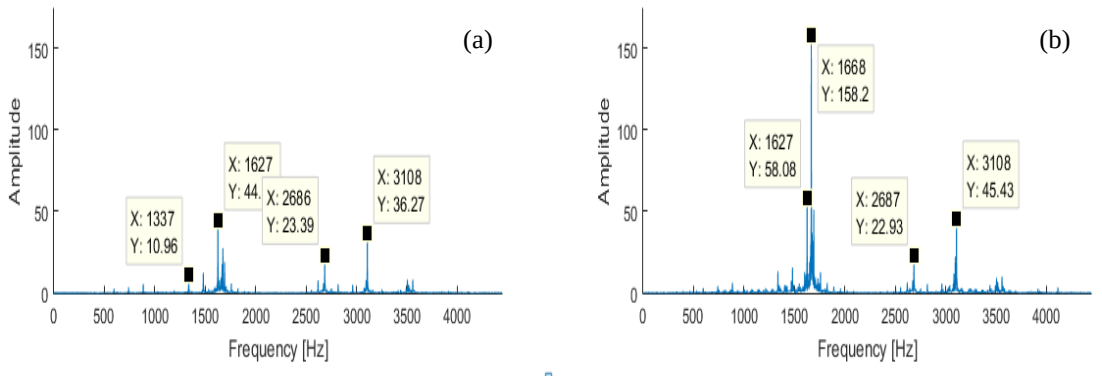

Figure 6.55 Frequency waveform of the bearing, 180° load direction on the y axis and node number 372 a) healthy bearing b) defect bearing

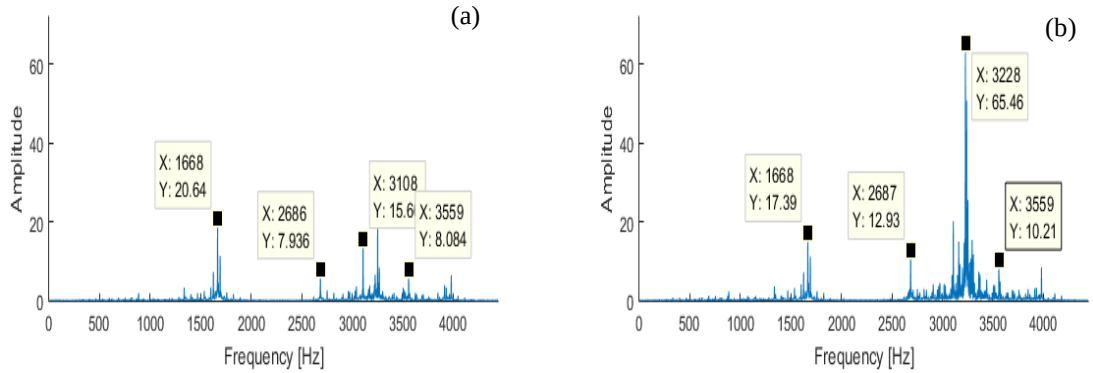

Figure 6.56 Frequency waveform of the bearing, 270° load direction on the x axis and node number 152 a) healthy bearing b) defect bearing

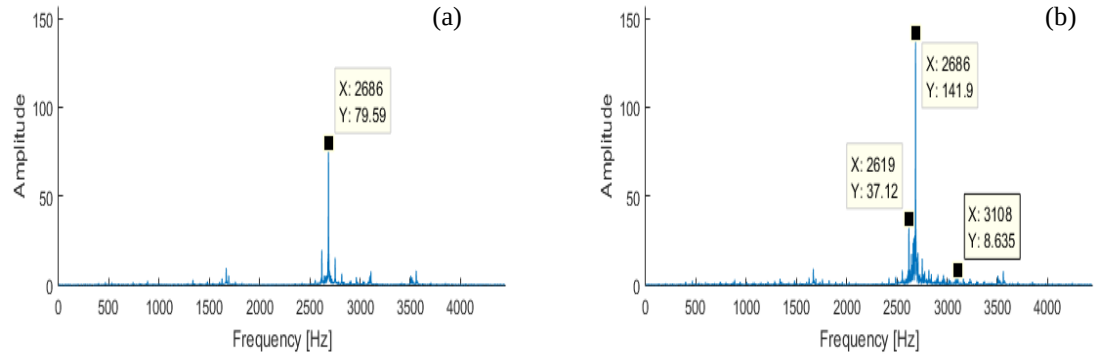

Figure 6.57 Frequency waveform of the bearing, 270° load direction on the y axis and node number 152 a) healthy bearing b) defect bearing

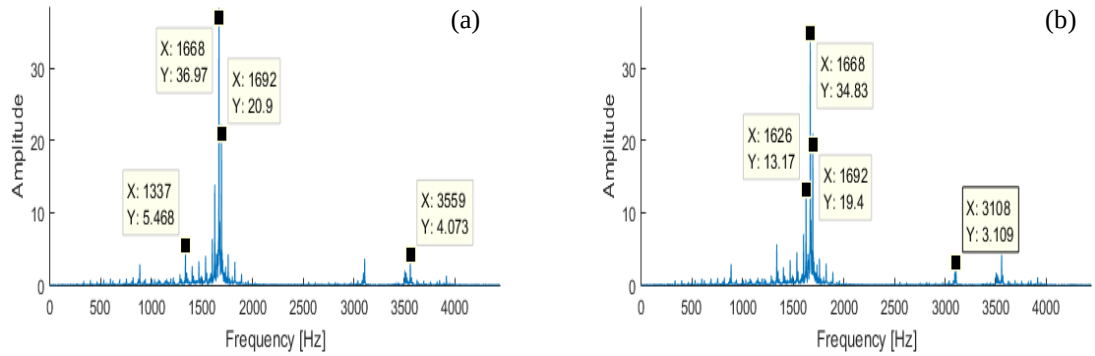

Figure 6.58 Frequency waveform of the bearing, 270° load direction on the x axis and node number 262 a) healthy bearing b) defect bearing

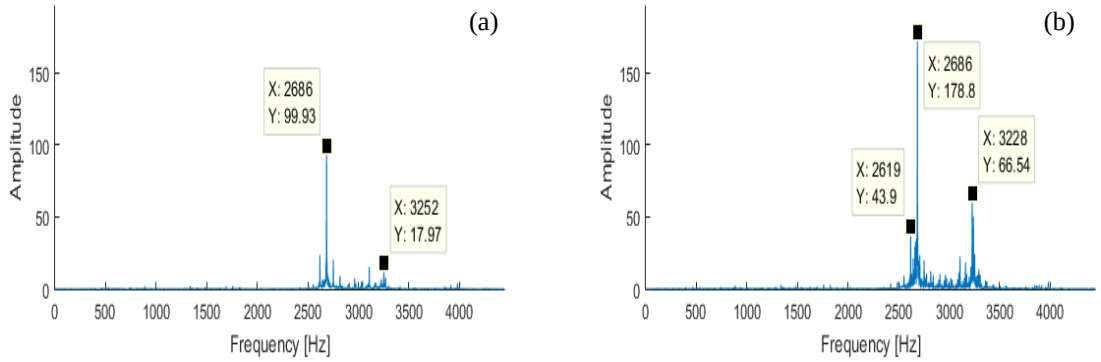

Figure 6.59 Frequency waveform of the bearing, 270° load direction on the y axis and node number 262 a) healthy bearing b) defect bearing

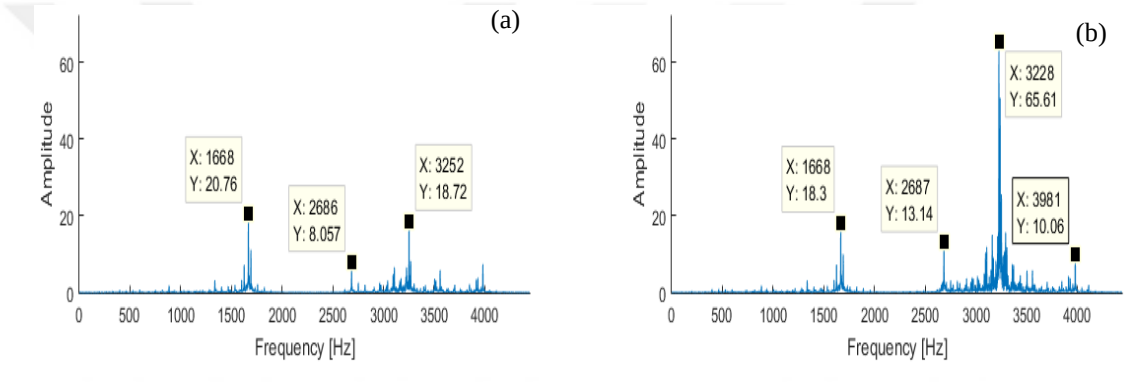

Figure 6.60 Frequency waveform of the bearing, 270° load direction on the x axis and node number 372 a) healthy bearing b) defect bearing

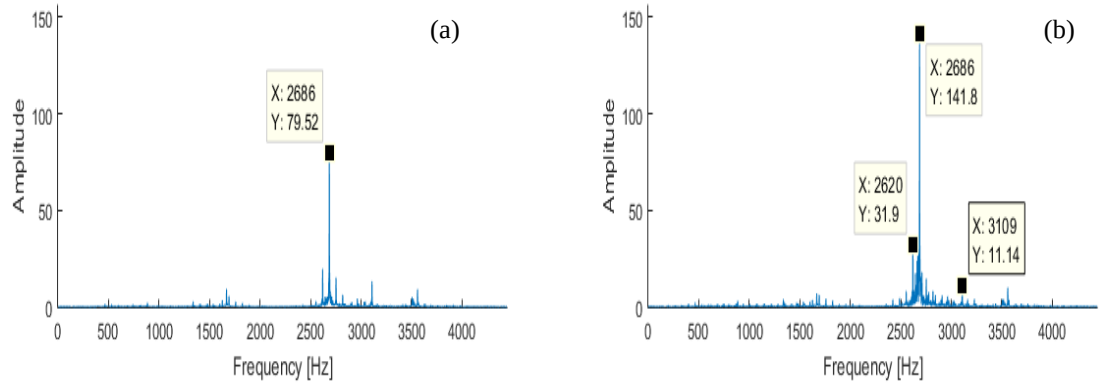

Figure 6.61 Frequency waveform of the bearing, 270° load direction on the y axis and node number 372 a) healthy bearing b) defect bearing

6.4 Determining Ideal Sensor Positions According To Statistical Parameters

In Figure 6.62-6.69, the results of the acceleration and velocity responses of the statistical parameters of a faulty bearing are compared.

In Figure 6.62, kurtosis values for x componentof the acceleration response are lower than those for the velocity response. If the kurtosis value is calculated from the x component of acceleration to detect a defect at 1000 rpm under different loading conditions, the sensorpositions N1, N2, N3 are suitable. While at N1 and N3 each sensor can take close measurements with each other, for 270 degrees of loaddirection, the N2 sensor remains weak in finding the fault.

Likewise, if the kurtosis value is calculated from the x component of the velocity signal, the sensor can detect faults more accurately than the N1 and N3 positions. Point N2 is weaker under all loading conditions.

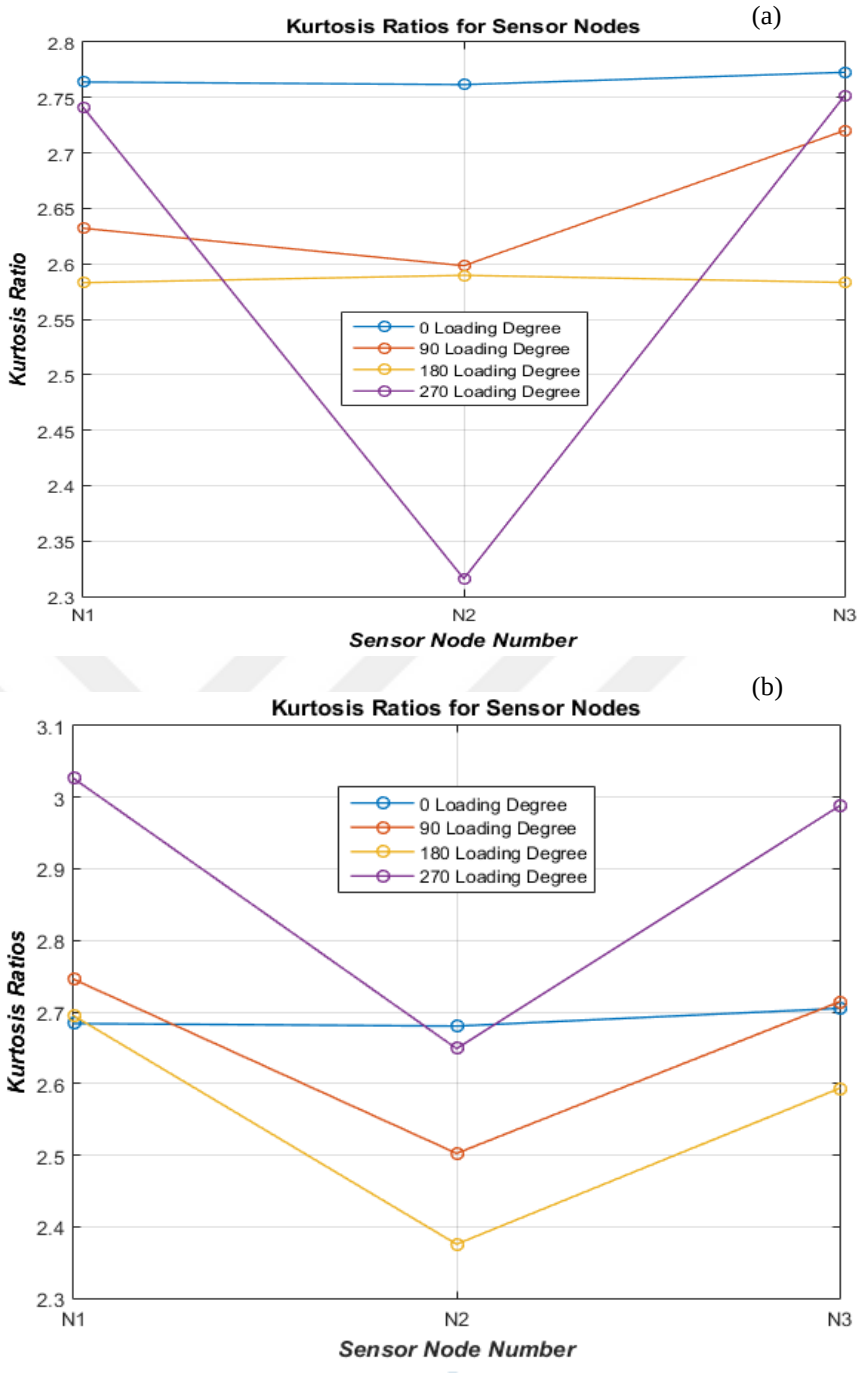

Figure 6.62 Kurtosis ratios of an faulty bearing for x component of a) acceleration responses b) velocity responses

Likewise, in Figure 6.63, the kurtosis values for the y component of the acceleration response are lower than for the velocityresponse. If the kurtosis value is calculated from the acceleration y component to detect a fault, the N1 and N3 sensor perform close to each other at 0, 90 and 180 degree loads, while the N2 sensor does

not take a healthy measurement under 90 degree radial load. 270 degrees is a non-ideal loading condition for all sensors. On the other hand, the calculation of the y component of the velocity value was found to be the ideal location for the N2 sensor's fault detection under 90 degrees of load.

(a)

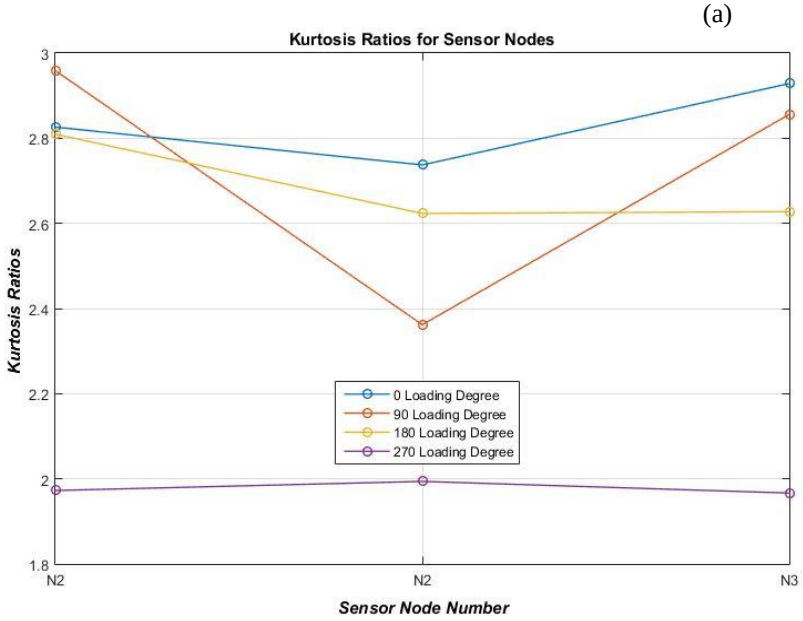

(b)

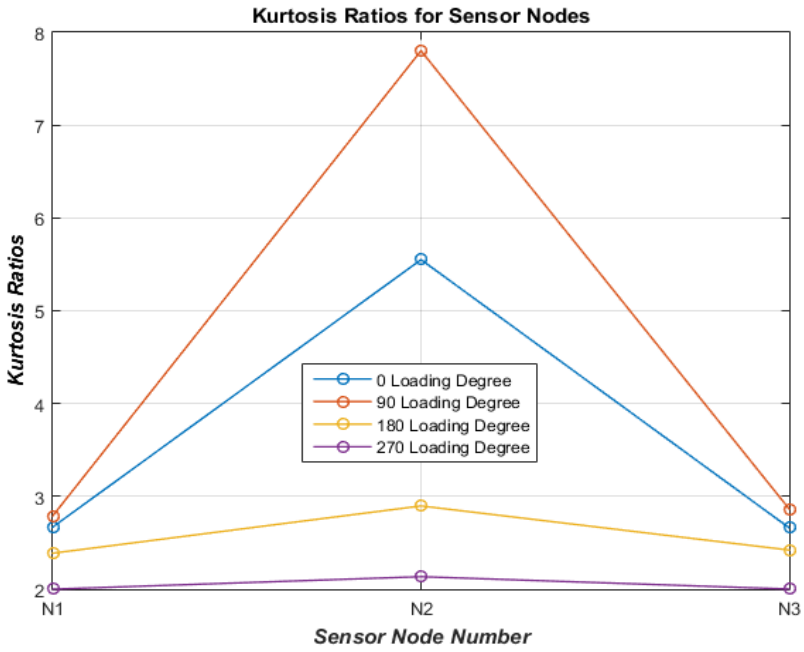

Figure 6.63 Kurtosis ratios of an faulty bearing for y component of a) acceleration responses b) velocity responses

When the crest factor is calculated from the *x* value of acceleration in Figure 6.64, it is seen that the most ideal sensor position is N_3 sensor under 0 degree load. When the crest factor was calculated from the *x* value of the velocity, it was observed that the N_1 and N_3 sensors were close to each other and gave appropriate results under 90 and 270 degrees loading conditions. The ideal sensor is the N_3 sensor at 270 degrees.

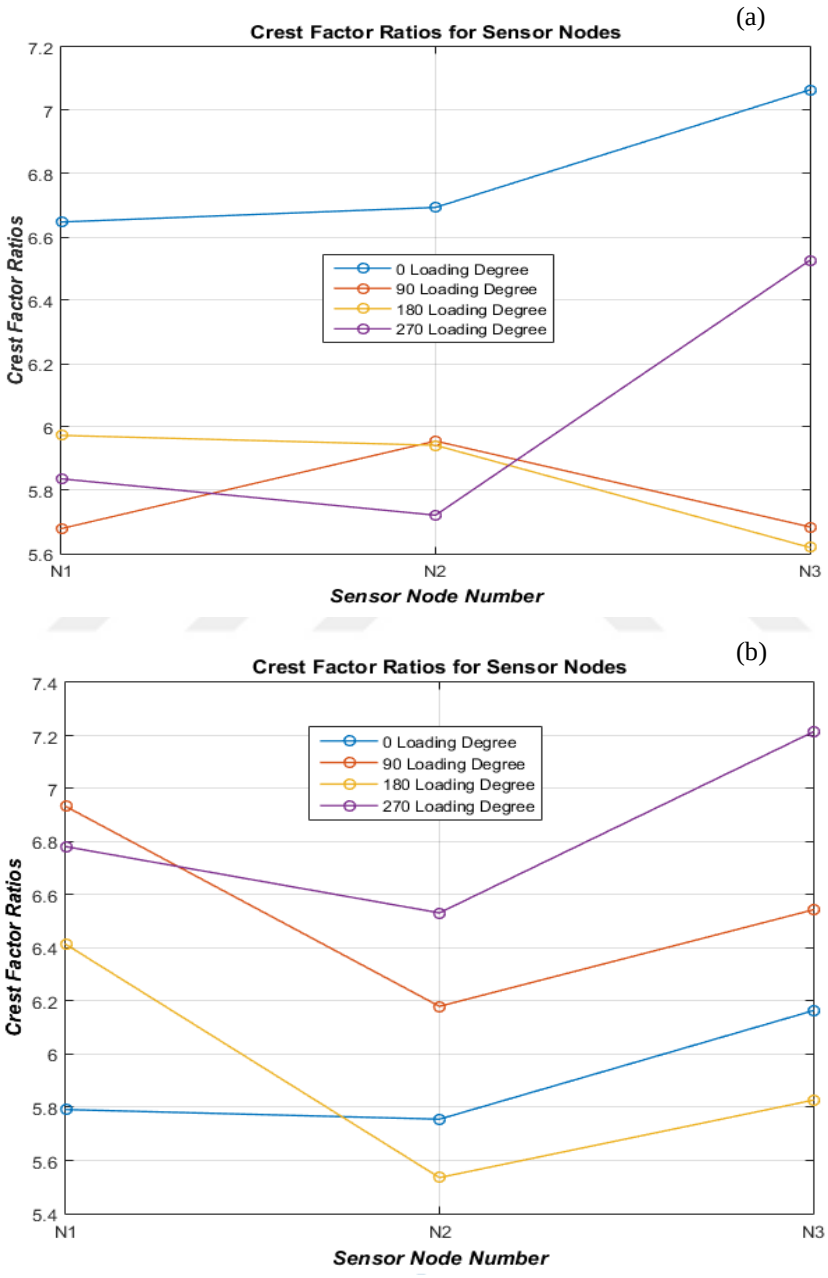

Figure 6.64 Crest Factor ratios of an faulty bearing for x component of a) acceleration responses b) velocity responses

When the crest factor is calculated from the *y* component of the acceleration, the N_1 sensor has similar results under 0, 90,180 degree loading, while the most ideal sensor position is N_3 sensor under 0 degree load. When the *y* component of the velocity is calculated, all sensors behave similarly in position N_1 and N_3, while the ideal sensor position is N_2 at 90 degrees.

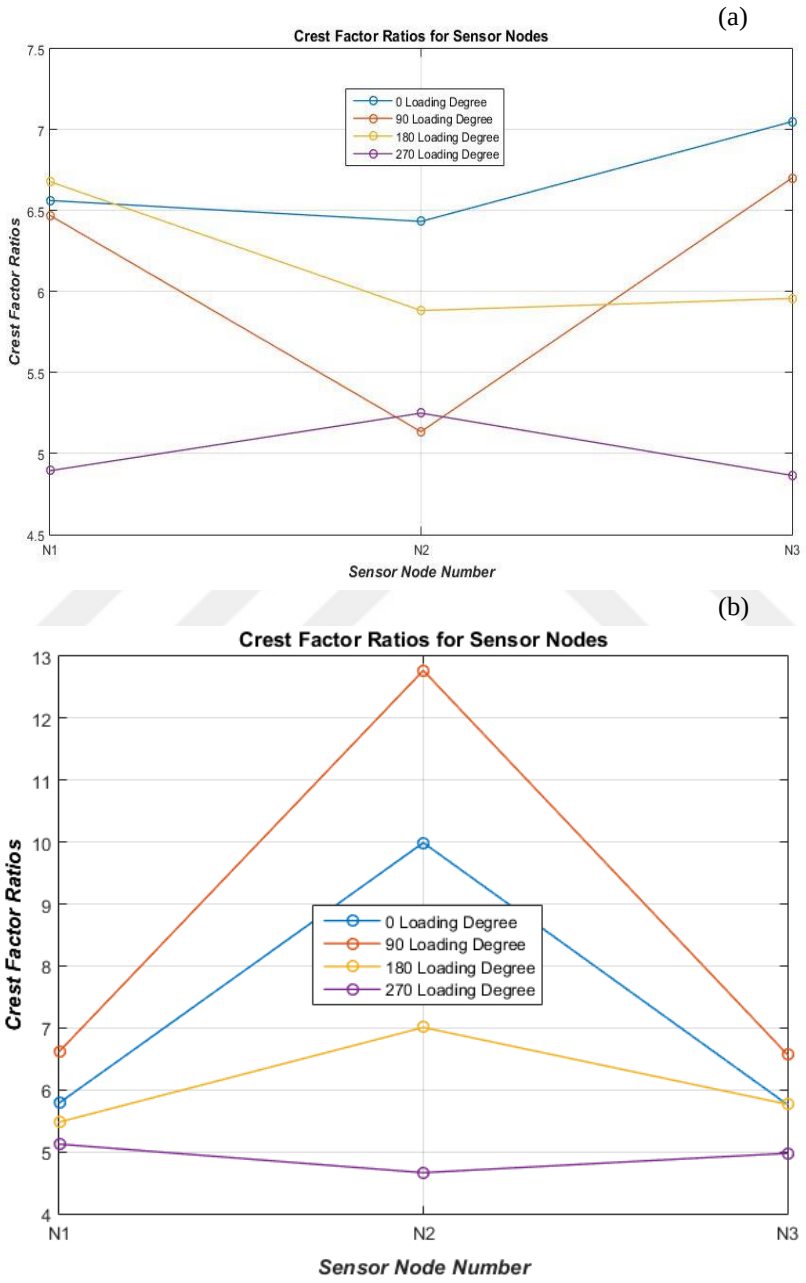

Figure 6.65 Crest Factor ratios of an faulty bearing for y component of a) acceleration responses b) velocity responses

When the RMS is calculated from both the acceleration x values and the velocity *x* values given in Figure 6.66, it is seen that the most ideal sensor position is N_2 sensor under 0 degree load. The N_2 sensor also provides good results for 90 and 180 degree radial load types.

(a)

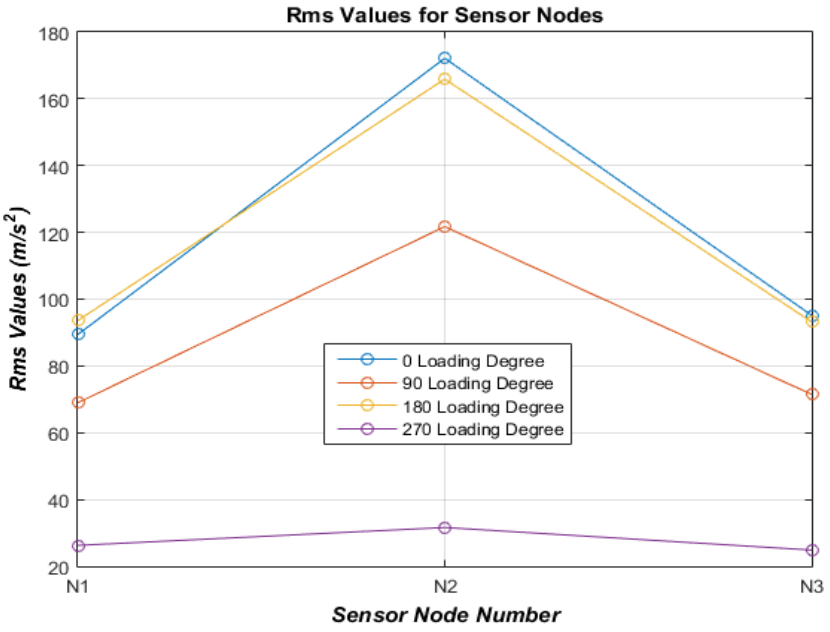

(b)

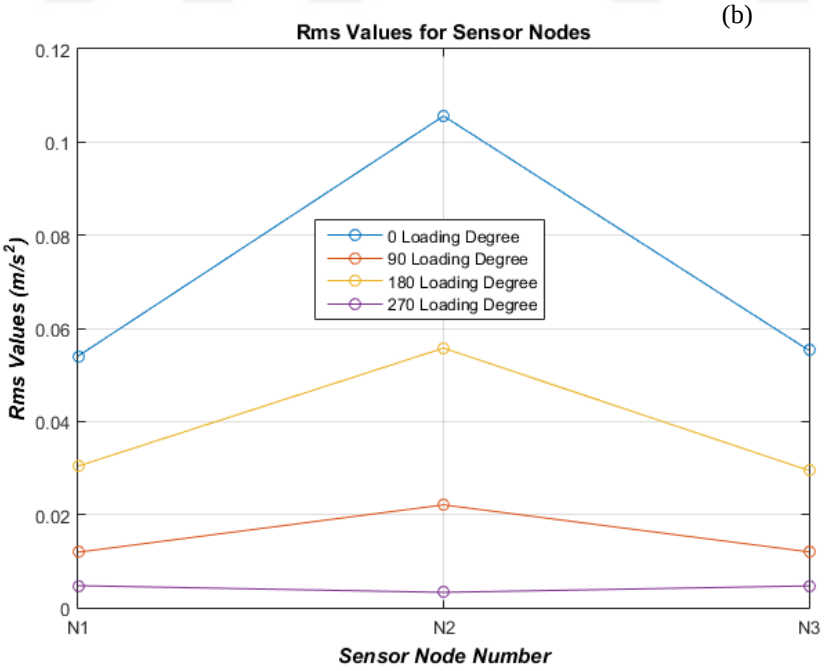

Figure 6.66 RMS values of an faulty bearing for x component of a) acceleration responses b) velocity responses

When the RMS is calculated from the acceleration *y* value in Figure 6.67, it is seen that the most ideal sensor position is N_2 sensor under 270 degrees load. In the 0 and 180 degree load positions, the N_1 and N_3 sensors showclose behavior. When the RMS velocityis calculated from the *y* value, it is observed that the N_1 and N_3 sensors are close to each other and give good results for radial loading at 0 degrees. The N_2 sensor gives good results at 270 degrees.

(a)

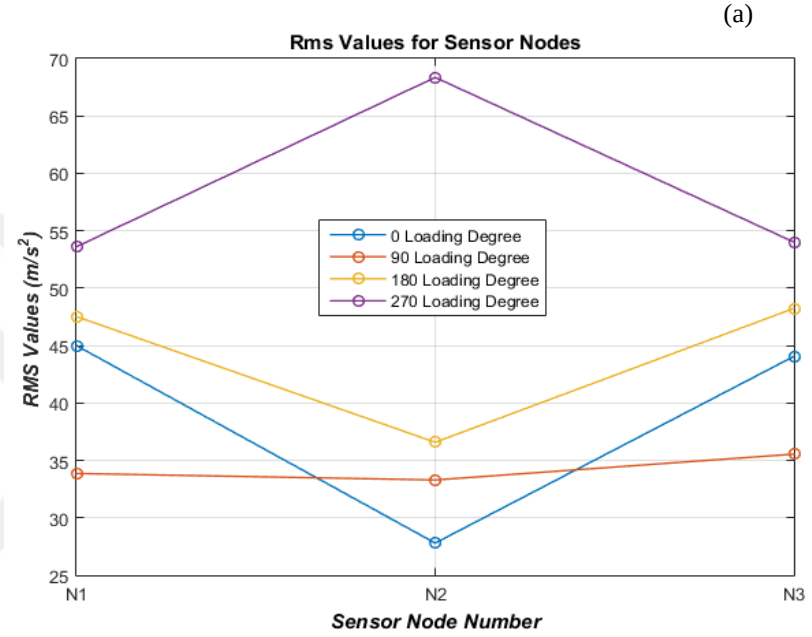

(b)

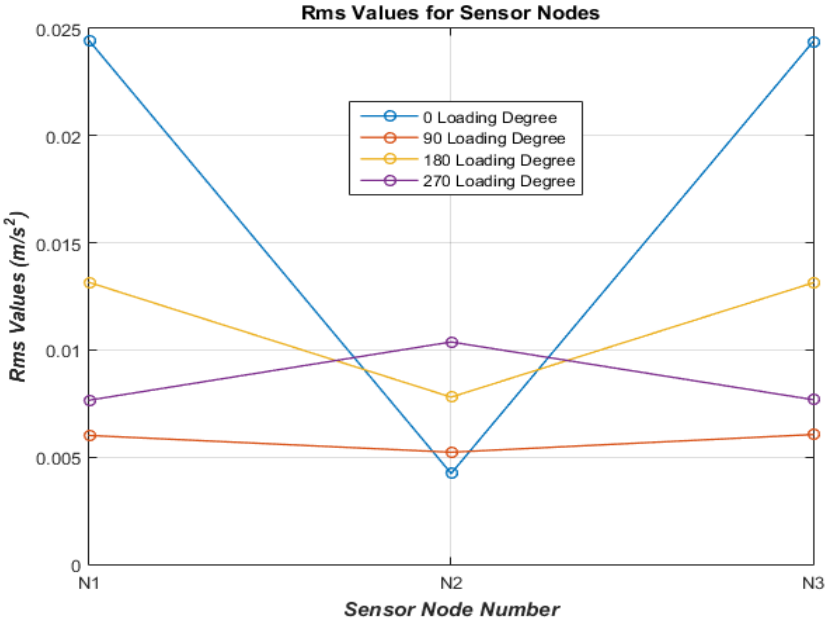

Figure 6.67 RMS values of an faulty bearing for y component of a) acceleration responses b) velocity responses

The peak to peak value is similar when calculated from the acceleration *x* value and the *x* value of the velocity in Figure 6.68. Healthy results can be obtained from positions N_1, N_2 and N_3 for all loading types other than 270 degrees of radial loading. However, the ideal sensor point is N_2 under 0 degrees of radial load.

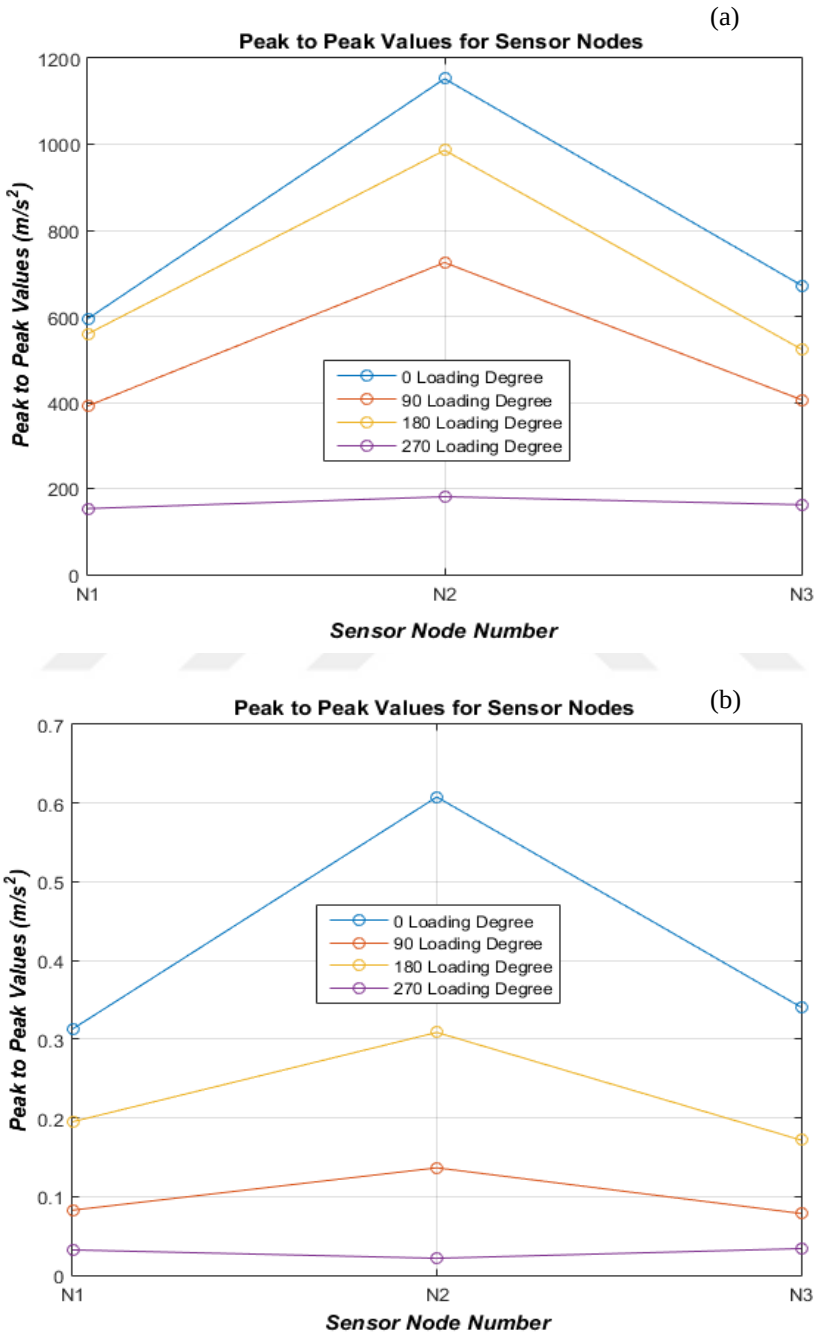

Figure 6.68 Peak to Peak values of an faulty bearing for x component of a) acceleration responses b) velocity responses

In Figure 6.69, the Peak to Peak values for the *y* component of the acceleration response yield similar results at all sensor positions at 0 and 180 degrees. The ideal sensor position is the N_2 sensor at 270 degrees. Similarly, if the peak to peak value is calculated from the *y* component of the velocity, the sensor can detect faults more accurately than N_1 and N_3 under 0 degrees of radial load.

(a)

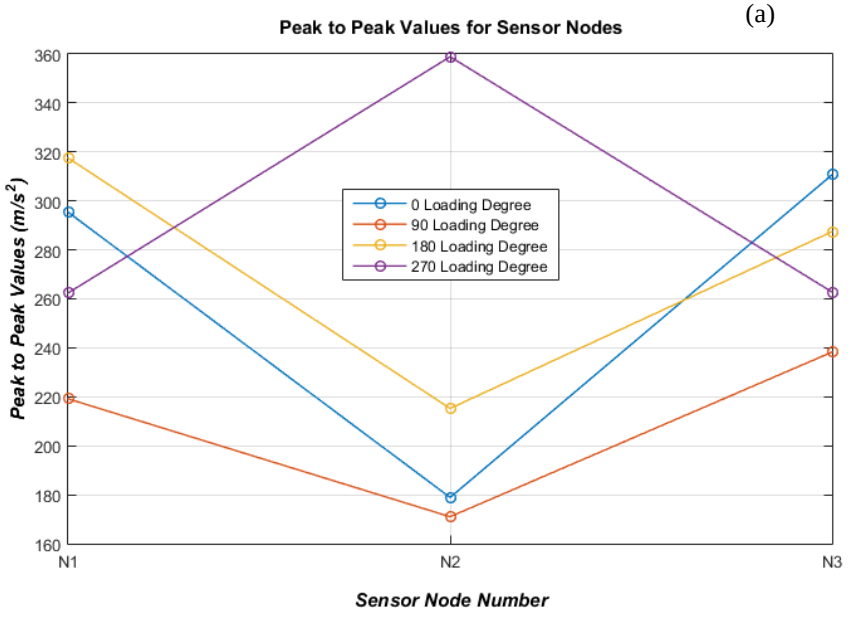

(b)

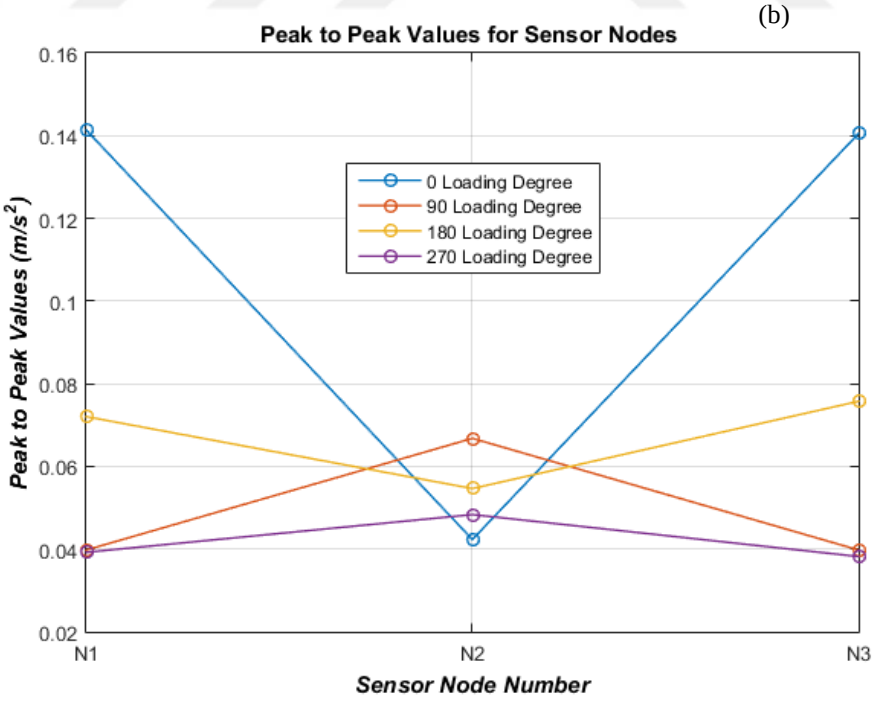

Figure 6.69 Peak to Peak values of an faulty bearing for y component of a) acceleration responses b) velocity responses

CHAPTER SEVEN
CONCLUSIONS

In this study, it is shown that vibration analysis under different loading conditions can be obtained by using a commercial finite element program when the suitable dynamic loading models of faulty and healthy bearings are created. The ANSYS APDL code was developed to obtain the parametric model of the bearing housing's finite element model. The dynamic loading of the bearing structure was created by considering the bearing kinematics and the direction of the radial loading. All data was processed with the codes developed in Visual BASIC and Matlab programming languagesto perform the vibration analysis. To create the proper time dependent loading functions in ANSYS finite element package, an interpolation procedure was applied to produce necessary loading functions for vibration analysis and loading files were created with .txt extension for performing vibration analyses. With this study, it was possible to obtain the simulated vibration signals, which are the response of the bearing structure to dynamic loads for different loading conditions in order to design the appropriate condition monitoring technique. The effects of the localized fault on the time waveforms and frequency spectra were observed. The results were evaluated for three different measuring points. In this study, it is possible to carry out a condition monitoring study which saves significant money and time wastes as a result of experimental studies with parametric modeling and vibration analysis procedure. Especially in high-budget and critical industrial studies, it is possible to select the appropriate sensor location and signal processing method at the design stage. In addition, engineering analyzes such as vibration, stress or fatigue caused by dynamic loading in roller bearing structures can be easily performed with this study.

From the results of this study, the following discussion points are summarized:

- Commercial finite element packages can be effectivelyused to model structures subjected to dynamic loads and perform vibration analysis. As in

the rolling element bearing applications, it is possible to perform vibration analysis with ANSYS APDL program for a rotating distributed bearing load.

- Healty and faulty bearing models can be obtained in the ANSYS APDL analysis program under the desired loading conditions. The results can be listed, graphed, and used to obtain statistical parameters based on velocity and acceleration responses.

- The presence of the fault at any point on the bearing can be determined by statistical parameters obtained from time analysis and frequency analysis conversion.

- All of the statistical parameters such as peak to peak, root mean square, crest factor and kurtosis can be used for error detection. However, since these parameters cannot indicate the source of the fault, the position selection of the sensor points is very important.

- Vertical and horizontal measurement points for statistical parameters give similar results.

- While RMS and peak to peak values are good for fault detection at speeds as high as 1000 rpm, crest factor and kurtosis valuesdo not produce reliable results at high speeds.

- The change in loading direction affects thestatistical parameters, and the RMS value is often influenced by loading changes.

- The statistical values for faulty bearings at all measuring points N_1, N_2 and N_3 are higher than those obtained for healthy bearings.

- In the graphs generated forthe frequency spectra based on the accelerationsignalsat N_1, N_2 and N_3 measurement points, the values of BPFO

and harmonics in both *x* and *y* directions have higher amplitude values for faulty bearings than healthy bearings.

- This work can be applied to faults other than the outer ring under different loading conditions and speed conditions.

- The accuracy of the study should be supported by experimental studies.

- It has been concluded that, instead of particularly difficult experimental studies, design of the proper condition monitoring applications can be carried out by vibration analysis for rolling element bearings using the commercial finite element packages.

REFERENCES

Bearing failure and analysis. (n.d.). Retrieved January 20, 2019, from https://www.schaeffler.com/remotemedien/media/_shared_media/08_media_library/01_publications/barden/brochure_2/downloads_24/barden_bearing_failures_us_en.pdf

Bearing failure: Causes and cures. (n.d.). Retrieved January 20, 2019, from https://www.schaeffler.com/remotemedien/media/_shared_media/08_media_library/01_publications/barden/brochure_2/downloads_24/barden_bearing_failures_us_en.pdf

Bearing timeline, (n.d.). Retrieved February 4, 2019, from https://www.americanbearings.org/page/bearing_timeline

Choudhury, A.,& Tandon, N. (2006). Vibration response of rolling element bearings in a rotor bearing system to a local defect under radial load. *Journal of Tribology*, *128*, 252-261.

Chan, T.H., Yu, L., & Law, S.S. (2000). Comparative studies on moving force identification from bridge strains in laboratory, *Journal of Sound and Vibration*, *235*, 87-104.

Chen, A., & Kurfess, T. R. (2019). Signal processing techniques for rolling element bearing spall size estimation. *Mechanical Systems and Signal Processing, 117*, 16–32.

Damped free vibration, (2007). Retrieved April 15, 2019, from http://www.wikizero.biz/index.php?q=aHR0cHM6Ly9lbi53aWtpcGVkaWEub3JnL3dpa2kvRmlsZTpEYW1wZWRfRnJlZV9WaWJyYXRpb24ucG5n

FAG Rolling Bearings. (1985). *Rolling element damage*. Schweinfurt:Georg Schäfer.

FAG Rolling Bearing Damage, (2001).Retrieved February 4, 2019, fromhttp://www.endas.com/images/Appic/PDF/FileUploadPDFTRinsert00456000.pdf

Geometrical parameters of engine bearings, (2019). Retrieved April 7, 2019, from http://www.substech.com/dokuwiki/doku.php?id=geometrical_parameters_of_engine_bearings

Holm-Hansen, B.T, & Gao, R.X.(2000). Structural design and analysis for a sensorintegrated ball bearing. *Finite Element Analysis and Design*, *34*, 257-270.

Holm-Hansen, B.T, & Gao, R.X. (2000). Vibration analysis of a sensor-integrated ball bearing. *Transactions of the ASME, 122*, 384-392.

Hizarci, B., Umutlu, R. C., Ozturk, H., & Kıral, Z. (2019). Vibration Region Analysis for Condition Monitoring of Gearboxes Using Image Processing and Neural Networks. *Experimental Techniques*, 1-17.

Jayaswal, P., Wadhwani, A. K., & Mulchandani, K. B. (2008). Machine fault signature analysis. *International Journal of Rotating Machinery*, 1-10.

Kiral Z.,& Karagulle, H. (2006). Vibration analysis of rolling element bearings with various defects under the action of an unbalanced force. *Mechanical Systems and Signal Processing*, *20*, 1967-1991.

Kiral, Z. (2002). *Simulation and analysis of vibration signals generated by rolling element bearings with defects*. Phd Thesis, Dokuz Eylül University, İzmir.

Kiral, Z.,& Karagulle, H. (2003). Simulation and analysis of vibration signals generated by rolling element bearings with defects. *Tribology International*, *36*, 667-678.

Kiral, Z.,& Karagulle, H.(2001). Hareketli yük etkisindeki sistemlerin IDEAS ile dinamik analizi. UMTS 2001, *10. Ulusal Makine Teorisi Sempozyumu*, *2*, 862-870.

Koyo Ball & Roller Bearings: Failure, causes and countermeasures, (2015). Retrieved March 20, 2019, from http://donoupoglou.gr/wp/wp-content/uploads/2015/03/catb3001e.pdf

Kurtosis, (2009). Retrieved February 5, 2019, from http://azimadli.com/vibman/kurtosis.htm

Laha, S. K. (2017). Enhancement of fault diagnosis of rolling element bearing using maximum kurtosis fast nonlocal means denoising. *Measurement*, *100*, 157–163

Kankar, P. K., Sharma, S. C., & Harsha, S. P. (2011). Rolling element bearing fault diagnosis using wavelet transform. *Neurocomputing*, *74*(10), 1638–1645.

Lawry, M.H. (1998). *I-DEAS Master series*. Milford: Structural Dynamics Research Corporation.

Leonardo and the strife-ridden renaissance, (n.d.). Retrieved February 8, 2019, from https://en.unesco.org/courier/octubre-1974/leonardo-and-strife-ridden-renaissance

Mathew, J.,& Alfredson, R. J. (1984). The condition monitoring of rolling element bearings using vibration analysis. *Journal of Vibration, Acoustics, Stress, and Reliability in Design*, *106*(3), 447-453.

McFadden, P. D.,& Smith, J. D. (1984). Model for the vibration produced by a single point defect in a rolling element bearing. *Journal of Sound and Vibration*, *96*(1), 69-82.

Metravib Technologies, (n.d.). Retrieved February 5, 2019, from http://www.plant-maintenance.com/articles/bearing_vibration_monitoring.pdf

McFadden, P.D, & Smith, J.D. (1984). Vibration monitoring of rolling element bearings by the high-frequency resonance technique- a review. *Tribology International*, *17*, 3 10.

Norton, P. (1998). *Peter Norton's guide to Visual Basic 6*, SAMS. Indiana: A Division of Macmillan Computer Publishing

Nabhan, A., Nouby, M., Sami, A. M., & Mousa, M. O. (2016). Vibration analysis of deep groove ball bearing with outer race defect using ABAQUS. *Journal of Low Frequency Noise Vibration and Active Control*, *35*(4), 312-325.

NTN Bearing Care and Maintenance of Bearings, (2017). Retrieved January 20, 2019, from https://www.ntn-snr.com/sites/default/files/2017-03/care_and_maintenance_of_bearings_en.pdf

Orhan, S., Akturk, N., & Celik, V. (2006). Vibration monitoring for defect diagnosis of rolling element bearings as a predictive maintenance tool: Comprehensive case studies. *NDT & E International*, *39*(4), 293-298.

Patel, R. K., Agrawal, S., & Joshi, N. C. (2012). Induction motor bearing fault identification using vibration measurement. *Conference: Engineering and Systems (SCES)*, 1-5.

Patidar, S.,& Soni, P. K. (2013). An overview on vibration analysis techniques for the diagnosis of rolling element bearing faults. *International Journal of Engineering Trends and Technology (IJETT)*, *4*(5), 1804-1809.

Peng, Y., Cai, J., Wu, T., Cao, G., Kwok, N., Zhou, S., & Peng, Z. (2019). Online wear characterisation of rolling element bearing using wear particle morphological features. *Wear, 430-431,* 369–375.

Rao, S. S. (2004). *Mechanical vibrations*. (5th ed.). London: Pearson Education.

Randall, R.B., & Antoni, J. (2011). Rolling element bearing diagnostics. *Mechanical System and Signal Processing*, *25*,485-520.

Roller type rolling guides, (n.d.). Retrieved April 7, 2019, from https://www.ikont.com/L2oU/7eMf-ZHvfu.html

Rao, V. G. (2000). Linear dynamics of an elastic beam under moving loads. *Journal of Vibration and Acoustics, 122,* 281-289.

Razpotnik, M., Čepon, G., & Boltežar, M. (2018). A smooth contact-state transition in a dynamic model of rolling-element bearings. *Journal of Sound and Vibration, 430,* 196–213.

Shah, D. S., & Patel, V. N. (2019). A dynamic model for vibration studies of dry and lubricated deep groove ball bearings considering local defects on races. *Measurement, 137*,535-555.

Schmidt, S., Heyns, P.S., & Gryllians, K.C. (2019). A discrepancy analysis methodolgy for rolling element bearing diagnostics under variable speed conditions. *Mechanical Systems and Signal Processing, 116,*40-61.

Singh, S., Howarda, C.Q., Hansena, C.H., Köpke, U. G.(2018).Analytical validation of an explicit finite element model of a rolling element bearing with a localised line spall. *Journal of Sound and Vibration, 416,* 94-110.

SKF. (1996). *SKF electronic handbook*. Sweden: Leif Lewinschal.

Scheffer, C. (Ed.). (2004). *Practical machinery vibration analysis and predictive maintenance*. Oxford: Elsevier.

Segla, M., Wang, S., & Wang, F. (2012). Bearing fault diagnosis with an improved high frequency resonance technique. *IEEE 10th International Conference on Industrial Informatics*, 580-585.

Simple harmonic motion, (n.d). Retrieved April 8, 2019, from https://www.augusta.k12.va.us/cms/lib01/VA01000173/Centricity/Domain/396/Simple_Harmonic_Motion_(SHM).pdfc

SKF Gauging machine health with "overall" vibration, (n.d.). Retrieved April 15, 2019, from https://www.skf.com/group/services/services-and-solutions/introduction-to-condition-monitoring/gauging-machine-health.html

SKF super-precision double direction angular contact thrust ball bearings, (2012). Retrieved April 8, 2019, from https://www.skf.com/binary/21-279300/Super-precision-double-direction-angular-contact-thrust-ball-bearings-BTW-series_10097_3_EN.pdf

SKF thrust ball bearings, (2014). Retrieved February 8, 2019, from http://sopetra.com.br/view/catalogo/rolamentos-axiais-de-esferas-catalogo.pdf

Tandon, N.,& Choudhury, A. *(1999)*. A review of vibration and acoustics measurement methods for the detection of defects in rolling element bearings. *Tribology International*, *32*, 469-480.

Types of ball bearings, (2012). Retrieved April 8, 2019, from https://nptel.ac.in/courses/116102012/bearings/types%20of%20ball%20bearings.htl

Xiang, J., Zhong, Y., & Gao, H. (2015). Rolling element bearing fault detection using PPCA and spectral kurtosis. *Measurement, 75*, 180–191

Yang, Y., Yang, W., & Jiang, D. (2018). Simulation and experimental analysis of rolling element bearing fault in rotor-bearing-casing system. *Engineering Failure Analysis, 92*, 205–221

Yiğit, A. (2008).*Detection of rolling element bearing faults via vibration analysis*. Msc Thesis, Dokuz Eylül University, İzmir.

Zhang, M., Jiang, Z., & Feng, K. (2017). Research on variational mode decomposition in rolling bearings fault diagnosis of the multistage centrifugal pump. *Mechanical Systems and Signal Processing, 93*, 460-493.

APPENDICES

APPENDIX 1: Creation of Parametric Model and Obtaining the Natural Frequency

```
/prep7
R=0.04
t=0.03
b=0.2
b1=0.14
a=0.1
h1=0.02
h2=0.05
h3=0.1
h=0.16
et,1,shell281
SECTYPE,1,SHELL
SECDATA,t
!r,1,t
mp,ex,1,2.1e11
mp,dens,1,7800
mp,nuxy,1,0.3
K,1,-b/2,-h3,0
K,2,-b/2,-(h3-h2),0
K,3,-a/2,-(h3-h2),0
K,4,-a/2,h-h3,0
K,5,a/2,h-h3,0
K,6,a/2,-(h3-h2),0
K,7,b/2,-(h3-h2),0
K,8,b/2,-h3,0
K,9,b1/2,-h3,0
K,10,b1/2,-(h3-h1),0
```

```
K,11,-b1/2,-(h3-h1),0
K,12,-b1/2,-h3,0
K,13,0,0,0
L,1,2
L,2,3
L,3,4
L,4,5
L,5,6
L,6,7
L,7,8
L,8,9
L,9,10
L,10,11
L,11,12
L,12,1
CIRCLE,13,R
A,1,2,3,4,5,6,7,8,9,10,11,12
AL,13,14,15,16
ASBA,1,2,KEEP1
LSEL,S,LINE,,13,16,1
LESIZE,ALL,,,20
ESIZE,0.002
AMESH,3
LSEL,ALL
!....Modal Solution.....
/SOLU
ANTYPE,MODAL,NEW
MODOPT,LANB,10
DL,8,3,ALL,0
DL,12,3,ALL,0
SOLVE
FINISH
```

*get,F1,mode,1,freq

!/POST1

!SET,LIST

APPENDIX 2: 0 Degree Radial Loading Position for Vibration Analysis and Sample Code File on 152thNode

model.txt

/config,nres,50000

/solu

antype , trans

outres , All, All

kbc , 0

deltim , 0.0000625

time , 0.00005

f,762,fx,555.556000

f,766,fx,4.007000

f,768,fx,0.000000

f,770,fx,0.000000

f,772,fx,0.000000

f,774,fx,0.000000

f,776,fx,0.000000

f,778,fx,0.000000

f,780,fx,0.000000

f,782,fx,0.000000

f,784,fx,299.516000

f,788,fx,0.000000

f,788,fx,0.000000

f,790,fx,0.000000

f,792,fx,0.000000

f,794,fx,0.000000

f,796,fx,0.000000

f,798,fx,0.000000

f,800,fx,0.000000

f,804,fx,0.000000

f,806,fx,0.000000

f,808,fx,0.000000

f,810,fx,0.000000

"

"

"

solve

finish

APPENDIX 3: Code Created to Process Data in Visual Program and Run It in Ansys Program

```
VERSION 5.00
Begin VB.Form Form1
   Caption        =   "Form1"
   ClientHeight   =   3015
   ClientLeft     =   120
   ClientTop      =   465
   ClientWidth    =   4560
   LinkTopic      =   "Form1"
   ScaleHeight    =   3015
   ScaleWidth     =   4560
   StartUpPosition =   3  'Windows Default
   Begin VB.CommandButton Command1
      Caption        =   "Command1"
      Height         =   1455
      Left           =   1560
      TabIndex       =   0
      Top            =   840
      Width          =   3975
   End
End
Attribute VB_Name = "Form1"
Attribute VB_GlobalNameSpace = False
Attribute VB_Creatable = False
Attribute VB_PredeclaredId = True
Attribute VB_Exposed = False
Private Sub Command1_Click()

Call count1
Call dt_calc
```

```
Call interp1
End Sub

Attribute VB_Name = "Module1"
Public Const nnum = 300
Public fl1 As String, fl As String, node_number(nnum) As String, node_dir(nnum)
As String
Public ncount(nnum) As Integer, tson As Double, n As Integer, dt As Single
Public te(nnum, nnum) As Single, fxe(nnum, nnum) As Double, dte(nnum) As
Single, dt_min(nnum) As Single
Sub count1()
fl1 = CurDir + "\"
fl = fl1 + "ANIM.PRG"

 n = 1: ncount(n) = 0
Open fl For Input As 1
11 Input #1, xc
xc = Mid(xc, 5, Len(xc))
If Val(xc) > 10 Then node_number(n) = xc
If xc = "X" Or xc = "Y" Then node_dir(n) = xc
If xc = 0 Or Mid(xc, 1, 1) = "." Then
If Val(xc) <= 1 Then
Input #1, yc
ncount(n) = ncount(n) + 1: te(n, ncount(n)) = xc: fxe(n, ncount(n)) = yc
If xc <> 0 Then dte(ncount(n) - 1) = te(n, ncount(n)) - te(n, ncount(n) - 1)
If ncount(n) > 2 Then
If dte(ncount(n) - 1) < dte(ncount(n) - 2) Then dt_min(n) = dte(ncount(n) - 1)
End If
End If
GoTo 11
End If
```

```
If ncount(n) <> 0 And xc = "" Then n = n + 1: ncount(n) = 0
If EOF(1) = True Then n = n - 1: Close #1: Exit Sub
GoTo 11
End Sub

Sub dt_calc()
Open fl1 + "dtmin.txt" For Output As 1
For nn = 1 To n
Write #1, node_number(nn), node_dir(nn), dt_min(nn), ncount(nn)
If nn < n And dt_min(nn) < dt_min(nn + 1) Then dt = Round(dt_min(nn), 5)
Next nn
Close #1
Form1.Print n, "dt =" & dt
End Sub

Sub interp1()
For nn = 1 To n
Open fl1 + "f" + node_number(nn) + node_dir(nn) + ".txt" For Output As nn
kt = 0: kk = 0
For k = 1 To ncount(nn)
'If k = 1 Then Write #nn, te(nn, k), fxe(nn, k)
If k > 1 Then
kk = kt + 1
Do While Round(kk * dt, 5) <= Round(te(nn, k), 5)
t1 = Round(te(nn, k - 1), 5): t2 = Round(te(nn, k), 5): f1 = fxe(nn, k - 1): f2 = fxe(nn,
k)
If Round((k - 1) * dt, 5) = Round(te(nn, k), 5) Then Write #nn, te(nn, k), fxe(nn, k)
If Round(kk * dt, 5) <= Round(te(nn, k), 5) Then
 If fxe(nn, k - 1) = fxe(nn, k) Then dtn = Round(kk * dt, 5): Write #nn, dtn, fxe(nn, k)
If fxe(nn, k - 1) <> fxe(nn, k) Then
fxn = (f2 - f1) * ((Round(kk * dt, 5) - t1) / (t2 - t1)) + f1
dtn = Round(kk * dt, 5)
```

```
Write #nn, dtn, fxn
End If
End If
kk = kk + 1
Loop
End If
kt = kk - 1
Next k
'Write #nn, te(nn, k), fxe(nn, k)
Close #nn
Next nn
End Sub
```

APPENDIX 4: An Example View of the ASCII File with Dynamic Extension Prg

K : $ mpos :; /CR T FD

K : f 11x

K : P

K : LAB

K : 11

K : X

K : U

K : 0, 0

K : .007, 0

K : .0075,-12808.5483521351

K : .00825,-12808.5483521351

K : .009,-12808.5483521351

K : .0095, 0

K : .02425, 0

K : .02475,-12808.5483521351

K : .0255,-12808.5483521351

K : .026, 0

K : .04075, 0

K : .04125,-12808.5483521351

K : .042,-12808.5483521351

K : .04275,-12808.5483521351

K : .04325, 0

K : .058, 0

"

"

"

K : $ return

K : $ return

K : $ mpos :; /F PR E

APPENDIX 5: Installation Dates Applied with Interpolation with Code Created in Visual Basic Program to Carry Out Ansys Analysis

0,0
.0005,0
.001,0
.0015,0
.002,0
.0025,0
.003,0
.0035,-5.69732017550807E-08
.004,-1.13946349176308E-07
.0045,-1.13946349176308E-07
.005,0
.0055,0
.006,0
.0065,0
.007,0
.0075,0
.008,0
.0085,0
.009,0
.0095,0
.01,0
.0105,0
.011,0
.0115,0
.012,0

APPENDIX 6: Frequency and Time Code Used for Creating Domain Analysis and Obtaining Statistical Indicators

```
clc;clear;close all
% HATASIZ SİNYAL İÇİN
dat=load('C:\Users\Nur\Desktop\sonucc_son_0\152ay.txt');
tm=dat(:,1); % Zaman sütunu
dt=(tm(2)-tm(1));
acc=dat(:,2); %İvme sütunu
b1=length(tm);
tm1=tm([1000:b1],1);acc=acc([1000:b1],1);
d1=acc; % Sinyal d değişkenine aktarıldı
byt=length(d1); %Sinyalin uzunluğu
fs=1/dt; %Örnekleme frekansı
% İstatistiksel değerler hesaplanıyor (hatasız rulman için)
sigmin=min(d1); % En küçük değer
sigmax=max(d1); % En büyük değer
%*****************************************************************
display
 ('=================== Hatasız Rulman İçin ====================')
p2p=sigmax-sigmin                % peak to peak
rms=sqrt(sum(d1.^2)/length(d1))      % rms
cf=p2p/rms                       % crest factor
kurtosis=sum((d1-mean(d1)).^4)/(length(d1).*(std(d1)^4)) % kurtosis
%*****************************************************************
display
('============================================================')
%FFT hesaplanıyor (hatasız rulman için)
nfft=256*32; % Kullanılacak FFT nokta sayısı
f_fft=abs(fft(d1,nfft))*dt*2*pi;
wf1=(0:(nfft/2-1))/(nfft/2)*(fs/2);
f_fft1=f_fft(1:length(f_fft)/2);
```

```
fmin=0; % x ekseni frekans başlangıcı
fmax=6000; % x ekseni frekans bitişi
% HATALI SİNYAL İÇİN
dat=load('C:\Users\Nur\Desktop\clhd_sn_0\152ay.txt');
tm=dat(:,1); % Zaman sütunu
dt=(tm(2)-tm(1)); % Örnekleme periyodu
acc=dat(:,2); % İvme sütunu
tm2=tm([1000:b1],1);acc=acc([1000:b1],1);
d=acc; % Titreşim sinyali d değişkenine aktarıldı
d2=d;
byt=length(d2); % Sinyal uzunluğu
fs=1/dt; % Örnekleme frekansı
aa=[max(d1), max(d2)];aa=max(aa);
tt=[max(tm1), max(tm2)];tt=max(tt);
subplot(2,2,1),
axis([0 tt -aa-aa*0.1 aa+aa*0.1]);
hold on;plot(tm1,d1)  % Hatasız sinyal çiziliyor
xlabel('Time [mS]'),ylabel('Acceleration [m/s^2]')
subplot(2,2,2),
axis([0 tt -aa-aa*0.1 aa+aa*0.1]);
hold on;plot(tm2,d2)
xlabel('Time [mS]'),ylabel('Acceleration [m/s^2]')
% İstatistiksel değerler hesaplanıyor (hatalı rulman için)
sigmin=min(d); % En küçük değer
sigmax=max(d); % En büyük değer
%**********************************************************************
display
('================== Hatalı Rulman İçin ====================')
p2p=sigmax-sigmin                % peak to peak
rms=sqrt(sum(d.^2)/length(d))       % rms
cf=p2p/rms                       % crest factor
kurtosis=sum((d-mean(d)).^4)/(length(d).*(std(d)^4)) % kurtosis
```

```
%*****************************************************************
display
('============================================================')
% FFT hesaplanıyor (hatalı rulman için)
f_fft=abs(fft(d,nfft))*dt*2*pi;
wf2=(0:(nfft/2-1))/(nfft/2)*(fs/2);
f_fft2=f_fft(1:length(f_fft)/2); % FFT sinyali (FFT düşey eksene göre simetrik
olduğu için yarısı kullanılır)
%fmin=0; % x ekseni başlangıç frekansı (Hz)
%fmax=2000; % x ekseni bitiş frekansı (Hz)
aa=[max(f_fft), max(f_fft)];aa=max(aa);
tt=[max(wf1), max(wf2)];tt=max(tt);
subplot(2,2,3);axis([0 tt 0 aa+0.1*aa]);hold on;plot(wf1,f_fft1)
%axis([fmin fmax min(f_fft) max(f_fft)*1.2]);
xlabel('Frequency [Hz]');ylabel('Amplitude')
subplot(2,2,4);axis([0 tt 0 aa+0.1*aa]);hold on;plot(wf2,f_fft2)
%axis([fmin fmax min(f_fft) max(f_fft)*1.2]);
xlabel('Frequency [Hz]');ylabel('Amplitude')
```

APPENDIX 7: Code for Comparing Rms, Kurtosis, Peak to Peak and Crest Factor Values According to Sensor Positions

```
clc;clear;close all
% HATASIZ SİNYAL İÇİN
dat1=load('C:\Users\Nur\Desktop\clhd_sn_0\152ux.txt');
dat2=load('C:\Users\Nur\Desktop\clhd_sn_0\262ux.txt');
dat3=load('C:\Users\Nur\Desktop\clhd_sn_0\372ux.txt');
dat4=load('C:\Users\Nur\Desktop\clhd_sn_90\152ux.txt');
dat5=load('C:\Users\Nur\Desktop\clhd_sn_90\262ux.txt');
dat6=load('C:\Users\Nur\Desktop\clhd_sn_90\372ux.txt');
dat7=load('C:\Users\Nur\Desktop\clhd_sn_180\152ux.txt');
dat8=load('C:\Users\Nur\Desktop\clhd_sn_180\262ux.txt');
dat9=load('C:\Users\Nur\Desktop\clhd_sn_180\372ux.txt');
dat10=load('C:\Users\Nur\Desktop\clhd_sn_270\152ux.txt');
dat11=load('C:\Users\Nur\Desktop\clhd_sn_270\262ux.txt');
dat12=load('C:\Users\Nur\Desktop\clhd_sn_270\372ux.txt');
tm1=dat1(:,1);dt1=(tm1(2)-tm1(1));d1=dat1(:,2);b1=length(tm1);
tm1=tm1([1000:b1],1);d1=d1([1000:b1],1);sigmin1=min(d1);sigmax1=max(d1);
p2p1=sigmax1-
sigmin1;rms1=sqrt(sum(d1.^2)/length(d1));cf1=p2p1/rms1;kurtosis1=sum((d1-
mean(d1)).^4)/(length(d1).*(std(d1)^4)) % kurtosis
tm2=dat2(:,1);dt2=(tm2(2)-tm2(1));d2=dat2(:,2);b2=length(tm2);
tm2=tm2([1000:b2],1);d2=d2([1000:b2],1);sigmin2=min(d2);sigmax2=max(d2);
p2p2=sigmax2-
sigmin2;rms2=sqrt(sum(d2.^2)/length(d2));cf2=p2p2/rms2;kurtosis2=sum((d2-
mean(d2)).^4)/(length(d2).*(std(d2)^4)) % kurtosis
tm3=dat3(:,1);dt3=(tm3(2)-tm3(1));d3=dat3(:,2);b3=length(tm3);
tm3=tm3([1000:b3],1);d3=d3([1000:b3],1);sigmin3=min(d3);sigmax3=max(d3);
p2p3=sigmax3-
sigmin3;rms3=sqrt(sum(d3.^2)/length(d3));cf3=p2p3/rms3;kurtosis3=sum((d3-
mean(d3)).^4)/(length(d3).*(std(d3)^4)) % kurtosis
```

```
pp1=[p2p1 p2p2 p2p3];rr1=[rms1 rms2 rms3];cc1=[cf1 cf2 cf3];kk1=[kurtosis1
kurtosis2 kurtosis3];
 tm1=dat4(:,1);dt1=(tm1(2)-tm1(1));d1=dat4(:,2);b1=length(tm1);
tm1=tm1([1000:b1],1);d1=d1([1000:b1],1);sigmin1=min(d1);sigmax1=max(d1);
p2p1=sigmax1-
sigmin1;rms1=sqrt(sum(d1.^2)/length(d1));cf1=p2p1/rms1;kurtosis1=sum((d1-
mean(d1)).^4)/(length(d1).*(std(d1)^4)) % kurtosis
tm2=dat5(:,1);dt2=(tm2(2)-tm2(1));d2=dat5(:,2);b2=length(tm2);
tm2=tm2([1000:b2],1);d2=d2([1000:b2],1);sigmin2=min(d2);sigmax2=max(d2);
p2p2=sigmax2-
sigmin2;rms2=sqrt(sum(d2.^2)/length(d2));cf2=p2p2/rms2;kurtosis2=sum((d2-
mean(d2)).^4)/(length(d2).*(std(d2)^4)) % kurtosis
tm3=dat6(:,1);dt3=(tm3(2)-tm3(1));d3=dat6(:,2);b3=length(tm3);
tm3=tm3([1000:b3],1);d3=d3([1000:b3],1);sigmin3=min(d3);sigmax3=max(d3);
p2p3=sigmax3-
sigmin3;rms3=sqrt(sum(d3.^2)/length(d3));cf3=p2p3/rms3;kurtosis3=sum((d3-
mean(d3)).^4)/(length(d3).*(std(d3)^4)) % kurtosis
pp2=[p2p1 p2p2 p2p3];rr2=[rms1 rms2 rms3];cc2=[cf1 cf2 cf3];kk2=[kurtosis1
kurtosis2 kurtosis3];
tm1=dat7(:,1);dt1=(tm1(2)-tm1(1));d1=dat7(:,2);b1=length(tm1);
tm1=tm1([1000:b1],1);d1=d1([1000:b1],1);sigmin1=min(d1);sigmax1=max(d1);
p2p1=sigmax1-
sigmin1;rms1=sqrt(sum(d1.^2)/length(d1));cf1=p2p1/rms1;kurtosis1=sum((d1-
mean(d1)).^4)/(length(d1).*(std(d1)^4)) % kurtosis
tm2=dat8(:,1);dt2=(tm2(2)-tm2(1));d2=dat8(:,2);b2=length(tm2);
tm2=tm2([1000:b2],1);d2=d2([1000:b2],1);sigmin2=min(d2);sigmax2=max(d2);
p2p2=sigmax2-
sigmin2;rms2=sqrt(sum(d2.^2)/length(d2));cf2=p2p2/rms2;kurtosis2=sum((d2-
mean(d2)).^4)/(length(d2).*(std(d2)^4)) % kurtosis
tm3=dat9(:,1);dt3=(tm3(2)-tm3(1));d3=dat9(:,2);b3=length(tm3);
tm3=tm3([1000:b3],1);d3=d3([1000:b3],1);sigmin3=min(d3);sigmax3=max(d3);
```

```
p2p3=sigmax3-
sigmin3;rms3=sqrt(sum(d3.^2)/length(d3));cf3=p2p3/rms3;kurtosis3=sum((d3-
mean(d3)).^4)/(length(d3).*(std(d3)^4)) % kurtosis
pp3=[p2p1 p2p2 p2p3];rr3=[rms1 rms2 rms3];cc3=[cf1 cf2 cf3];kk3=[kurtosis1
kurtosis2 kurtosis3];
tm1=dat10(:,1);dt1=(tm1(2)-tm1(1));d1=dat10(:,2);b1=length(tm1);
tm1=tm1([1000:b1],1);d1=d1([1000:b1],1);sigmin1=min(d1);sigmax1=max(d1);
p2p1=sigmax1-
sigmin1;rms1=sqrt(sum(d1.^2)/length(d1));cf1=p2p1/rms1;kurtosis1=sum((d1-
mean(d1)).^4)/(length(d1).*(std(d1)^4)) % kurtosis
tm2=dat11(:,1);dt2=(tm2(2)-tm2(1));d2=dat11(:,2);b2=length(tm2);
tm2=tm2([1000:b2],1);d2=d2([1000:b2],1);sigmin2=min(d2);sigmax2=max(d2);
p2p2=sigmax2-
sigmin2;rms2=sqrt(sum(d2.^2)/length(d2));cf2=p2p2/rms2;kurtosis2=sum((d2-
mean(d2)).^4)/(length(d2).*(std(d2)^4)) % kurtosis
tm3=dat12(:,1);dt3=(tm3(2)-tm3(1));d3=dat12(:,2);b3=length(tm3);
tm3=tm3([1000:b3],1);d3=d3([1000:b3],1);sigmin3=min(d3);sigmax3=max(d3);
p2p3=sigmax3-
sigmin3;rms3=sqrt(sum(d3.^2)/length(d3));cf3=p2p3/rms3;kurtosis3=sum((d3-
mean(d3)).^4)/(length(d3).*(std(d3)^4)) % kurtosis
pp4=[p2p1 p2p2 p2p3];rr4=[rms1 rms2 rms3];cc4=[cf1 cf2 cf3];kk4=[kurtosis1
kurtosis2 kurtosis3];
t=[1 2 3];
figure;hold on;plot(t,pp1,'-o');plot(t,pp2,'-o');plot(t,pp3,'-o');plot(t,pp4,'-o');
title('peak to peak');legend('0','90','180','270')
figure;hold on;plot(t,rr1,'-o');plot(t,rr2,'-o');plot(t,rr3,'-o');plot(t,rr4,'-o');
title('rms');legend('0','90','180','270')
figure;hold on;plot(t,cc1,'-o');plot(t,cc2,'-o');plot(t,cc3,'-o');plot(t,cc4,'-o');
title('crist');legend('0','90','180','270')
figure;hold on;plot(t,kk1,'-o');plot(t,kk2,'-o');plot(t,kk3,'-o');plot(t,kk4,'-o');
title('kurtosis');legend('0','90','180','270')
```

APPENDIX 8: Nomenclature

D	: Outer diameter
d	: Bore diameter
d_b	: Ball diameter
b	: Spring gap in the length in the foundation
Dd	: Dynamic magnification factor
dm	: Pitch diameter
Z	: Number of ball
α	: Contact angle
E	: Modulus of elasticity
fc	: Cage frequency
Fc	: Crest Factor
f_s	: Shaft frequency
f_{ir}	: Inner ring defect frequency
f_r	: Rolling element spin frequency
f_{or}	: Outer ring defect frequency
f_{re}	: Rolling element defect frequency
c	: Damping
f	: Frequency of oscillation
k	: Stiffness
m	: mass
S	: Shaft speed
t	: Time
T	: Period
V	: Velocity
ω	: Angular frequency
ω_n	: Natural frequency
ω_r	: Resonance frequency
σ	: Standard deviation
Ø	: Phase

N	: Number of nodes that satisfies the condition
N_s	: Sample number of discrete vibration signal
Nz	: Total number of nodes
q	: Column matrix of nodal displacements
q_i	: Generalized coordinates
q_o	: Maximum load intensity
θ_{ni}	: Angular position of nodes
θ_{bj}	: Angle of balls
ε	: Load distribution factor
φ	: Angular coordinates in the load zone
φ_z	: Load zone angle
FFT	: Fast Fourier transform
HFRT	: High frequency resonance technique
RPM	: Revolution per minute